Available online at www.sciencedirect.com
SCIENCE DIRECT
Pergamon
Cement and Concrete Research 34 (2004) 1733–1777
CEMENT AND CONCRETE RESEARCH

# Tobermorite/jennite- and tobermorite/calcium hydroxide-based models for the structure of C-S-H: applicability to hardened pastes of tricalcium silicate, β-dicalcium silicate, Portland cement, and blends of Portland cement with blast-furnace slag, metakaolin, or silica fume

I.G. Richardson*

*Civil Engineering Materials Unit, School of Civil Engineering, University of Leeds, Leeds LS2 9JT, UK*

Received 26 May 2004; accepted 27 May2004

**Abstract**

The purpose of this article is to discuss the applicability of the tobermorite–jennite (T/J) and tobermorite–'solid-solution' calcium hydroxide (T/CH) viewpoints for the nanostructure of C-S-H present in real cement pastes. The discussion is facilitated by a consideration of the author's 1992 model, which includes formulations for both structural viewpoints; its relationship to other recent models is outlined. The structural details of the model are clearly illustrated with a number of schematic diagrams. Experimental observations on the nature of C-S-H present in a diverse range of cementitious systems are considered. In some systems, the data can only be accounted for on the T/CH structural viewpoint, whilst in others, both the T/CH and T/J viewpoints could apply. New data from transmission electron microscopy (TEM) are presented. The 'inner product' (Ip) C-S-H in relatively large grains of $C_3S$ or alite appears to consist of small globular particles, which are ≈ 4–8 nm in size in pastes hydrated at 20 °C but smaller at elevated temperatures, ≈ 3–4 nm. Fibrils of 'outer product' (Op) C-S-H in $C_3S$ or β-$C_2S$ pastes appear to consist of aggregations of long thin particles that are about 3 nm in their smallest dimension and of variable length, ranging from a few nanometers to many tens of nanometers. The small size of these particles of C-S-H is likely to result in significant edge effects, which would seem to offer a reasonable explanation for the persistence of $Q^0$(H) species. This would also explain why there is more $Q^0$(H) at elevated temperatures, where the particles seem to be smaller, and apparently less in KOH-activated pastes, where the C-S-H has foil-like morphology. In blended cements, a reduction in the mean Ca/Si ratio of the C-S-H results in a change from fibrillar to a crumpled-foil morphology, which suggests strongly that as the Ca/Si ratio is reduced, a transition occurs from essentially one-dimensional growth of the C-S-H particles to two-dimensional; i.e., long thin particles to foils. Foil-like morphology is associated with T-based structure. The C-S-H present in small fully hydrated alite grains, which has high Ca/Si ratio, contains a less dense product with substantial porosity; its morphology is quite similar to the fine foil-like Op C-S-H that forms in water-activated neat slag pastes, which has a low Ca/Si ratio. It is thus plausible that the C-S-H in small alite grains is essentially T-based (and largely dimeric). Since entirely T-based C-S-H is likely to have different properties to C-S-H consisting largely of J-based structure, it is possible that the C-S-H in small fully reacted grains will have different properties to the C-S-H formed elsewhere in a paste; this could have important implications.


*Keywords:* Calcium-silicate-hydrate (C-S-H); Cement paste; Granulated blast-furnace slag; Metakaolin; Silica fume

## 1. Introduction

What is it that is produced during the hydration of Portland cement (PC) that results in the formation of a hardened mass? This rather fundamental question was first addressed experimentally by Henri Le Chatelier and Wilhelm Michaëlis in their classic works of the late 19th and early 20th centuries. Their competing theories for the hardening of cement resulted in a long-continued and somewhat polarized debate: Michaëlis' 'colloids' theory (e.g., Refs. [1,2]) (and its derivatives, e.g., Ref. [3]), against Le Chatelier's 'crystalloids' theory (e.g., Refs. [4,5]). Le Chatelier believed that the principal binding phase was a calcium silicate hydrate of formula $CaO{\cdot}SiO_2{\cdot}2.5H_2O$; Newberry and Smith [6] also thought that it was a calcium silicate hydrate, but with the formula 1.5–2 $CaO{\cdot}SiO_2{\cdot}$(aq), whilst Rankin [7] thought it a

* Tel.: +44-113-343-2331; fax: +44-113-343-2265.
*E-mail address:* i.g.richardson@leeds.ac.uk (I.G. Richardson).

0008-8846/$ – see front matter © 2004 Elsevier Ltd. All rights reserved.
doi:10.1016/j.cemconres.2004.05.034

hydrous silica. Bogue concluded in his book in 1955 that the probable composition was close to $1.5CaO{\cdot}SiO_2{\cdot}(aq)$ [8]. Bernal et al. [9] found through X-ray studies on hydrated $C_3S$ pastes that the calcium silicate hydrate (C-S-H) that was formed was nearly amorphous and thus difficult to characterize structurally; they did, however, consider that it was related to C-S-H phases formed in dilute suspensions, which they called calcium silicate hydrates (I) and (II) [10], which had low and high Ca/Si ratios, respectively. Calcium silicate hydrate (I) had a layer structure, with the layers elongated in one direction that resulted in a fibrous structure, and showed similarities to tobermorite, a rare crystalline calcium silicate hydrate that had been found in Northern Ireland, which has the approximate constitutional formula $Ca_4(Si_6O_{18}H_2){\cdot}Ca{\cdot}4H_2O$ and a Ca/Si ratio of 0.83. Its structure—first described by Megaw and Kelsey in 1956 [11]—contains linear silicate chains of the 'dreierkette' form in which the silicate tetrahedra coordinate themselves to $Ca^{2+}$ ions by linking in such a way as to repeat a kinked pattern after every three tetrahedra. Two of the three tetrahedra share O–O edges with the central Ca–O part of the layer; these are linked together and are often referred to as 'paired' tetrahedra (P). The third tetrahedron, which shares an oxygen atom at the pyramidal apex of a Ca polyhedron, connects the two 'paired' tetrahedra and so is termed 'bridging' (B). The dreierkette-type chain present in tobermorite is illustrated in Fig. 1. Taylor and Howison [13] suggested that the Ca/Si ratio could be raised above 0.83 by the removal of some of these 'bridging' tetrahedra and replaced by interlayer $Ca^{2+}$ ions. Various dreierkette-based models have subsequently been proposed, which broadly fall into two categories that have different ways of raising the Ca/Si ratio to the value observed experimentally in $C_3S$ or neat PC pastes, i.e., 1.7–1.8. The first category envisages elements of tobermorite-like structure interstratified with layers of calcium hydroxide: the so-called tobermorite–'solid-solution' calcium hydroxide, or T/CH, viewpoint [14–16]. The second category envisages elements of tobermorite-like structure intermixed with others of jennite-like structure [17]: the tobermorite–jennite, or T/J, viewpoint. Jennite is another crystalline calcium silicate hydrate that has dreierkette silicate chains, but it has a much higher Ca/Si ratio than tobermorite (formula $Ca_9Si_6O_{18}(OH)_6{\cdot}8H_2O$; Ca/Si ratio of

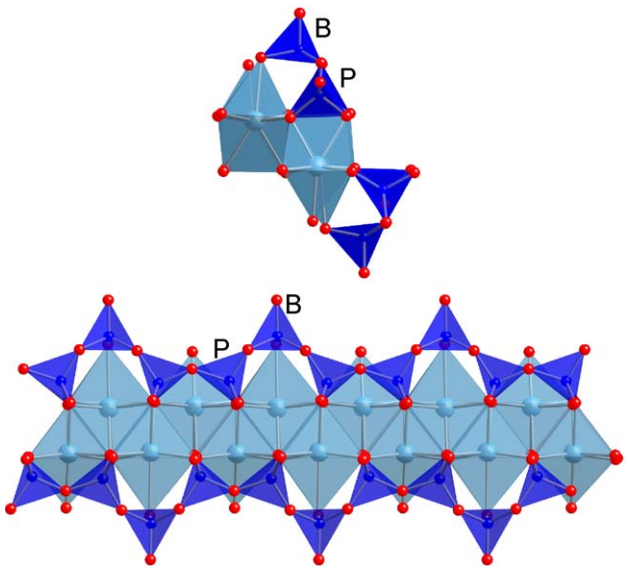


Fig. 1. Schematic diagrams showing dreierkette chains present in 14 Å tobermorite (which in theory are of infinite length) projected along [010] (top) and [210] (crystal structure data from Bonaccorsi et al. [12] and private communication). The chains have a kinked pattern where some silicate tetrahedra share O–O edges with the central Ca–O layer (called 'paired' tetrahedra, P) and others that do not (called 'bridging' tetrahedra, B).

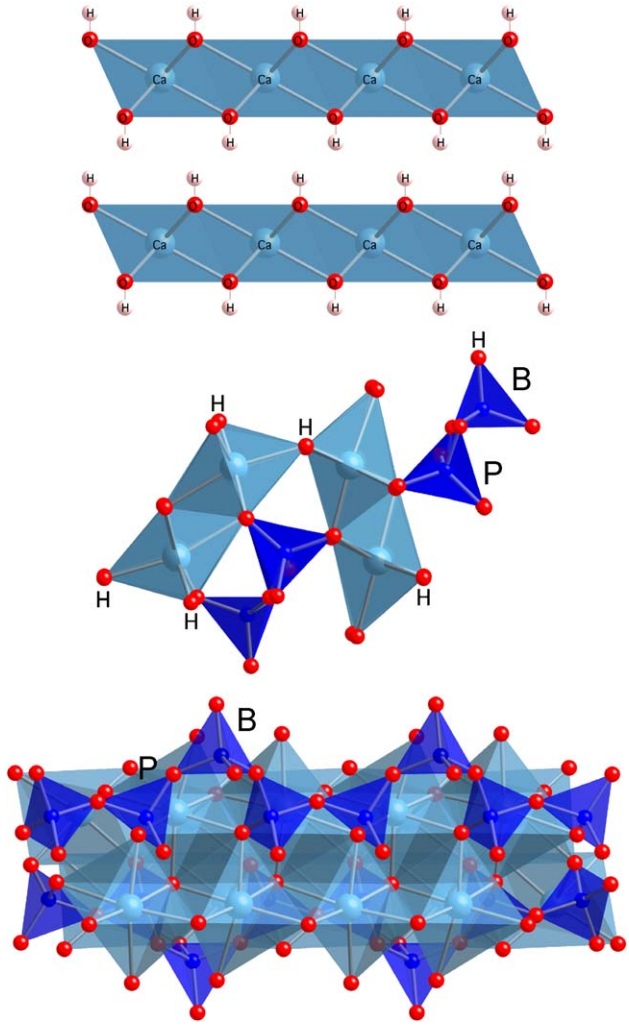


Fig. 2. Schematic diagrams showing layers of $Ca(OH)_2$ (top) and dreierkette chains present in the structure of jennite (which in theory are of infinite length) projected along [010] (middle; hydroxyl groups are indicated by 'H') and [100] (bottom) (jennite data from Bonaccorsi et al. [20]). 'Paired' and 'bridging' tetrahedra are labelled 'P' and 'B', respectively. The oxygen atom labelled 'H' on the 'bridging' tetrahedron is only likely to be Si–OH in synthetic jennites, which are generally deficient in Ca (i.e., the deficit in positive charge resulting from the absence of interlayer $Ca^{2+}$ is balanced by $OH^-$ groups).

1.5), and the central Ca–O part of its structure is corrugated, as illustrated in Fig. 2. The purpose of this article is to discuss the applicability of the T/J and T/CH viewpoints for the nanostructure of C-S-H present in real cement pastes. The discussion in this article is facilitated by a consideration of the author's 1992 model [18,19], which includes formulations for both structural viewpoints; its relationship to other recent models is outlined. The structural details of the model are clearly illustrated with a number of schematic diagrams, some of which have only been made possible by the recent determinations of the crystal structures of 1.4 nm tobermorite and jennite [12,20]. The model is shown to account for a number of experimental observations on the nature of C-S-H present in a diverse range of cementitious systems. The T/J and T/CH viewpoints and many other aspects of calcium silicate hydrates formed both naturally and in cements and also those synthesized in the laboratory, are discussed at length in a forthcoming RILEM report [21].

## 2. Experimental

The experimental details for all the systems discussed in this article are reported in other publications, which are referenced as appropriate, and should be consulted when necessary. The specimens for transmission electron microscopy (TEM) were prepared as outlined in Ref. [22]. Excessive beam damage was avoided by restricting the maximum magnification to $\times 25{,}000$; the problems associated with attempting to view hardened cement specimens at higher magnifications in the TEM are discussed in detail in Ref. [22].

## 3. Results and discussion

Significant advances in the characterization of C-S-H have been achieved in the past 40 years through the application of a variety of new techniques: the electron microprobe in the 1960s; scanning electron microscopy (SEM) in the 1970s; trimethylsilylation gel permeation chromatography (TMS-GPC), analytical TEM, and solid-state nuclear magnetic resonance (NMR) spectroscopy in the 1980s and 1990s. Whilst these studies confirmed that the principal binding phase in hardened cements is a C-S-H with linear (alumino)silicate chains of the dreierkette form, they also showed that its exact nature is affected by many factors—including the composition of the cement, the water-to-cement ratio (w/c), the curing temperature, the degree of hydration, and the presence of chemical and mineral admixtures—with the result that there is tremendous variation in its composition, nanostructure, and morphology. Any model for the structure of C-S-H must account for these observations. The most important of them are summarized in the following sections, with some additional new results.

### 3.1. Chemical composition

Any model for the structure of C-S-H must account for the observed compositional variations and distributions of composition within any particular system; it must account for the following:

(i) The mean Ca/Si ratio of C-S-H phases present in commercial cements varies considerably, from $\approx 2.3$ to $\approx 0.7$ [23].
(ii) C-S-H displays very fine-scale compositional heterogeneity; for example, in neat $C_3S$ or $\beta$-$C_2S$ pastes where the mean Ca/Si ratio is about 1.75 [24–29], different regions analysed in the TEM (at the scale of about 100 nm) have values ranging between 2.1 and 1.2 [28,29].
(iii) C-S-H tends to become compositionally more homogeneous with age; for example, the C-S-H present in neat ordinary PC (OPC) pastes has been observed to have a bimodal distribution at young age, which becomes unimodal as hydration progresses [28].
(iv) The mean Ca/Si ratio of C-S-H in neat $C_3S$ or OPC pastes does not vary with age (see, e.g., the top part of Fig. 2 in Ref. [29]).
(v) The C-S-H present in many types of cement contains significant amounts of substituent ions, the most important being $Al^{3+}$. For example, in granulated iron blast-furnace slag–PC blends the Al/Ca ratio increases linearly with increasing Si/Ca ratio [30]; the compositions of the C-S-H present in the 'outer product' (Op)[1] region and in the slag and alite 'inner product' (Ip) regions are all affected similarly. A number of examples that will be discussed in this article in terms of models for the nanostructure of C-S-H are shown in Figs. 3, 4, and 5 [31–33]. These figures show Al/Ca against Si/Ca ratio scatter plots for TEM analyses of C-S-H present in water- and KOH-activated slag–white PC blends, in a KOH-activated 20% metakaolin–80% white PC blend, and in a KOH-activated synthetic slag glass. Each point represents an analysis of Op C-S-H at the scale of about 100 nm, which had been checked by selected area electron diffraction (SAED) to be free of admixture with crystalline phases. The labels on the figures—which relate to the models for the structure of C-S-H—are discussed in Section 4.

### 3.2. Morphology and structural order of C-S-H

Any model for the structure of C-S-H must account for the various morphologies of C-S-H and varying degrees of structural order; many of these are outlined in the following sections.

[1] C-S-H that forms within the original volume of reacting cement grains is termed *Ip C-S-H* and the C-S-H that forms in the originally water-filled spaces is termed *Op C-S-H*. There is not necessarily an exact correspondence between the positions of the outer boundaries of Ip and the original grains.

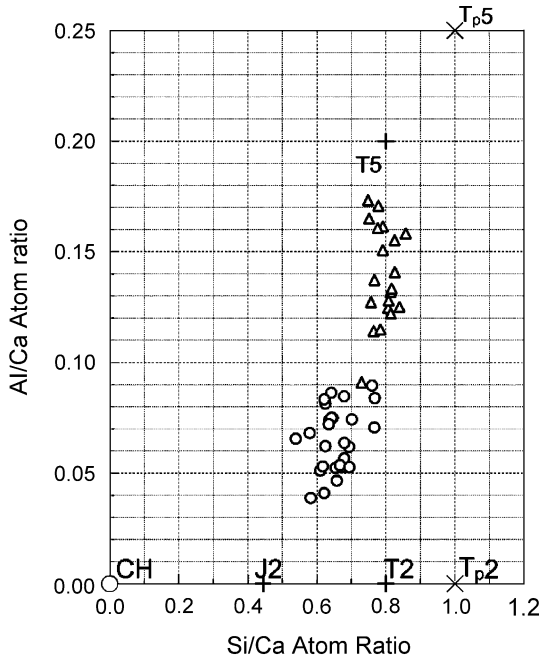


Fig. 3. Al/Ca against Si/Ca atom ratio plot of TEM analyses of Op C-S-H present in hydrated samples of water-activated white PC/GGBS blends with 50% (○) and 90% (△) slag. Experimental details are given in Ref. [31].

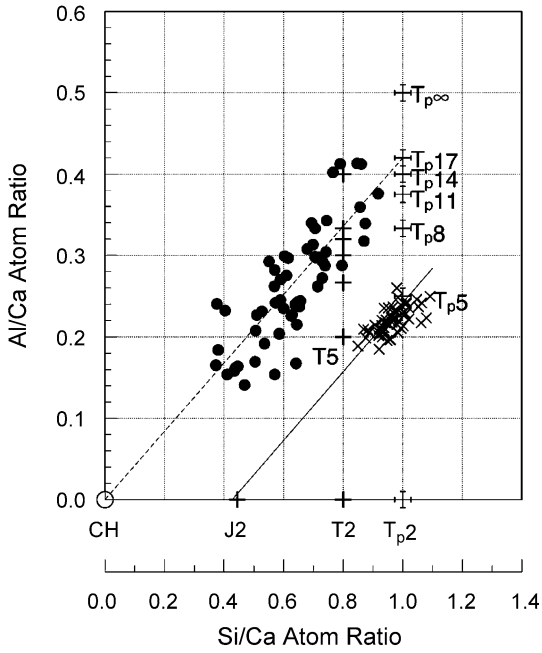


Fig. 5. Al/Ca against Si/Ca atom ratio plot of TEM analyses of Op C-S-H present in hydrated samples of a hardened white PC/20% metakaolin blend (●) [45] and a synthetic slag glass (×) [33] both activated with 5 M KOH solution.

### 3.2.1. C-S-H in hardened pastes of $C_3S$, $\beta$-$C_2S$ or PC hydrated at 20 °C and 80 °C

(i) *Inner product.* Ip C-S-H that forms from the reaction of reasonably large grains of $C_3S$ or alite has a compact, fine-scale, and homogeneous morphology (see, e.g., SEM [34] and TEM [35]); the morphology of C-S-H present in small fully reacted grains is discussed in Section 3.2.6. Groves [35] estimated from TEM that the pores in this type of Ip C-S-H are less than ≈ 10 nm, which is consistent with results from small-angle neutron scattering experiments [36,37]. The fine morphology of this Ip C-S-H is illustrated on the left of Fig. 6(a), which shows a TEM micrograph of a region in a hardened $C_3S$ paste hydrated for 8 years at 20 °C with w/c = 0.4. Fig. 6(b) shows an enlargement of an area of the Ip; the Ip C-S-H appears to consist of aggregates of small globular particles, the particles being 4–6 nm in diameter. The pores—if simplistically considered to be the regions of lighter contrast—are certainly less than 10 nm. If the boundary between the Ip and Op product regions is assumed to be along the area indicated by the white arrows, then it is evident that in some of the Ip the globules are aligned so as to give a fan-like texture. Fig. 7(a) shows an example of fine-textured C-S-H present in a PC paste (hydrated for 12 months at 20 °C; w/c = 0.4). Fig. 7(b) shows an enlargement of part of the micrograph; again, the Ip C-S-H appears to consist of small globular particles, but in this case, they are more homogeneously distributed than in Fig. 6 and perhaps a bit larger, between 6 and 8 nm in diameter. Whilst the fine-textured morphology is certainly the most common form in grains greater than a few micrometers in size, C-S-H with a more pronounced

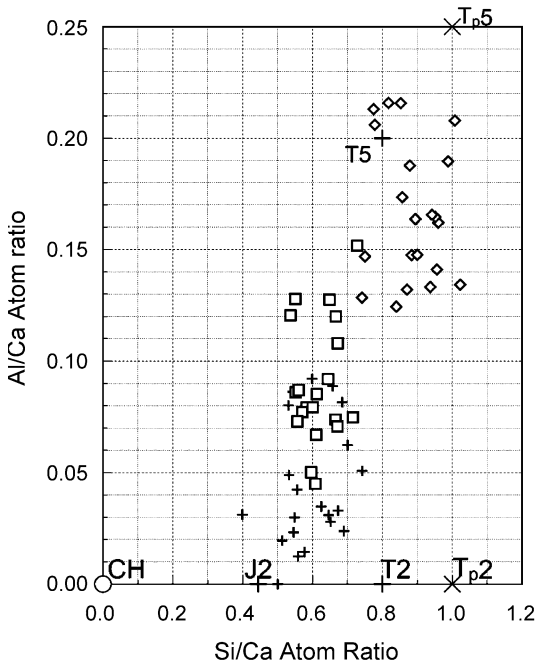


Fig. 4. Al/Ca against Si/Ca atom ratio plot of TEM analyses of Op C-S-H present in hydrated samples of 5 M KOH-activated white PC/GGBS blends with 0% (+), 50% (□), and 90% (◇) slag. Experimental details are given in Ref. [31].

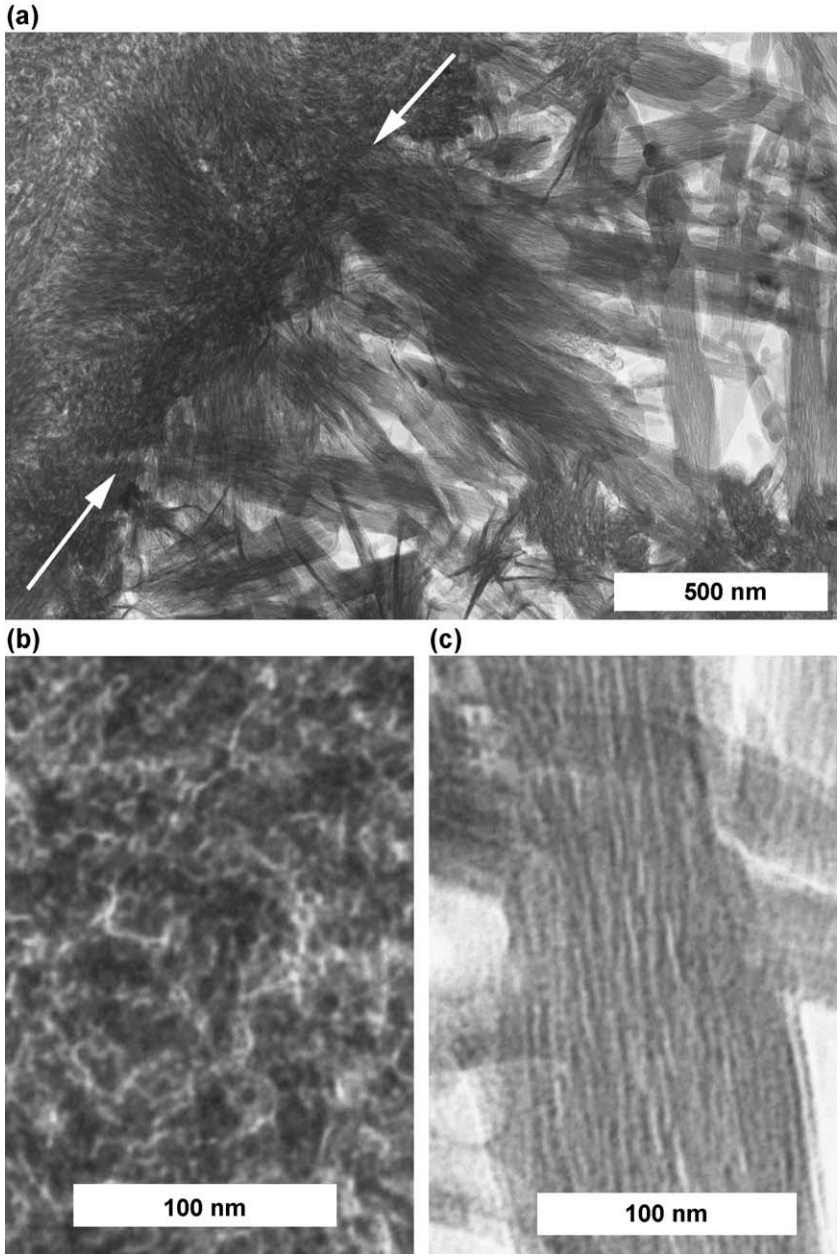


Fig. 6. (a) A TEM micrograph showing Ip and Op C-S-H present in a hardened $C_3S$ paste with w/c = 0.4 hydrated at 20 °C for 8 years. White arrows indicate the Ip–Op boundary; the Ip is in the upper left of the micrograph. (b) An enlargement of a region of Ip C-S-H. (c) An enlargement of a fibril of Op C-S-H.

texture is also sometimes observed in PC pastes, as well as in $C_3S$ pastes (example in Fig. 6); an example is shown in Fig. 8. The globules of C-S-H are of similar dimensions to those in Fig. 7, but they are packed together differently (compare Figs. 7(b) and 8(b)).

Fig. 9(a) shows a micrograph illustrating C-S-H present in a $C_3S$ paste hydrated at elevated temperature (at 80 °C for 8 days with w/c = 0.51). The Ip C-S-H again has a fine homogeneous morphology, similar to that in Fig. 6. However, the globules of C-S-H appear to be significantly smaller, between 3 and 4 nm: Comparison of Figs. 6(b) and 9(b) shows that the particles of C-S-H in the higher temperature system are about half the size of those present at lower temperature. Careful examination of a number of regions in both systems led to the same conclusion.

(ii) *Outer product.* The Op C-S-H present in hardened $C_3S$ or OPC pastes has a fibrillar, directional morphology (e.g., SEM [34] and TEM [35,38]). This morphology is a function of space constraint: where it forms in large pore spaces, the fibrils form with a high length to width aspect ratio (which will be referred to as *coarse fibrillar*); in smaller spaces, it retains a directional aspect but forms in a more space-efficient manner ('fine fibrillar'); C-S-H morphological terminology is discussed in Ref. [22]. The spaces between the fibrils

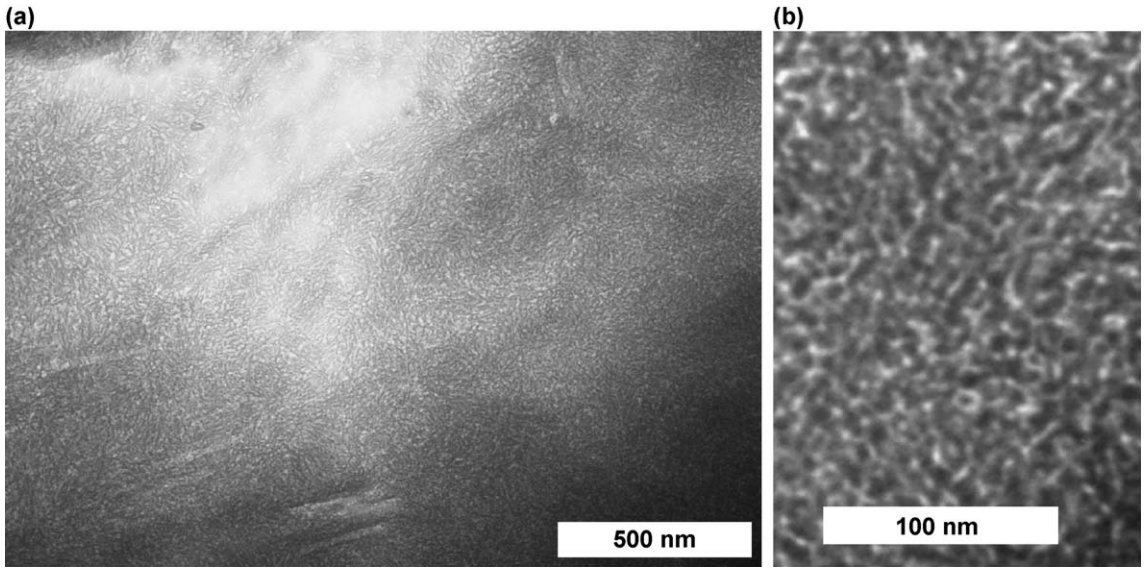


Fig. 7. (a) A TEM micrograph showing fine Ip C-S-H present in a hardened OPC paste with w/c = 0.4 hydrated at 20 °C for 1 year. (b) An enlargement of a region of Ip C-S-H. Experimental details are given in Ref. [28].

of Op C-S-H form a three-dimensional interconnected pore network: the capillary porosity. Op C-S-H present in a hardened $C_3S$ paste (hydrated for 8 years at 20 °C; w/c = 0.4) is shown on the right of Fig. 6(a), and an enlargement of a section of a coarse fibril is shown in Fig. 6(c). The fibril—which is about 100 nm wide—appears to consist of a large number of long thin particles aligned along its length. The particles are—like those in the Ip—about 3 nm in their smallest dimension, but they are of variable length from a few nanometers to many tens of nanometers. This is a common observation, both in hardened $C_3S$ and β-$C_2S$ pastes. Coarse fibrillar Op C-S-H present in a β-$C_2S$ paste is shown in Fig. 10 (hydrated for 1 month at 20 °C; w/c = 0.4). Op C-S-H formed by the hydration of $C_3S$ at elevated temperatures also appears to consist of long thin particles: Fig. 9(c) shows an enlargement of some of the fine fibrillar C-S-H present on Fig. 9(a). The Op C-S-H present in neat PC pastes typically has a finer morphology than that present in $C_3S$ or β-$C_2S$ pastes.

(iii) *Interlayer space and gel pores.* If in the micrographs discussed above the regions of lighter contrast in the C-S-H are taken to essentially correspond to pores, and if it is assumed that by drying the contrast has been enhanced, then these gel pores are clearly very small. If

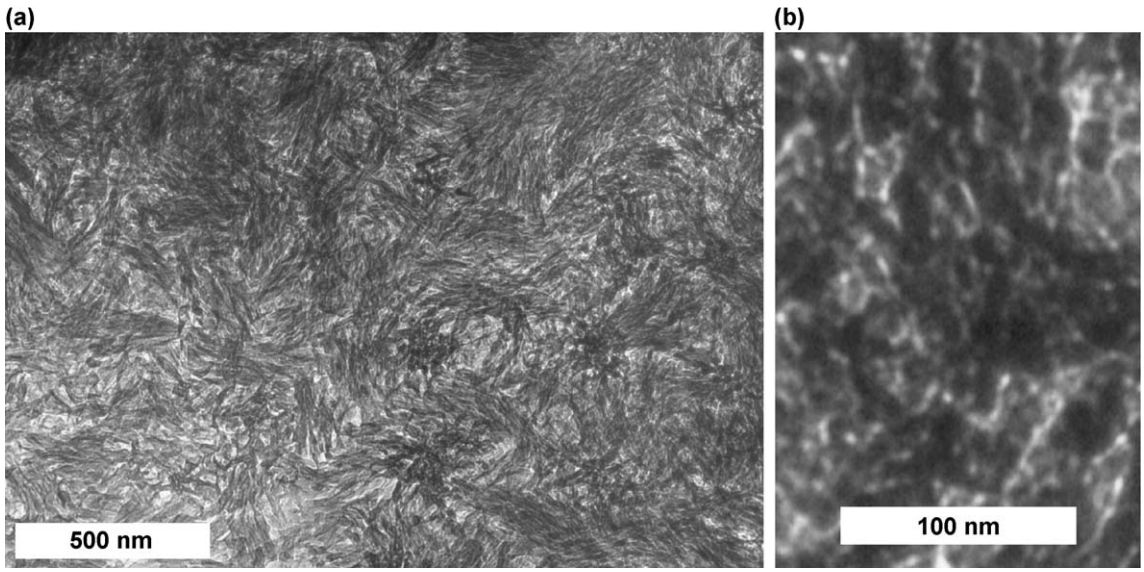


Fig. 8. (a) A TEM micrograph showing Ip C-S-H present in a hardened OPC paste with w/c = 0.4 hydrated at 20 °C for 1 year; the C-S-H has a more pronounced texture than that in Fig. 7. (b) An enlargement of a region of Ip C-S-H. Experimental details are given in Ref. [28].

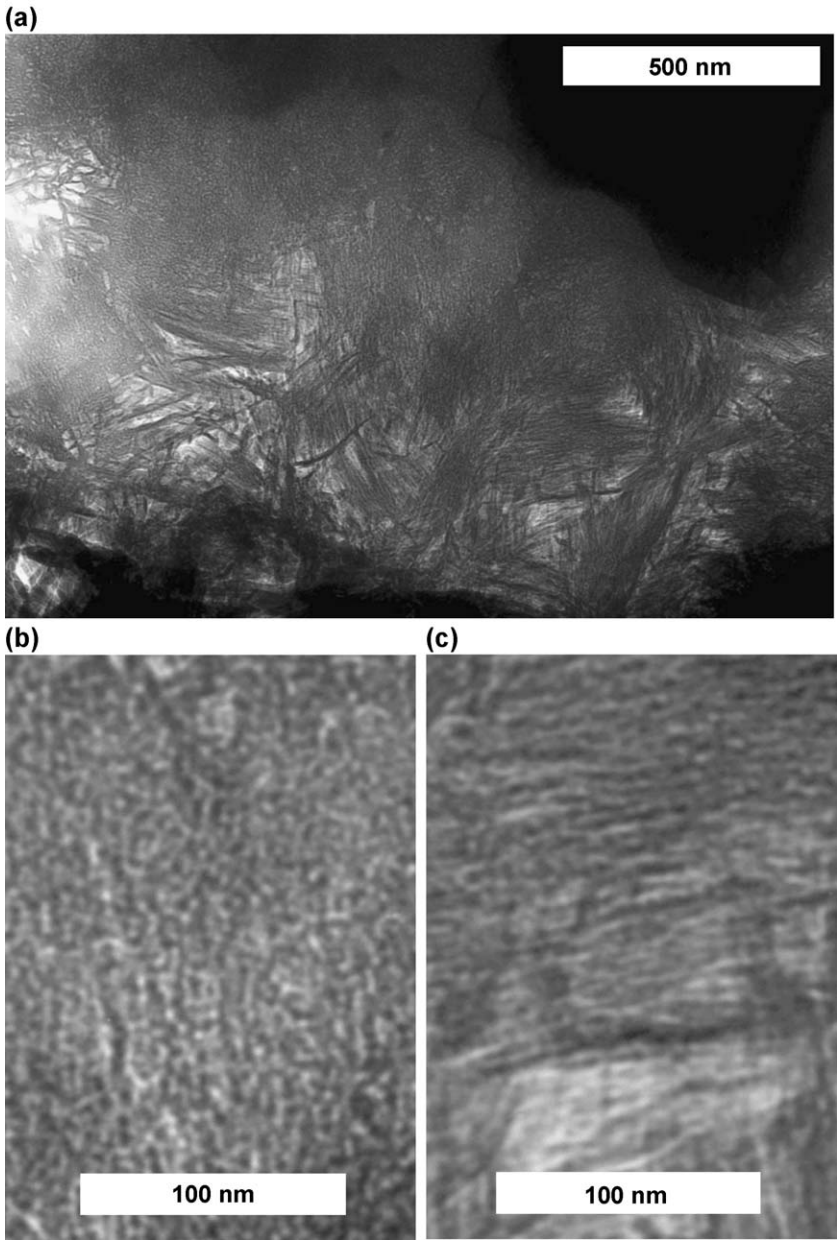


Fig. 9. (a) A TEM micrograph showing Ip and Op C-S-H present in a hardened $C_3S$ paste with w/c = 0.51 hydrated at 80 °C for 8 days. (b) An enlargement of a region of Ip C-S-H. (c) An enlargement of a fibril of Op C-S-H.

it is assumed that the particles of C-S-H consist of elements of structure based on tobermorite and/or jennite, then their dimensions are such that they must consist of very few layers of these structures, in some cases as few as two. It is clear that the boundary between interlayer space and gel pore space is likely to be very indistinct.

(iv) *Structural order.* Powder X-ray diffraction (XRD) of water-activated cement pastes show only two weak, broad peaks for C-S-H, centred between 3.2–2.7 and 1.86–1.79 Å [39,40]. There is never any sign of layer spacing. SAED studies have produced results consistent with those from XRD (e.g., Ref. [41]). As an example, Fig. 11 shows a SAED pattern for an area that contained both C-S-H and CH in a hardened paste of ordinary PC (hydrated for 12 months at 20 °C; w/c = 0.4). The figure consists of a diffuse C-S-H ring superimposed on a [031] zone axis pattern for CH. The diffuse ring ranges between about 3.2 and 2.7 Å. A faint ring at about 1.83 Å is also commonly observed. Spacings in the region of 3 and 1.8 Å correspond to important repeat distances in the Ca–O parts of the structures of tobermorite and jennite, as well as in the structure of CH, which is illustrated in Fig. 12.

(v) *Calcium hydroxide.* CH is typically observed as large crystals (several micrometers in size) in the Op regions

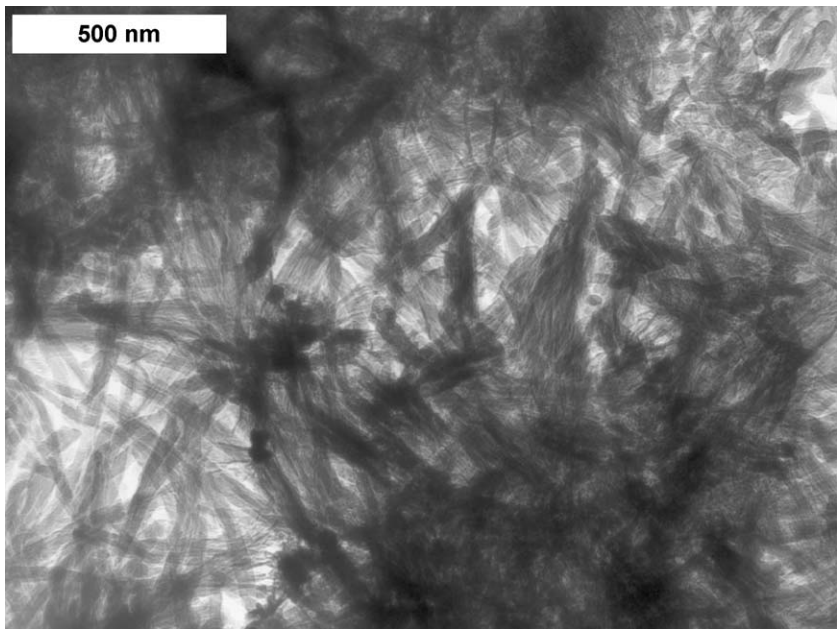


Fig. 10. A TEM micrograph showing coarse Op C-S-H present in a hardened β-$C_2S$ paste with w/c = 0.4 hydrated at 20 °C for 3 months.

of hardened pastes of $C_3S$, β-$C_2S$, and PC hydrated at around 20 °C. It is also commonly observed in the Ip of PC pastes. Whilst large crystals of CH also occur in pastes hydrated at elevated temperatures, microcrystalline CH is also present. Fig. 13(a) shows an example of CH microcrystals (which appear dark where they are oriented such that they Bragg-reflect electrons strongly and are blocked by the objective aperture in a bright field image) intermixed with C-S-H in a white PC hydrated at 80 °C; Fig. 13(b) shows an enlargement of part of the region and Fig. 13(c) shows a typical SAED.

*3.2.2. C-S-H in water-activated hardened pastes of PC blended with different amounts of blast-furnace slag*

(i) *Inner product.* As the fraction of slag increases the chemical composition of Ip C-S-H that forms from the reaction of reasonably large grains of alite changes: the mean Ca/Si ratio decreases whilst the mean Al/Ca increases [30]. However, it nevertheless retains the typical compact, fine-scale, and homogeneous morphology. The C-S-H present in small fully reacted grains has a different morphology, which is discussed in Section 3.2.6. An example for a 50% slag blend (hydrated at 25 °C for 3 weeks; w/s = 0.4) is shown on the right of Fig. 14(a), with an enlargement of part of the region shown in Fig. 14(b); the globules of C-S-H appear to be around 4–8 nm in diameter. C-S-H present in the Ip of reacted slag grains has a similar chemical composition, but it is intermixed on a range of scales with a hydrotalcite-type phase [30].

(ii) *Outer product.* The morphology of Op C-S-H is dependent on its chemical composition, which is determined by the amount of slag in the blend. Whilst some micrographs demonstrating the change in morphology that occurs on increasing the slag fraction have

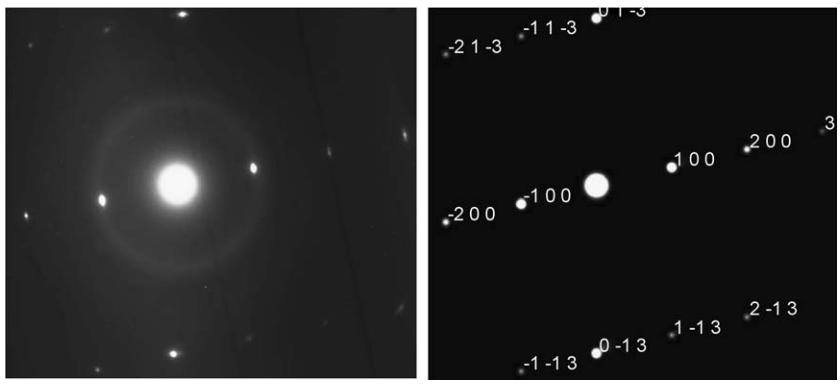


Fig. 11. SAED pattern for an area in a hardened paste of ordinary PC (hydrated for 12 months at 20 °C; w/c = 0.4) showing a C-S-H 'halo' superimposed on a [031] zone axis pattern for CH (calculated pattern shown on the right).

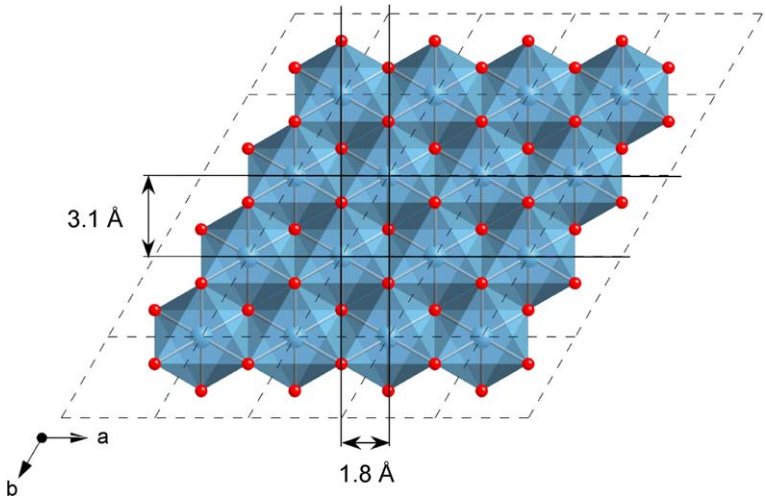


Fig. 12. A single layer of CH structure (SG = $P-3\ m\ 1$; $a = b = 3.593$ Å; $c = 4.909$ Å) illustrating the 3.1 ($= b \sin(60)$) and 1.8 ($= a/2$) Å repeat distances.

been published [22,23,29,30], additional examples are included here for the specific purpose of relating this change to possible changes in the nanostructure of C-S-H. These micrographs are at the same magnifications—including enlargements—as those discussed in Section 3.2.1 to facilitate comparison between the different systems, and thus the different chemical compositions. Figs. 14–17 show Op C-S-H present in blends with 50%, 75%, 90%, and 100% slag, respectively. The compositional data in Fig. 3 correspond to Figs. 14 (○) and 16 (△). The Op C-S-H in neat $C_3S$ pastes is, as discussed above, fibrillar; the fibrils are often quite coarse and appear to consist of agglomerations of long thin particles, approximately 3 nm in their smallest dimension. Coarse fibrils are generally less evident in neat PC pastes, the C-S-H generally having a finer morphology, which nevertheless retains a linear directional aspect (described as 'fine fibrillar'). This morphology is broadly maintained as the mean Ca/Si ratio of the C-S-H decreases from a mean value of about 1.75 in neat PC pastes to about 1.5 in pastes with 50% slag; the latter also contains a significant amount of Al (Al/Ca ≈ 0.07 to 0.10) (see Ref. [30] and Fig. 3). An example for a 50% slag blend is shown on the left of Fig. 14. Fig. 14(c) shows an enlargement of an area of this Op C-S-H; it still appears to consist of agglomerations of long thin particles, but in this case, they are perhaps thicker (say 3–6 nm) than in Fig. 6(c). The morphology of Op C-S-H changes more noticeably with further increases in the proportion of slag in the paste. Fig. 15 shows an example for a paste containing 75% slag where the mean Ca/Si ratio is 1.34 (and Al/Ca = 0.13) [30]. Much of the Op C-S-H in this micrograph retains a very linear, directional character, but it now seems to have a likeness to fanned-out crêpe paper (a description first used by Copeland and Schulz in 1962 [41]); other areas—for example on the left of Fig. 15(a), have lost the linear aspect. Examples of Op C-S-H present in a blend containing 90% slag (mean Ca/Si = 1.26 and Al/Ca = 0.14) and in a neat water-activated slag paste (mean Ca/Si = 1.18 and Al/Ca = 0.19) are shown in Figs. 16 and 17, respectively. The Op C-S-H in these two pastes has the appearance of crumpled sheet-like foils. Comparison of the Op C-S-H morphologies shown in Figs. 6(c), 14(c), 15(b), 16(b), and 17(b) suggests strongly that as the mean Ca/Si ratio decreases (and the Al/Ca ratio increases) a transition occurs from essentially one- to two-dimensional growth; i.e., long thin particles to thin foils.

(iii) *Structural order.* SAED patterns of Op C-S-H in water-activated slag–PC blends show only a diffuse ring ranging between about 3.2 and 2.7 Å, and occasionally a faint ring at around 1.8 Å, regardless of chemical composition.

### 3.2.3. C-S-H in alkali-activated blast-furnace slag pastes

(i) *Inner product.* The Ip of hydrated slag grains in KOH- or NaOH-activated slag pastes is very similar to that formed in water-activated slag–PC blends. Again, it consists of a hydrotalcite-type phase mixed over a range of scales with C-S-H that has a similar composition to the Op C-S-H in the same paste [33,42]. An example is shown in Fig. 18(a) (left centre and upper right) with an enlargement of part of one of the regions shown in Fig. 18(b) (slag activated with 5 M KOH and hydrated for 8 years at 20 °C; s/s = 0.4). The laths or platelets present in the Ip—which are quite small in this example—are the hydrotalcite-type phase. The fine scale intermixing of the hydrotalcite-type phase and the Al-substituted C-S-H might be due to a strong attraction between their oppositely charged main layers [43].

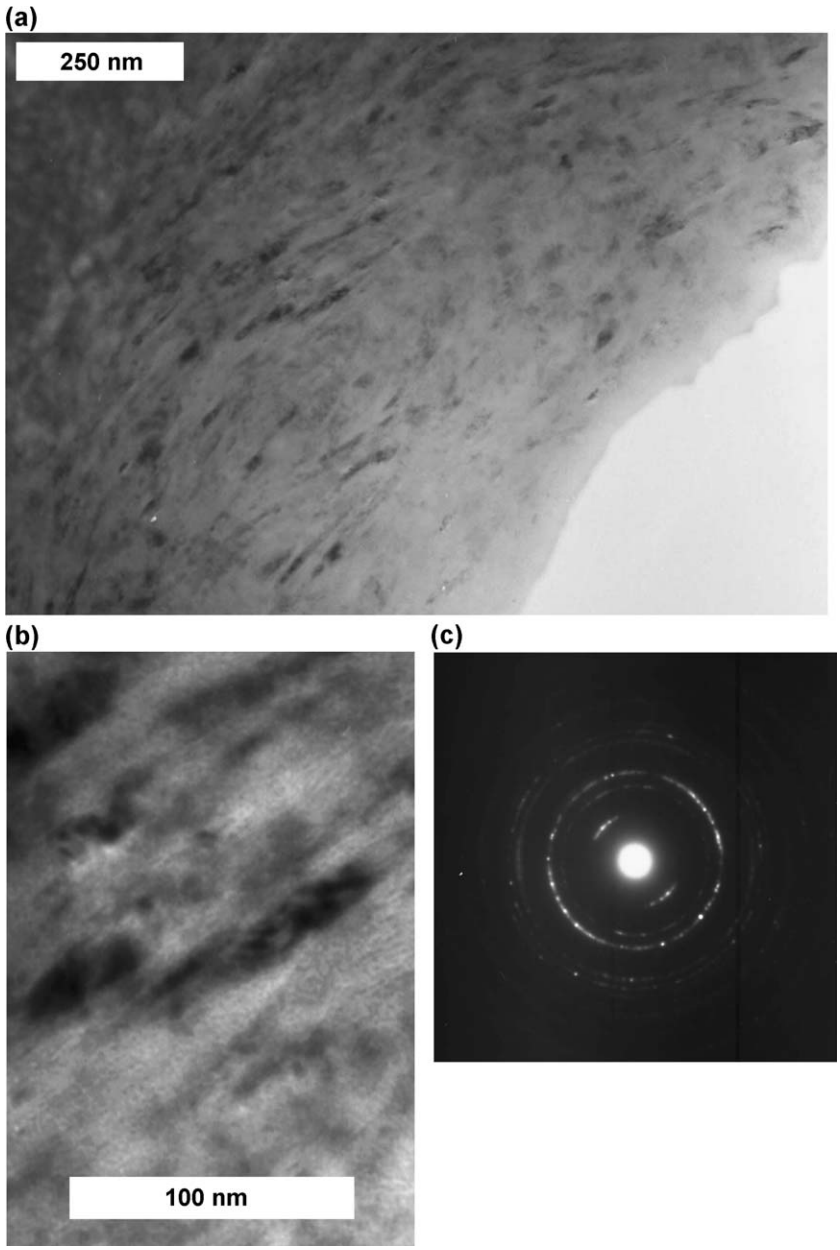


Fig. 13. (a) A TEM micrograph showing microcrystalline CH present in a hardened white PC paste with w/c = 0.4 hydrated at 80 °C for 19 days. (b) An enlargement of a region in (a). (c) SAED pattern for an area in (a) showing reflections characteristic of microcrystalline CH.

(ii) *Outer product.* The morphology of the Op C-S-H present in KOH- or NaOH-activated slag pastes is, like that in the neat water-activated slag paste, foil-like, but the foils tend to be less crumpled, which suggests a greater degree of structural order. An example is shown in the central region of Fig. 18(a) with an enlargement of part of the region shown in Fig. 18(c). The Op C-S-H in this paste had a mean Ca/Si = 0.99 and Al/Ca = 0.20.

(iii) *Structural order.* As suggested by its morphology, the C-S-H in an alkali hydroxide-activated slag is indeed structurally better ordered than in a water-activated slag paste. SAED patterns of Op C-S-H in KOH- or NaOH-activated slag pastes show ring patterns corresponding to C-S-H (I), which is structurally related to 14 Å tobermorite; the peaks at 3.07, 2.80, and 1.83 Å represent the three shortest repeat distances in the plane of a distorted CH layer [40]. An example of a pattern is given in Ref. [33]; the layer spacing in the example was smaller than detected by powder XRD due to drying during sample preparation and/or examination in the electron microscope. C-S-H (I) synthesized in the laboratory has been observed by TEM to have a foil-like morphology [44]. Since the C-S-H in Fig. 18 has structural order intermediate between that in the water-activated neat slag paste

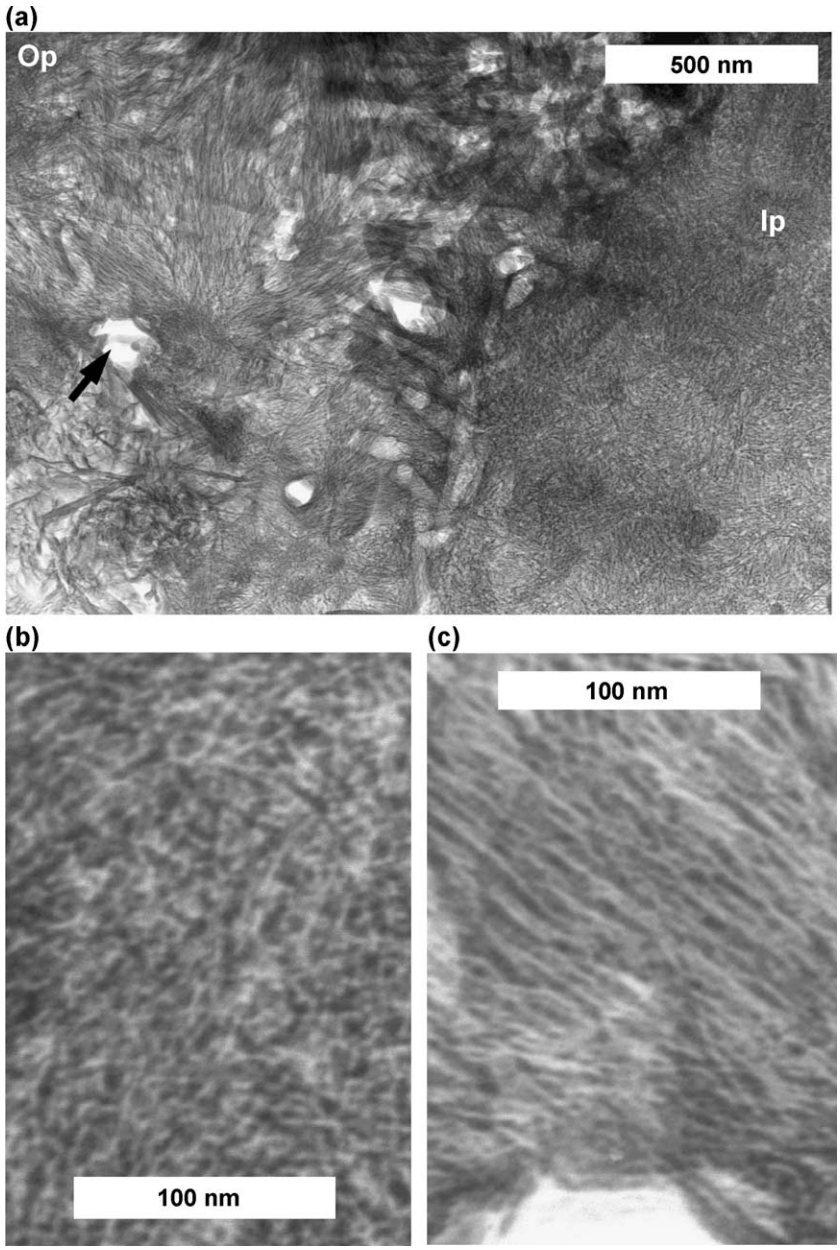


Fig. 14. (a) A TEM micrograph showing Ip and Op C-S-H present in a hardened white PC-50% GGBS paste with w/s = 0.4 hydrated at 25 °C for 3 weeks; the Ip is on the right of the micrograph. A black arrow indicates the location of a relict of AFt; there are number of others in the micrograph. (b) An enlargement of a region of Ip C-S-H. (c) An enlargement of a region of Op C-S-H. Experimental details are given in Ref. [31].

(Fig. 17) and crystalline tobermorite, crystals of the latter are shown at the same magnifications in Fig. 19 for comparison with the other micrographs.

*3.2.4. C-S-H in alkali hydroxide-activated hardened pastes of PC blended with different amounts of blast-furnace slag*

(i) *Inner product.* The Ip C-S-H that forms from the reaction of reasonably large grains of alite in KOH-activated slag–PC blends has the typical compact, fine-scale, and homogeneous morphology, regardless of the amount of slag in the paste. The Ip in hydrated slag grains is very similar to that formed in water-activated slag–PC blends. Again, it consists of a hydrotalcite-type phase mixed over a range of scales with C-S-H that has a similar composition to the Op C-S-H in the same paste. An example is shown on the right of Fig. 20(a) for a blend with 90% slag (activated with 5 M KOH solution and hydrated at 25 °C for 3 days; s/s = 0.4); Fig. 20(b) shows an enlargement of part of the region. Again, the laths or platelets present in the Ip are the hydrotalcite-type phase.

(ii) *Outer product.* The morphology of the Op C-S-H present in KOH-activated slag–PC blends is gener-

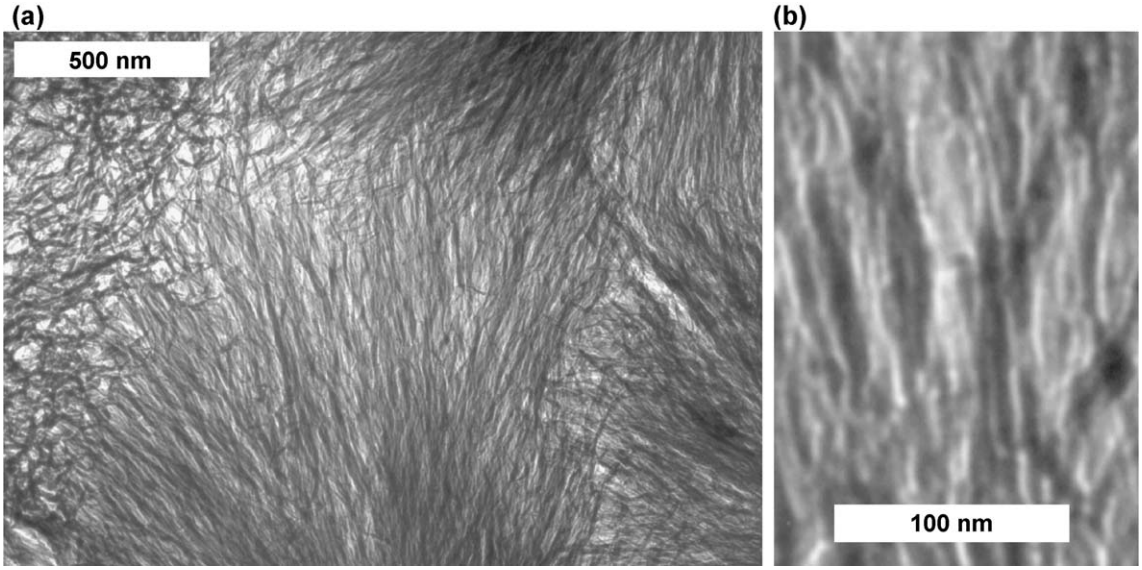


Fig. 15. (a) A TEM micrograph showing Op C-S-H present in a hardened ordinary PC-75% GGBS paste with w/s = 0.4 hydrated at 20 °C for 14 months. (b) An enlargement of a region of Op C-S-H. Experimental details are given in Ref. [30].

ally foil-like, regardless of the amount of slag in the paste; it is foil-like at low and high Ca/Si ratio. An example for a high-slag blend is shown on the left of Fig. 20(a) with an enlargement of part of the region shown in Fig. 20(c). The Op C-S-H in this paste had a mean Ca/Si = 1.14 and Al/Ca = 0.17 [31]. An example for a neat PC paste is shown on the lower right of Fig. 21(a), which is a modification of Fig. 5 of Ref. [31]; an enlargement of part of the region is shown in Fig. 21(b). The Op C-S-H in this paste had a mean Ca/Si = 1.69 and Al/Ca = 0.04, which is essentially the same as in water-activated pastes where the C-S-H has a fibrillar morphology. Op C-S-H also occurs as lath-like features, which often have lines of contrast running along them that readily coarsen in the electron beam (due to the formation of gaseous products), suggestive of a basal plane perpendicular to the plane of the page. An example for a low Ca system is indicated on Fig. 20(a) by a white arrow.

(iii) *Structural order.* Again, as suggested by its morphology, the C-S-H in alkali hydroxide-activated slag–PC blends is structurally better ordered than in water-activated pastes. XRD and SAED data are consistent with C-S-H (I). This is true at both low and high Ca/Si ratio.

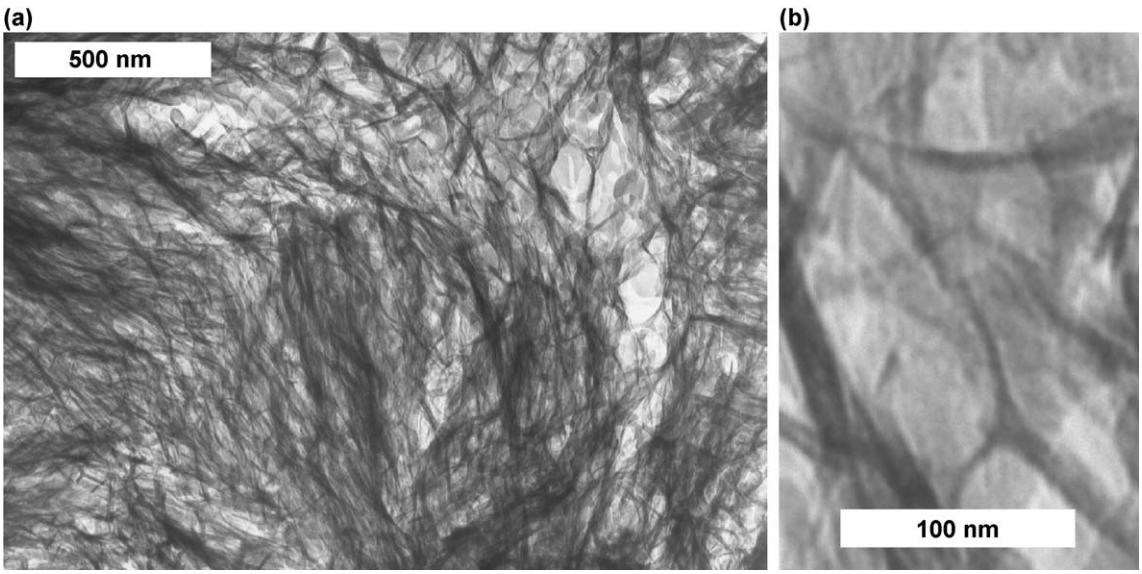


Fig. 16. (a) A TEM micrograph showing Op C-S-H present in a hardened white PC-90% GGBS paste with w/s = 0.4 hydrated at 25 °C for 3 weeks. (b) An enlargement of a region of Op C-S-H. Experimental details are given in Ref. [31].

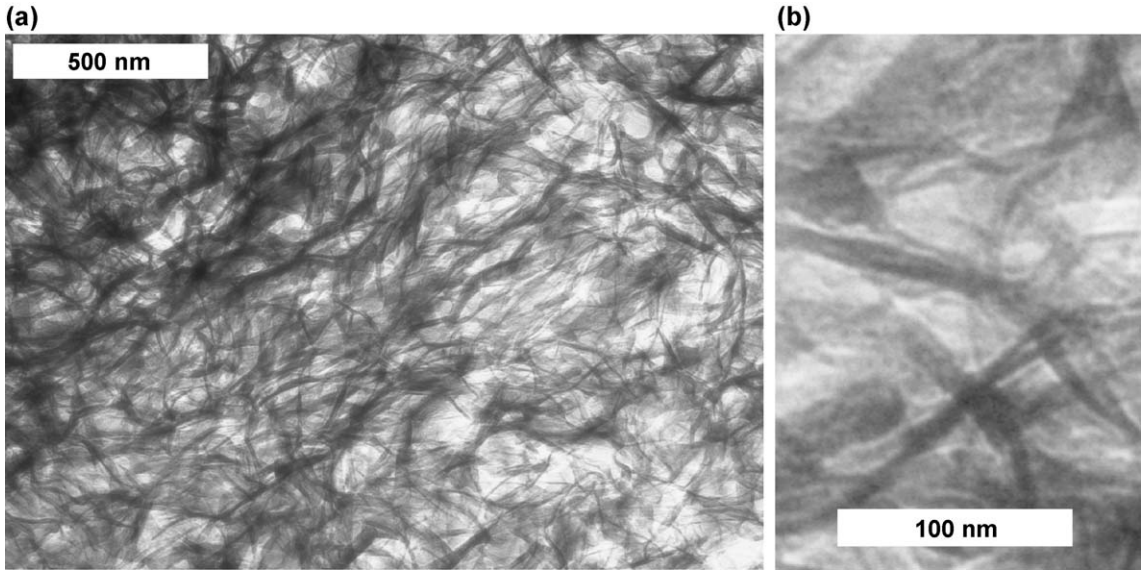


Fig. 17. (a) A TEM micrograph showing Op C-S-H present in a hardened neat GGBS paste with w/s = 0.4 hydrated at 40 °C for 3.5 years. (b) An enlargement of a region of Op C-S-H. Experimental details are given in Ref. [30].

(iv) *Calcium hydroxide.* CH is generally microcrystalline and occurs interstratified with C-S-H at the nanometer scale; the regions can extend over many micrometers. An example is shown in the top/left/centre of Fig. 21(a), with an enlargement of part of the region in Fig. 21(c). A typical SAED pattern is given in Ref. [31], which is obviously similar to that shown in Fig. 13(c), and CH peaks on powder XRD patterns are broader than with water activation, consistent with the smaller crystal size.

### 3.2.5. C-S-H in alkali hydroxide-activated hardened pastes of PC blended with 20% metakaolin

The morphology of the Op C-S-H present in a KOH-activated 20% metakaolin–PC blend is foil-like; micrographs are reported elsewhere [45]. TEM analyses for the blend are shown on Fig. 5.

### 3.2.6. C-S-H in small fully hydrated particles

TEM of ion-thinned sections has shown that the hydrated remains of relatively small particles—whether of PC, slag, or fly ash—contain a less dense product with substantial porosity, surrounded by a zone of relatively dense C-S-H [23,28,30,46]. An example from a PC paste, which is a modified version of Fig. 3 in Richardson and Groves [28], is shown in Fig. 22(a). The boundary between Ip and Op is well defined (indicated by the white arrows). The Ip C-S-H is clearly less dense than that present in larger grains, as is readily noted on comparison with Fig. 7. Indeed its morphology is quite similar to the fine foil-like Op C-S-H present in neat water-activated slag pastes, which has low Ca/Si ratio; an example for comparison is shown in Fig. 22(b).

### 3.2.7. C-S-H in carbonated PC pastes

When $C_3S$ or neat PC pastes undergo relatively gentle carbonation, the C-S-H is progressively decalcified and the spaces between the fibrils of Op C-S-H are filled with microcrystals of calcium carbonate [47,48]. The fibrillar morphology of the Op C-S-H is strikingly well preserved, as illustrated in Fig. 23(a), which is a modification of Fig. 2 of Ref. [48]. The C-S-H in this particular paste was only partially decalcified—the Ip C-S-H had a mean Ca/Si of 1.41—and the Op C-S-H still appears to consist of agglomerations of long thin particles; compare for example Fig. 23(b) with Fig. 14(c), which has a similar Ca/Si ratio. As carbonation proceeds and the C-S-H is decalcified further, the long thin particles are broken up, ultimately resulting in microporous silica. Compare, for example, Fig. 23(a) with Fig. 3 in Ref. [49]. This striking preservation of Op C-S-H morphology upon carbonation strongly supports the view—as does TEM of replicas (see discussion in Ref. [22])—that it is a genuine feature and not an artefact introduced by specimen preparation.

## 3.3. (Alumino)silicate anion structure

Any model for the structure of C-S-H must be able to account for experimental observations on the nature of its (alumino)silicate anions; it must account for the following:

(i) *Sequence of (alumino)silicate chain lengths.* Evidence from solid-state NMR spectroscopy [50–52] and TMS-GPC [24,53–55] have shown that the C-S-H that is formed during the first day of hydration of $C_3S$ or neat PC contains mostly dimeric silicate units (the end of the induction period is associated with the

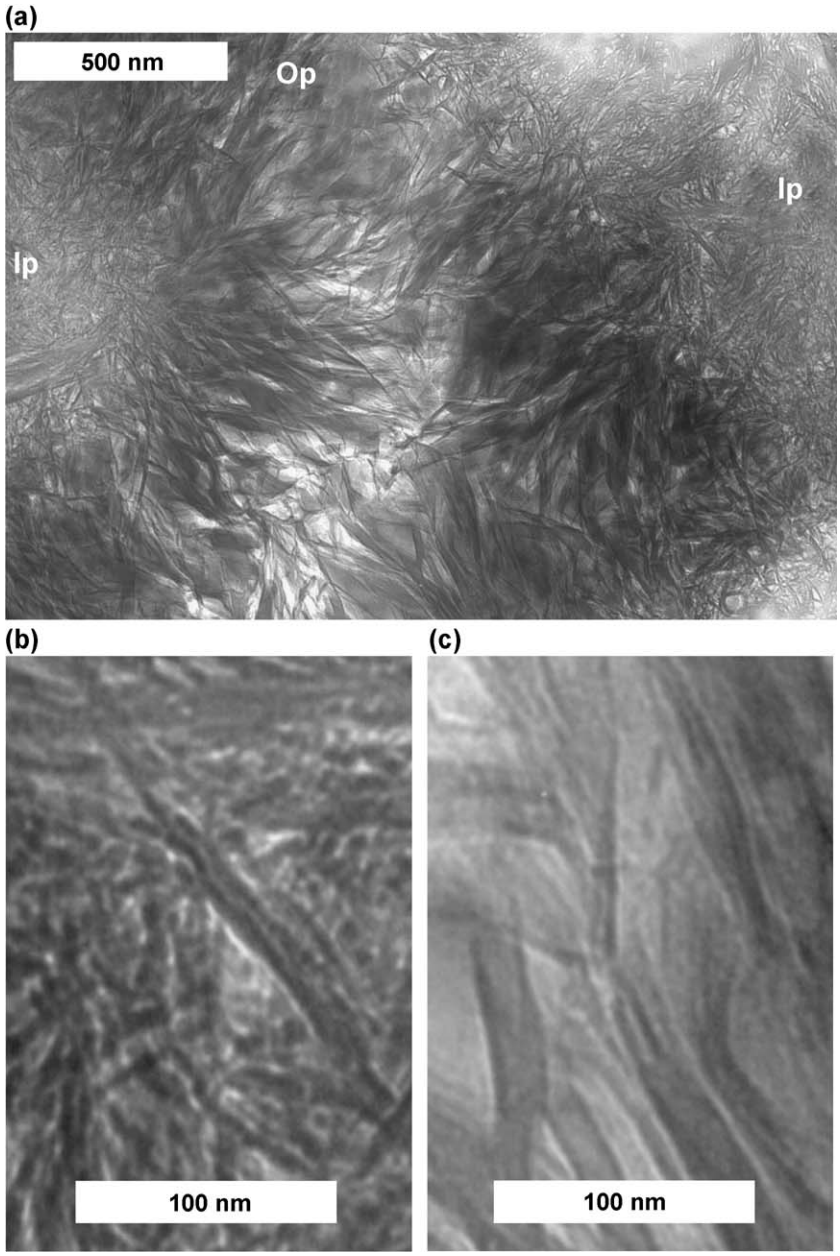


Fig. 18. (a) A TEM micrograph showing Ip and Op C-S-H present in a 5-M KOH-activated GGBS paste with s/s = 0.4 hydrated at 20 °C for 8 years. (b) An enlargement of a region of Ip C-S-H showing laths of a Mg,Al-rich phase intermixed with C-S-H. (c) An enlargement of a region of Op C-S-H. Experimental details are given in Ref. [33].

onset of the formation of dimer) and the TMS has shown that the C-S-H formed subsequently consists of both dimeric and higher polymeric species. The polymeric species are mainly linear pentamer and octamer, thus suggesting a 2, 5, 8...$(3n-1)$ chain length sequence, where $n$ is integer for individual structural units; $n$ would of course be noninteger for mixtures of units of different lengths. At greater ages, polymeric units form at the expense of existing dimer (dimer peaking at about 6 months), but dimer remains at $\approx 40\%$ when reaction is essentially complete [24,54,56], and even after ageing for 20–30 years [54]. The polymer fraction in very mature samples still contains pentamer and octamer in substantial amounts but larger anions, containing tens of tetrahedra, are also present [54]. NMR and TMS-GPC have shown that in systems where there is significant substitution of Al for Si the 2, 5, 8...$(3n-1)$ chain length sequence is maintained and the $Al^{3+}$ substitutes for $Si^{4+}$ in the bridging tetrahedra of dreierkette chains [23,57,58]. This point is confirmed by the observation that dimer is still the main species detected by TMS-GPC: since TMS only probes the silicate portion of aluminosilicate anions

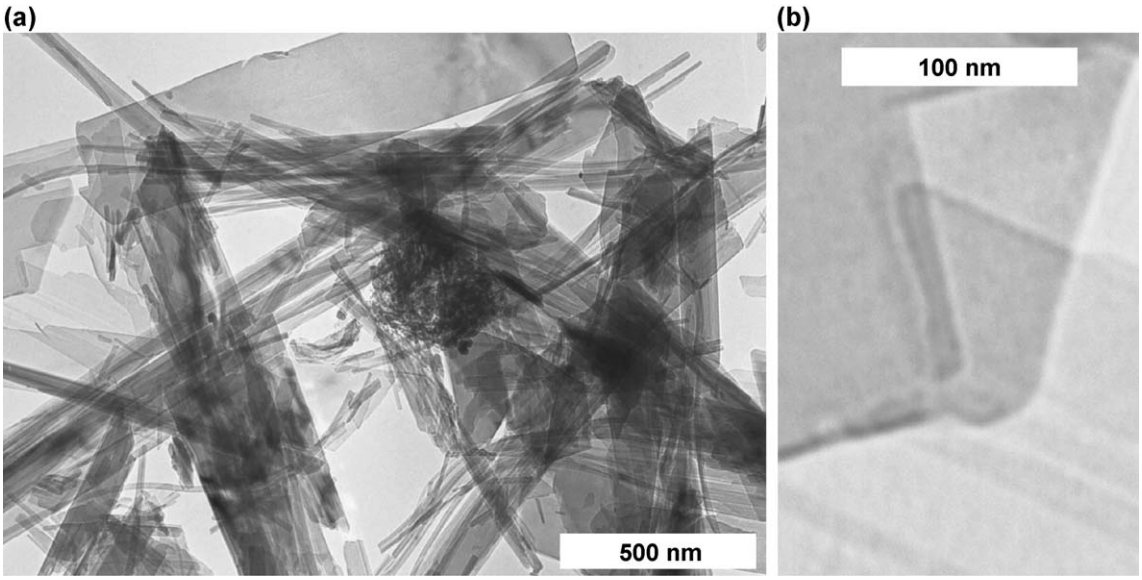


Fig. 19. (a) A TEM micrograph showing crystals of tobermorite. (b) An enlargement of overlapping crystals of tobermorite.

substitution of Al into paired tetrahedra would result in enhanced amounts of trimer and tetramer, which is not observed.

(ii) *Mean (alumino)silicate chain lengths.* In $C_3S$, β-$C_2S$, and neat PC pastes, there is only a gradual increase in the mean silicate chain length (MCL) with hydration time: for example, Rodger [59] and Rodger et al. [60] reported increases over 12 months from 2 to 2.7 for a β-$C_2S$ paste, 2 to 3.3 for a $C_3S$ paste, and 2 to 3.1 for a neat PC paste. Even after 26 years, the MCL for C-S-H in a $C_3S$ paste is less than 5 [50]. Maximum MCL and $Q^1/Q^2$ ratios[2] in hydrating $C_3S$ pastes have indicated that polymerization most probably occurs through the linking of dimers with monomers, in support of the $(3n-1)$ sequence of chain lengths observed by TMS [52]. Activation of $C_3S$ with KOH solution results in shorter chains than with water activation [61]. The MCL of C-S-H is longer in composite cements where the PC has been partially replaced by slag or a pozzolan. The following examples are discussed later in terms of models for the structure of C-S-H. Richardson and Groves [31] reported the MCL and Al/Si ratios calculated from $^{29}$Si NMR for C-S-H present in water-activated slag–PC blends [50% (○) and 90% (◇) slag] and KOH-activated slag–PC blends [50% (□) and 90% (◇) slag], and Love et al. [45] for C-S-H in a KOH-activated metakaolin–PC blend [20% (●) metakaolin]. The MCLs are 4.1 (○), 6.5 (△), 3.6 (□), 4.2 (◇), and about 18 (●), respectively. Analytical TEM data for the same pastes are reported in Figs. 3, 4, and 5 (only mean values were reported previously for the slag blends [31]). Note that the MCL are again less with alkali activation than with water. Long chains also develop in blends with high levels of amorphous silica; for example, the C-S-H formed in a $C_3S$–silica system with overall Ca/Si of 1.0 hydrated for 3 months at 40 °C (w/s = 0.7) had an MCL of 8 [62], and the C-S-H that formed in a PC–silica fume paste with >50% silica hydrated for 3 months at 40 °C (w/s = 0.7) had a mean Ca/Si ≈ 0.7 → 0.8 and MCL of 8.5 [63]. As noted in Section 3.2.7, relatively gentle carbonation of C-S-H results in decalcification; this reduction in Ca content is accompanied by an increase in MCL [48,64]. For example, Groves et al. [64] reported that a hardened $C_3S$ paste that had been carbonated for 2 months in air (at 72.6% relative humidity) contained a relatively homogeneous C-S-H with a mean Ca/Si ratio of 1.02; the MCL was 4.5—silica gel had not yet formed—which is longer than before it was carbonated. The MCL of the C-S-H in the sample represented by the micrograph in Fig. 23(a) was about 3.4, which is again longer than would be expected for an uncarbonated PC of similar age [25].

(iii) *Hydrated monomer.* Solid-state $^{29}$Si NMR techniques have shown that the product formed during the induction period of hydrating $C_3S$ contains exclusively hydrated monomeric silicate units ($Q^0$(H)) [60]. Hydrated monomer persists to high degrees of reaction at a level of ≈ 2% for curing at 20 °C and between 8% and 3% at 75 °C, depending on the degree of hydration [52,60]. The exact nature of this persistent $Q^0$(H) has yet to be established. Either it must be accounted for within the C-S-H or in some other way. Interestingly, there

[2] $Q^n$ ($0 \le n \le 4$). Q is a silicate tetrahedron and $n$ is the number of oxygen ions that bridge to adjacent tetrahedra; thus, $Q^0$ are isolated tetrahedra, $Q^1$ are chain-end groups, $Q^2$ middle groups, etc. Increased polymerization of the $Q^n$ building units causes characteristic up-field chemical shifts on $^{29}$Si NMR spectra. In aluminosilicates, the shifts are further influenced by the replacement of Si by Al; there are 15 possible $Q^n$(mAl) structural units where $n = 0-4$ and $m = 0-n$.

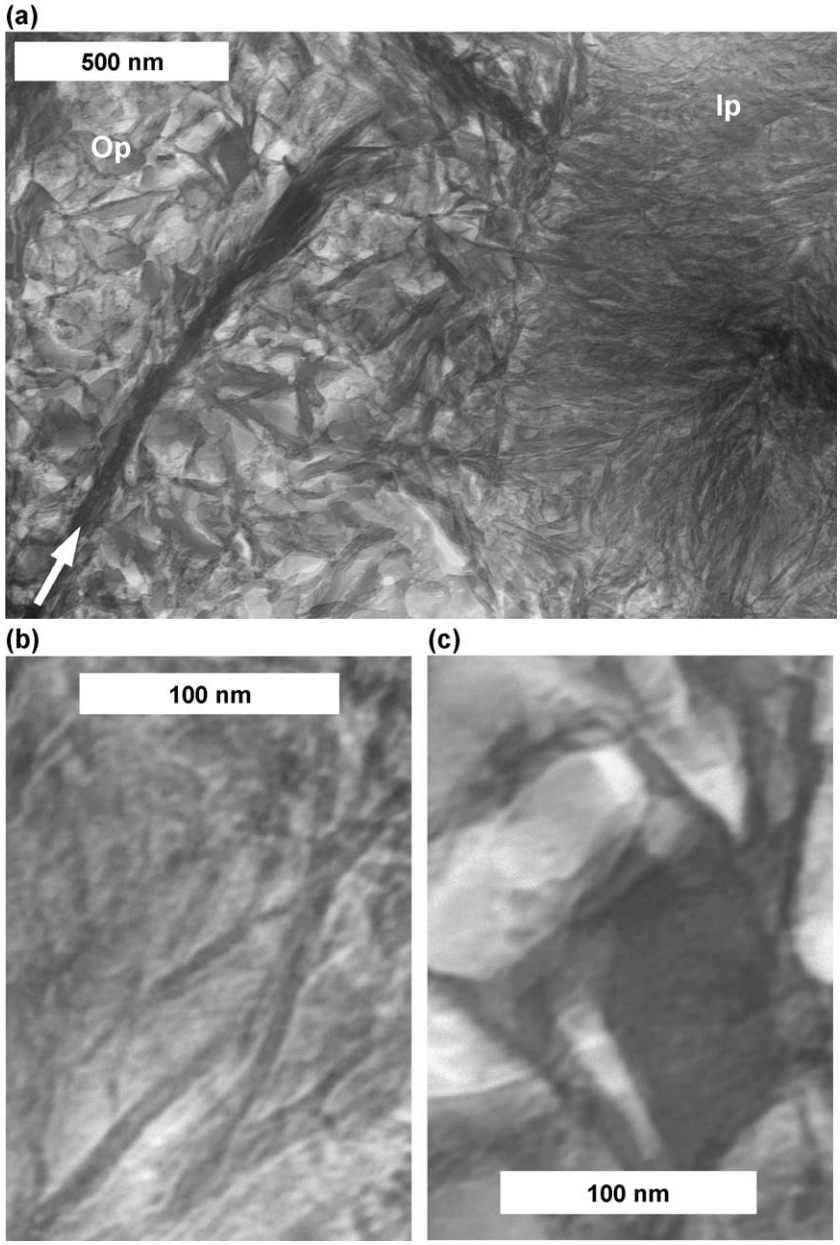


Fig. 20. (a) A TEM micrograph showing Ip and Op C-S-H present in a hardened 5-M KOH-activated white PC-90% GGBS paste with s/s = 0.4 hydrated at 25 °C for 3 days; the Ip is on the right of the micrograph. (b) An enlargement of a region of Ip showing laths of a Mg,Al-rich phase intermixed with C-S-H. (c) An enlargement of a region of Op C-S-H. Experimental details are given in Ref. [31].

does not appear to be very much, if any, $Q^0$(H) in KOH-activated $C_3S$ pastes (see Figs. 5 and 6 in Ref. [61]) or in water-activated slag–PC blends containing 90% slag (see Fig. 12 of Ref. [31], both of which have Op C-S-H with foil-like rather than fibrillar morphology.

## 4. Richardson and Groves' generalized model for the nanostructure of C-S-H

The following sections attempt to explain Richardson and Groves' model more clearly than previously [18,19] by the use of schematic diagrams; the model's applicability to the experimental data outlined in Section 3 is discussed.

### *4.1. C-S-H in hardened $C_3S$ or $\beta$-$C_2S$ pastes*

Richardson and Groves [18] proposed a generalized model that included formulations that could be interpreted from both the T/CH and T/J structural viewpoints. They started their discussion by giving the general form for a calcium silicate hydrate composed of isolated silicate chains of varying length and with a variable number of –OH

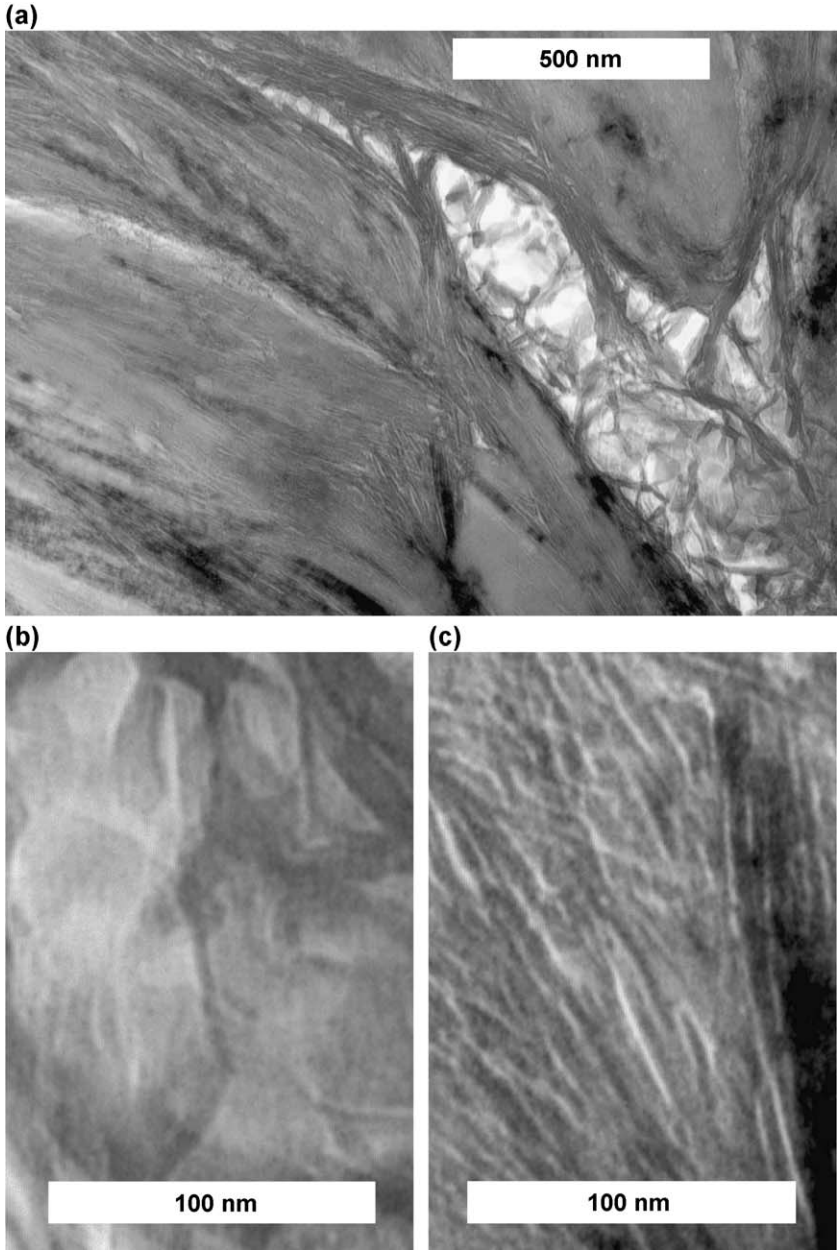


Fig. 21. (a) A TEM micrograph showing Op C-S-H and microcrystalline CH present in a hardened 5-M KOH-activated neat white PC paste with s/s = 0.5 hydrated at 25 °C for 5 months. (b) An enlargement of a region of crumpled-foil Op C-S-H. (c) An enlargement of a region of Op C-S-H interstratified with microcrystalline CH. Experimental details are given in Ref. [31].

groups attached to Si atoms, in 'solid solution' with a variable amount of $Ca(OH)_2$:

$$Ca_X H_{2(N+1-X)} Si_N O_{(3N+1)} \cdot z Ca(OH)_2 \cdot m H_2O \quad (1)$$

In this formula, $N$ is the mean length of the silicate chains, $X$ is the number of $Ca^{2+}$ ions necessary to charge-balance the silicate chains, $2(N+1-X)$ is the number of hydroxyl units attached to the chains, $z$ is the number of $Ca(OH)_2$ units in 'solid solution', and $m$ is the number of water molecules bound but not present as hydroxyl groups. They noted that the special case of this formula for dimer (the predominant form in young $C_3S$ or OPC pastes, as noted in Section 3.3), $N=2$, was the same as that given by Glasser et al. [65]. The model was then extended to account for the experimentally observed sequence of chain lengths, i.e., $3n-1$:

$$Ca_X H_{(6n-2X)} Si_{(3n-1)} O_{(9n-2)} \cdot z Ca(OH)_2 \cdot m H_2O \quad (2)$$

Formula (2)—the T/CH viewpoint—is essentially the polysilicate version of Glasser's compositional model for

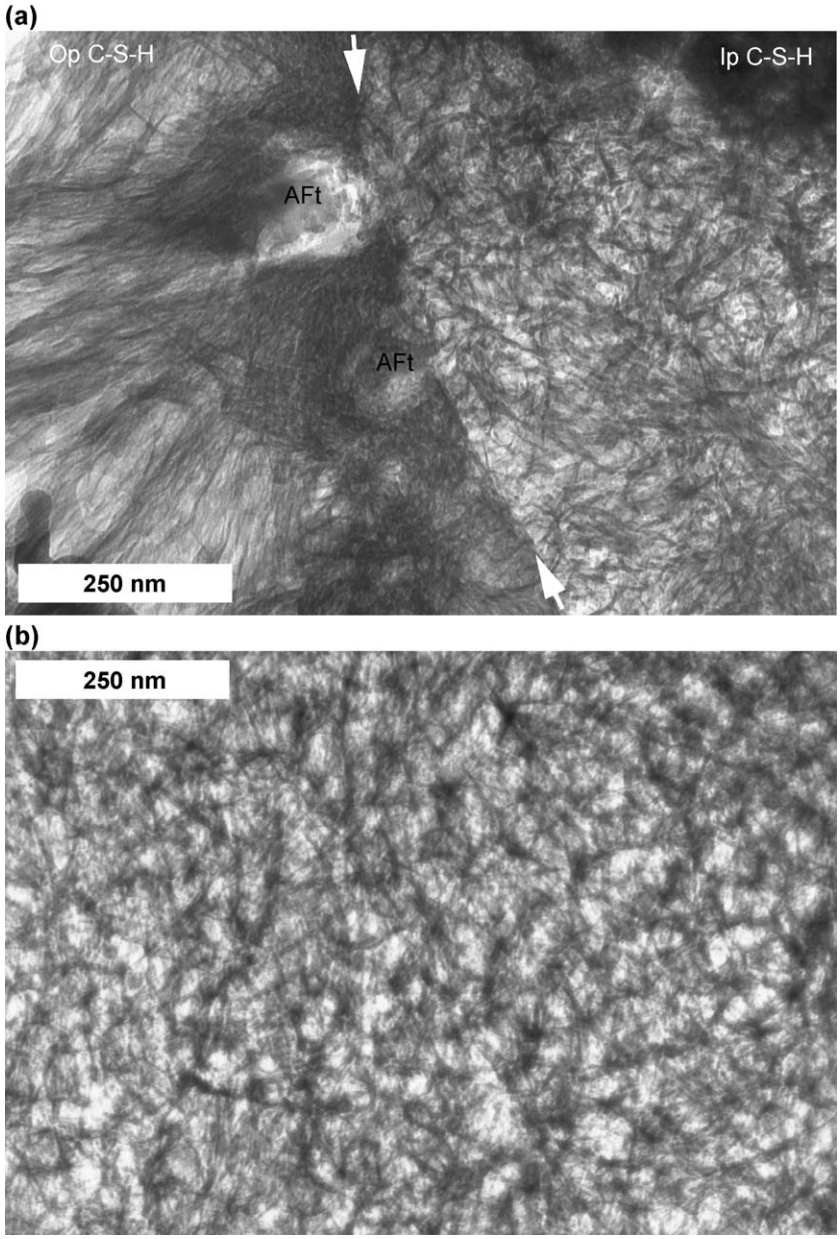


Fig. 22. (a) A TEM micrograph showing Ip C-S-H in a hardened PC paste (w/c = 0.4 hydrated at 20 °C for 1 week), which is typical of the product formed in relatively small grains; the Ip is less dense than that formed in larger grains (e.g., in Fig. 7) and is surrounded by a zone of relatively dense Op C-S-H (this figure is a modified version of Fig. 3 in Ref. [28]). (b) A TEM micrograph showing fine foil-like Op C-S-H present in a neat water-activated GGBS paste (w/s = 0.4 hydrated at 20 °C for 14 months), which has a morphology similar to the Ip in (a) but has a low Ca/Si ratio ( ≈ 1.1) rather than high ( ≈ 1.7–1.8). Experimental details are given in Ref. [30].

dimeric C-S-H. Richardson and Groves [18] gave an alternative formulation for their model:

$$\{Ca_{2n}H_wSi_{(3n-1)}O_{(9n-2)}\}\cdot(OH)_{w+n(y-2)}\cdot Ca_{\frac{ny}{2}}\cdot mH_2O \quad (3)$$

The number of silanol groups is given by $w$, and the degree of protonation of the silicate chains by $w/n$. The limiting values of the variables in these formulations, which are dictated by the requirement to maintain the layer structure and neutrality, are the following:

for $0\le y\le 2$, $\quad n(2-y)\le w\le 2n$

$2\le y\le 4$, $\quad 0\le w\le 2n$

$4\le y\le 6$, $\quad 0\le w\le n(6-y)$

and $X=\frac{1}{2}(6n-w)$

$z=\frac{1}{2}(w+n(y-2))$

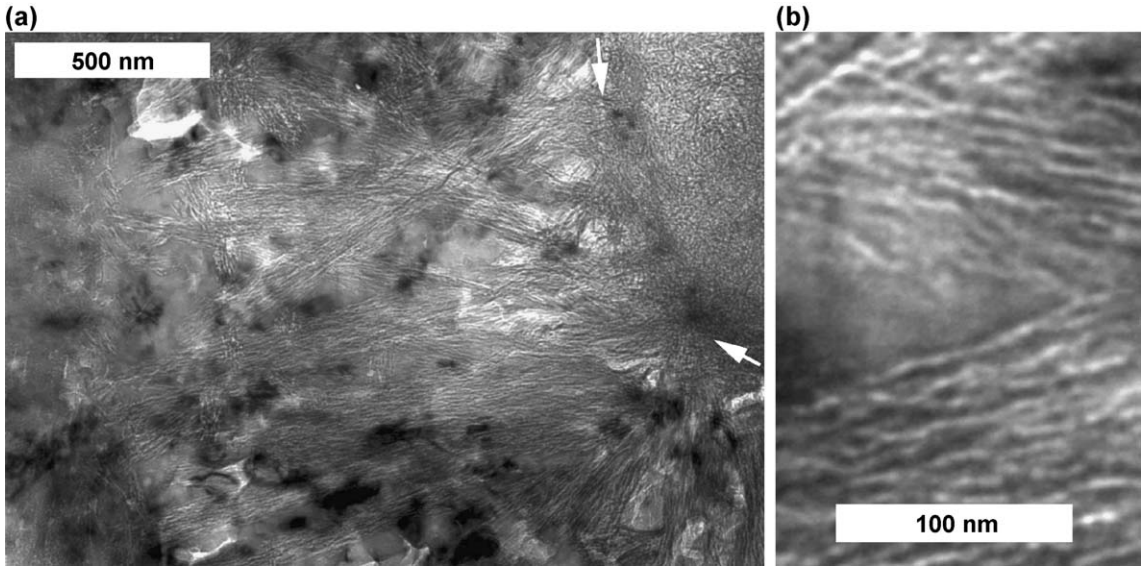


Fig. 23. (a) A TEM micrograph showing partially decalcified Op C-S-H and microcrystals of calcite in a carbonated white PC paste (this figure is a modified version of Fig. 2 in Ref. [48]). (b) An enlargement of a region of partially decalcified Op C-S-H.

The limits are illustrated graphically on Fig. 24. The Ca/Si ratio is given by

$$\mathrm{Ca/Si} = \frac{n(4+y)}{2(3n-1)} \tag{4}$$

On the T/CH viewpoint, the part of formula (3) contained within the braces is the tobermorite-like core. It consists of a highly disordered layer structure comprising finite silicate chains of mean length $3n-1$. Dimeric species ($n=1$) are linked during polymerization by bridging tetrahedra to form pentamer ($n=2$) and higher polymers, thus accounting for the experimentally observed sequence of silicate chain lengths (Section 3.3(i)). The $2n$ $Ca^{2+}$ ions within the braces are main layer $Ca^{2+}$ ions, and $n-(w/2)$ of the $(n{\cdot}y)/2$ $Ca^{2+}$ ions outside the braces are interlayer $Ca^{2+}$ ions required for charge-balance. The position of the remainder of the $(n{\cdot}y)/2$ $Ca^{2+}$ ions depends on the structural viewpoint adopted. On the T/CH viewpoint they occur in layers of CH sandwiched between silicate layers of tobermorite-like structure whilst on the T/J viewpoint they form part of the main layer of jennite-based structural units (as Si–O–Ca–OH). The structural units—and thus the parameters in the formulations—may vary from one region of the C-S-H to another thus accounting for the local variations in composition observed by TEM (Section 3.1). To aid this discussion, the structural units derived from either jennite or 1.4-nm tobermorite will be identified by the use of 'J' or 'T' as labels [18]. Hence, J2 and T2 correspond to dimeric structural units that result from omission of all bridging tetrahedra from jennite and

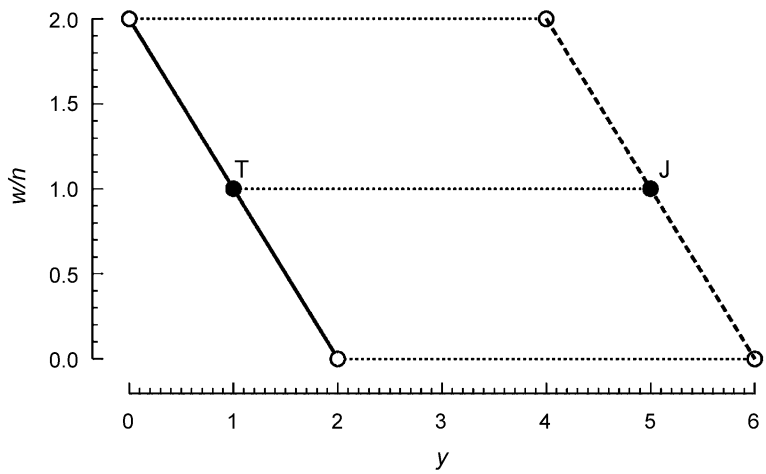


Fig. 24. The combinations of the degree of protonation, $w/n$, and $y$ that are possible in formula (3) whilst maintaining the layer structure and neutrality [18]. Taylor's [17] tobermorite-based structural units occur at T, and his jennite-based units at J.

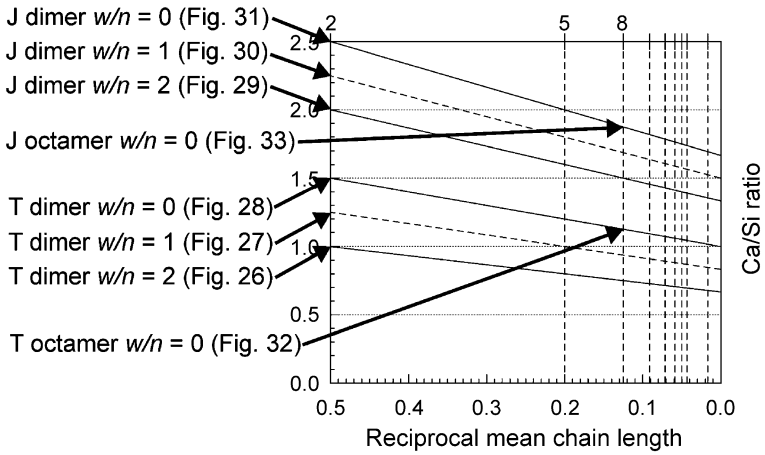


Fig. 25. Variation of Ca/Si ratio with mean chain length for structural units present in Richardson and Groves' model [18] with three different levels of protonation of the silicate chains: the minimum level ($w/n=0$), an intermediate level ($w/n=1$), which is equivalent to the units in Taylor's model [17], and the maximum level ($w/n=2$). The structures of the eight units that are labelled are illustrated in Figs. 26–33.

tobermorite, respectively, and J$\infty$ and T$\infty$ represent infinite chain lengths and so correspond to the crystalline phases themselves.

The degree of protonation of the silicate chains, $w/n$, is clearly flexible in the model: the line on Fig. 24 between $T^{w/n=2}$ and $T^{w/n=0}$ (O—O) represents tobermorite-based units, and, on the T/J viewpoint, the line between $J^{w/n=2}$ and $J^{w/n=0}$ (O- - - -O) represents jennite-based units. The effects of this flexibility in possible degree of protonation on the composition of the structural units is illustrated in Fig. 25, which shows the variation in Ca/Si ratio with the reciprocal of the MCL for structural units derived from both jennite (J) and 1.4 nm tobermorite (T), with the maximum, intermediate, and minimum levels of $w/n$ [18]. The compositional and structural details of a number of the units are outlined in greater detail in Figs. 26–33; the positions of these units are indicated in Fig. 25.

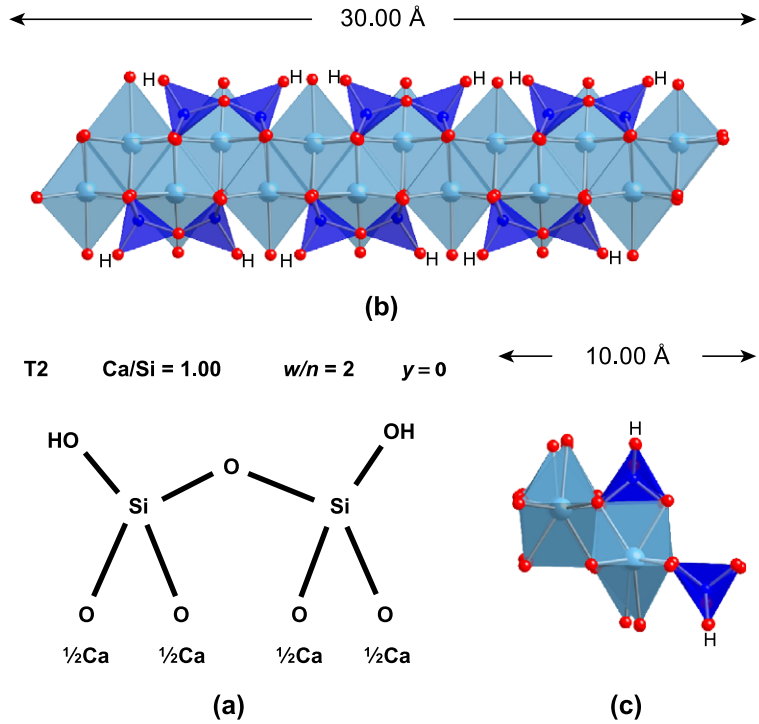


Fig. 26. Diagrams illustrating tobermorite-based dimer ($n=1$) that has the maximum degree of protonation of the silicate chains ($w/n=2$). (a) A highly schematic diagram demonstrating chemical accounting; the values of the variables in Richardson and Groves' model [18] are indicated. (b) and (c) show more realistic structural representations derived using crystal structure data for tobermorite [66–68] with the silicate chains either aligned along the plane of the page or perpendicular to the page (i.e., edge on).

Figs. 26–31 show highly schematic diagrams of tobermorite-based dimeric (Figs. 26(a), 27(a), and 28(a)) and jennite-based dimeric (Figs. 29(a), 30(a), and 31(a)) structural units with these three levels of protonation: the maximum level ($w/n=2$) in Figs. 26(a) and 29(a), an intermediate level ($w/n=1$) in Figs. 27(a) and 30(a), and the minimum level ($w/n=0$) in Figs. 28(a) and 31(a). The diagrams are purely for the purpose of demonstrating chemical accounting within the model and are not meant to represent accurately the actual arrangement of atoms in the structures: for example, the calcium atoms in the main layers of jennite or tobermorite are coordinated to six or seven oxygen atoms; these main layers are also of course very different in the two phases, as detailed in Figs. 1 and 2. The values of the variables $w/n$ and $y$ are included at the top of each of the schematic diagrams in Figs. 26–31, together with the Ca/Si ratio, which can vary between maximum and minimum values of 1.5 and 1.0 for T units, and 2.5 and 2.0 for J units. More realistic structural representations are shown in Figs. 26(b,c) Figs. 27(b,c) Figs. 28(b,c) Figs. 29(b,c) Figs. 30(b,c) Figs.31(b,c), which were derived using crystal structure data for tobermorite [66–68] and jaffeite [69]. Figs. 26(b)–31(b) show the silicate chains aligned along the plane of the page (one view for the T structures, two for the J), whilst Figs. 26(c)–31(c) show them perpendicular to the page (i.e., edge on).

Figs. 32 and 33 show similar schematic diagrams that illustrate the process of polymerization of the chains, in this case for chains with a minimum degree of protonation, i.e., $w/n=0$; Fig. 32 is for T- and Fig. 33 for J-based structures. In both cases, silicate monomers are inserted at bridging sites and the $Ca^{2+}$ ions that previously occupied those sites are displaced into the interlayer space; there is no change in the number of $Ca^{2+}$ ions, they are simply displaced. So, taking Fig. 32 as an example, six T-based dimers that have the composition and structure shown in Fig. 28, are polymerized to two octamers by the insertion of monomers at the four bridging sites, with the associated displacement of $Ca^{2+}$ ions into the interlayer. There is no change in $w/n$ or $y$, which in both cases are 0 and 2, respectively; polymerization simply involves an increase in $n$ from 1 to 3 (i.e., the MCL, $(3n-1)$, increases from 2 to 8). Substitution of $y=2$ and $n=1$ or 3 into Eq. (4) shows that the polymerization results in a decrease in the Ca/Si ratio from 1.5 for the dimer to 1.125 for octamer. The actual positions of the $Ca^{2+}$ ions that are displaced

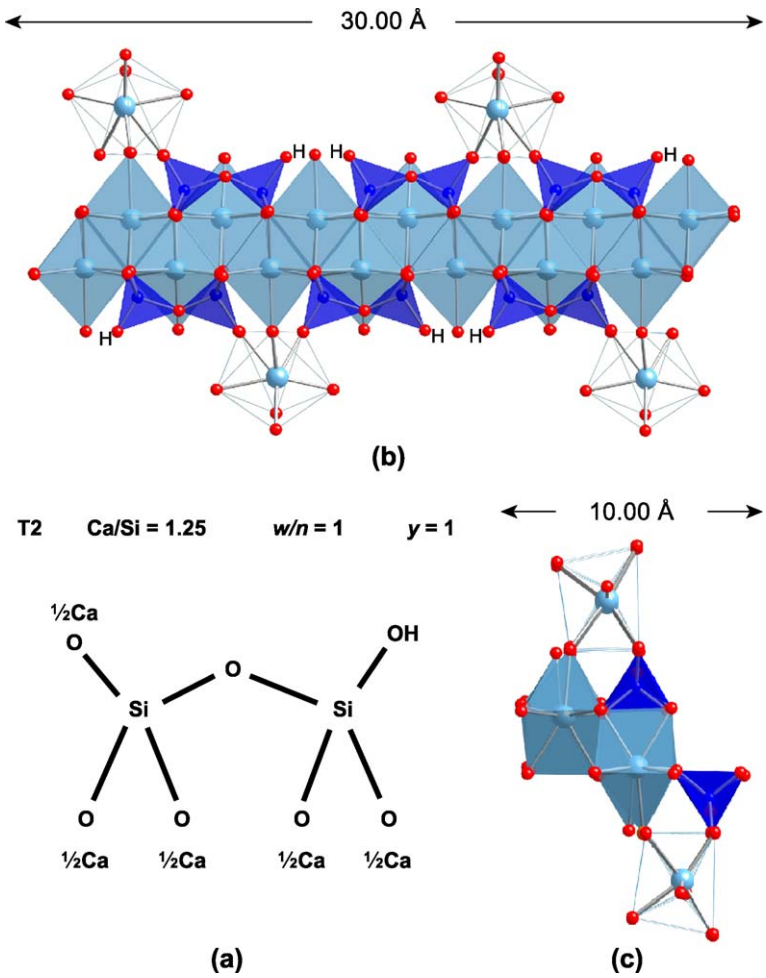


Fig. 27. As Fig. 26 but for an intermediate level of protonation of the silicate chains ($w/n=1$).

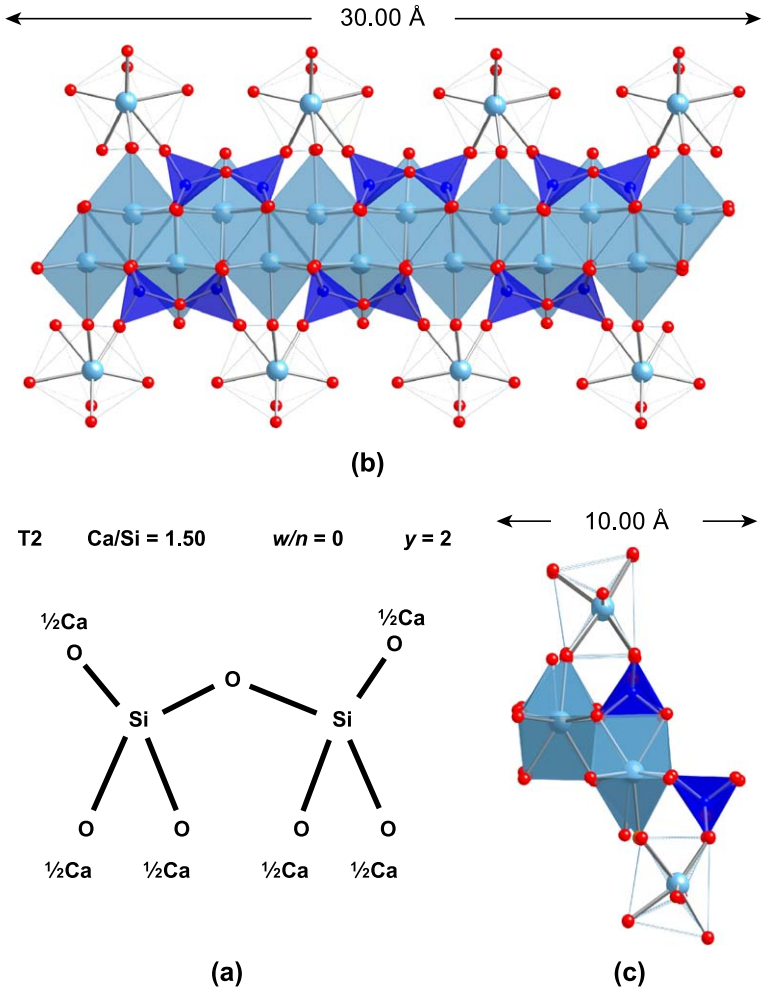


Fig. 28. As Fig. 26 but for the minimum degree of protonation of the silicate chains ($w/n = 0$).

from the bridging sites into the interlayer space (and the oxygen ions and water molecules to which they are coordinated) are of course likely to vary depending on the local environment. For example, two different positions in the J-type structure are shown in Figs. 33(a) and (b); these figures were derived from the structures of jennite [12,20] and metajennite [70], respectively, which of course have different layer spacings.

The smallest particles observed in the TEM micrographs discussed in Section 3 were in the Ip C-S-H of hardened $C_3S$ pastes that had been hydrated at elevated temperature (Fig. 9); they are about 3 nm in diameter. Figs. 34–36 are schematic diagrams showing different views of a particle of this approximate size. To keep the particle relatively straightforward it is entirely J dimer with the minimum degree of protonation. It is clear from these schematics that the number of structural elements present in one of these particles is not large, and that edge effects at the ends of the chains are therefore likely to have significant consequences. For example, monomeric silicate tetrahedra are present; the most easily noticed is in the top right-hand corner of Fig. 34. Chain-end edge effects would therefore seem to offer a reasonable explanation for the persistence of $Q^0$(H) species in hardened $C_3S$ pastes (see Section 3.3). The particle in Fig. 34 has a ratio of monomer to 'paired' tetrahedra of about 0.07. Calculations using Brough et al.'s data [52] for $C_3S$ pastes cured at 75 °C reveals a similar value at about 80% hydration, which corresponds to a similar age as the TEM specimen (which was hydrated at 80 °C). Interestingly, the same calculation using Brough et al's [52] 20 °C data gives a value of about 0.03 for a paste hydrated to 92%. This value would of course correspond to bigger or longer particles, if, as seems likely, this is the direction of chain growth. Bigger particles are consistent with the TEM evidence, which seems to show that the Ip particles in the 20 °C paste are perhaps 4–6 nm in diameter, rather than 3 nm in the 80 °C paste. More data are needed to assess whether the particles in the fibrils of Op C-S-H are shorter in the case of curing at elevated temperature. The apparently lower amount of $Q^0$(H) in KOH-activated $C_3S$ pastes would be consistent with the Op C-S-H having a foil-like morphology, which would presumably have far fewer chain-end

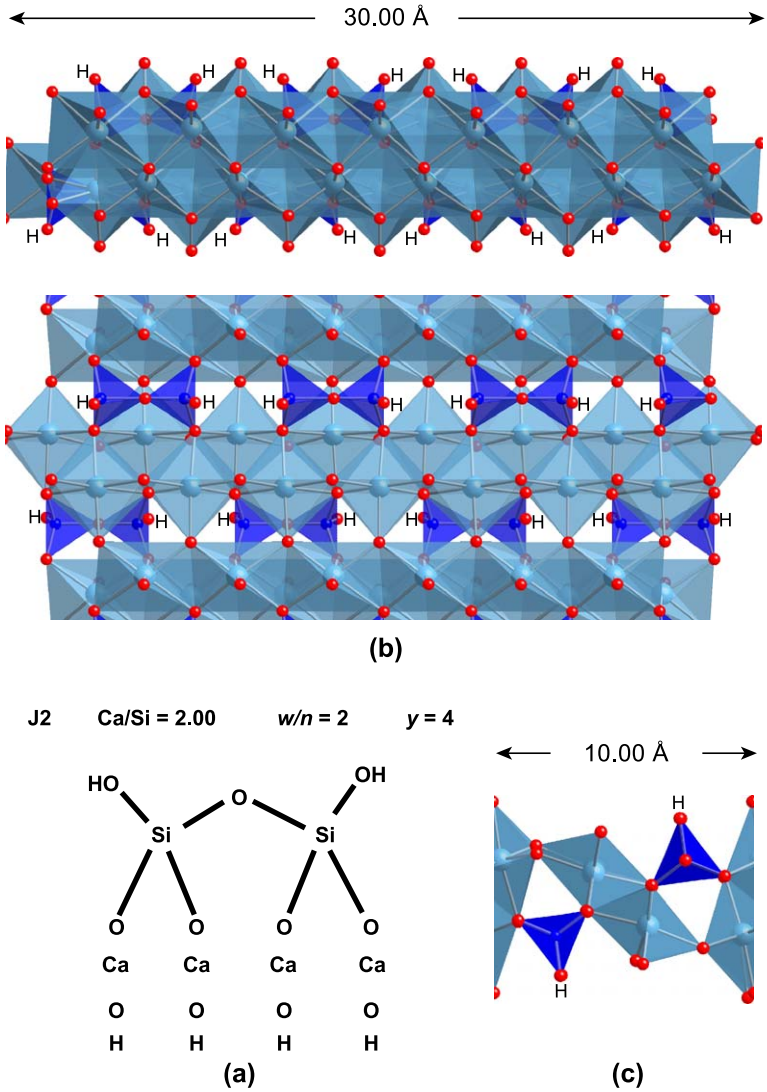


Fig. 29. Diagrams illustrating jennite-based dimer ($n=1$) that has the maximum degree of protonation of the silicate chains ($w/n=2$). (a) A highly schematic diagram demonstrating chemical accounting; the values of the variables in Richardson and Groves' model [18] are indicated. (b) and (c) show more realistic structural representations derived using crystal structure data for jaffeite [69] with the silicate chains either aligned along the plane of the page or perpendicular to the page (i.e., edge on).

edges than the particles in the fibrils of Op C-S-H present in water-activated pastes.

Figs. 35 and 36 show two additional views of the J dimer particle shown in Fig. 34, both as polyhedral (a) and space filling (b) models. The 3-nm size of the particle requires only two layers. In reality, the adjacent layers are quite probably not as close or aligned as shown; in this case, they are as close as they can get to one another and well-ordered, with Fig. 36(a) in particular betraying the model's origin (Ca-deficient jaffeite). Nevertheless, the figure raises an interesting point regarding the nature of polymerization in J-based particles. Fig. 37 shows the same projection as Fig. 36(a), but this time with bridging tetrahedra replacing $Ca^{2+}$ ions, which have been displaced. This figure is derived from a model structure for metajennite (unrefined) produced by Taylor [70], who used jaffeite as a starting point; the relationship between the two structures is clear from these two figures. It is equally clear that the displacement of $Ca^{2+}$ ions and insertion of silicate tetrahedra would be easier at the surfaces of the particle than within its interior. This point is reinforced by Fig. 38, which is the same projection but this time from jennite itself; in this case the main layers are much further apart. It seems quite plausible that in an early-age particle that consists entirely of J dimer (with some associated monomer due to chain-end edge effects), the main layers would be closer together than in crystalline jennite, and that the subsequent insertion of bridging tetrahedra would therefore be much easier at the particle's surfaces (those that are not chain-end surfaces). This is perhaps one reason why mean chain lengths do not get above five in $C_3S$ pastes hydrated at ambient temperatures, but can get longer at higher temperatures where a smaller

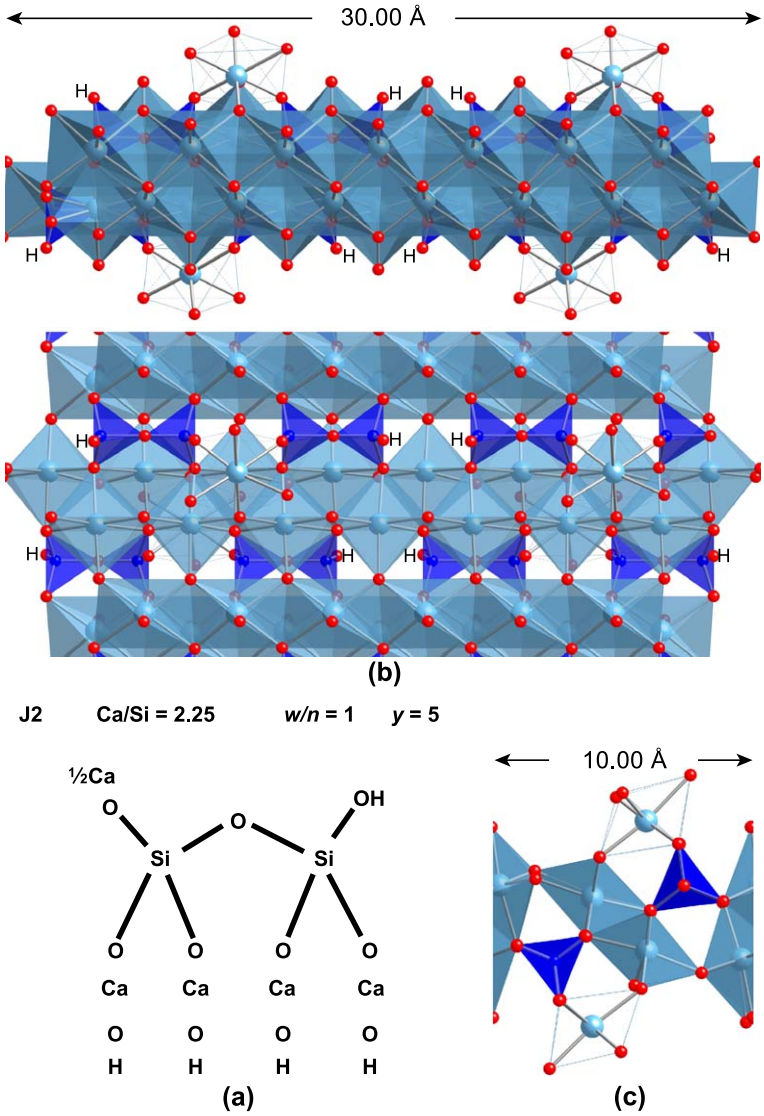


Fig. 30. As Fig. 29 but for an intermediate level of protonation of the silicate chains ($w/n = 1$).

proportion of the silicate chains are in the interior of particles (because the particles are smaller).

In many systems, both J- and T-type units are likely to be present, although the actual distribution between the two types is very flexible, depending on the Ca/Si ratio and hydroxyl water content. This point is illustrated in Fig. 39, which outlines how the distribution can be altered for a C-S-H of fixed MCL and Ca/Si ratio by varying the hydroxyl water content. The example has a Ca/Si ratio of 1.4 and a chain length of 5 (i.e., $n = 2$ and, from Eq. (4), $y = 3$). A pentamer has been chosen purely for simplicity of illustration: mixtures of structural units of different lengths would of course give noninteger mean chain lengths. The diagrams are highly schematic and again purely for the purpose of chemical accounting: each one really corresponds to a mixture of units that have either T- or J-based structure. So, with zero degree of protonation, $w/n = 0$, the mixture would be 25% J, 75% T; with $w/n = 1$ it would be 50% J 50% T; and with $w/n = 2$ it would be 75% J 25% T. It is also important to note that the J and T structural units would not necessary have the same degree of protonation, as implied in this illustration; indeed in real cement it is most likely that there would be variability. It is clear from Fig. 39 that for a given Ca/Si ratio and MCL the amount of hydroxyl water—which is defined by the variable $w$—is flexible within the limits imposed by the need to maintain the layer structure and neutrality: an increase in $w$ above its minimum value is compositionally equivalent to the addition of elements of $H_2O$, but structurally corresponds to increasing the number of –Ca–OH and Si–OH bonds at the expense of Si–O–Ca–O–Si.

Much useful information on the nature of the silicate chains can be obtained from solid-state $^{29}$Si NMR data; for example, if

$$q = \frac{Q^1}{Q^1 + Q^2} \tag{5}$$

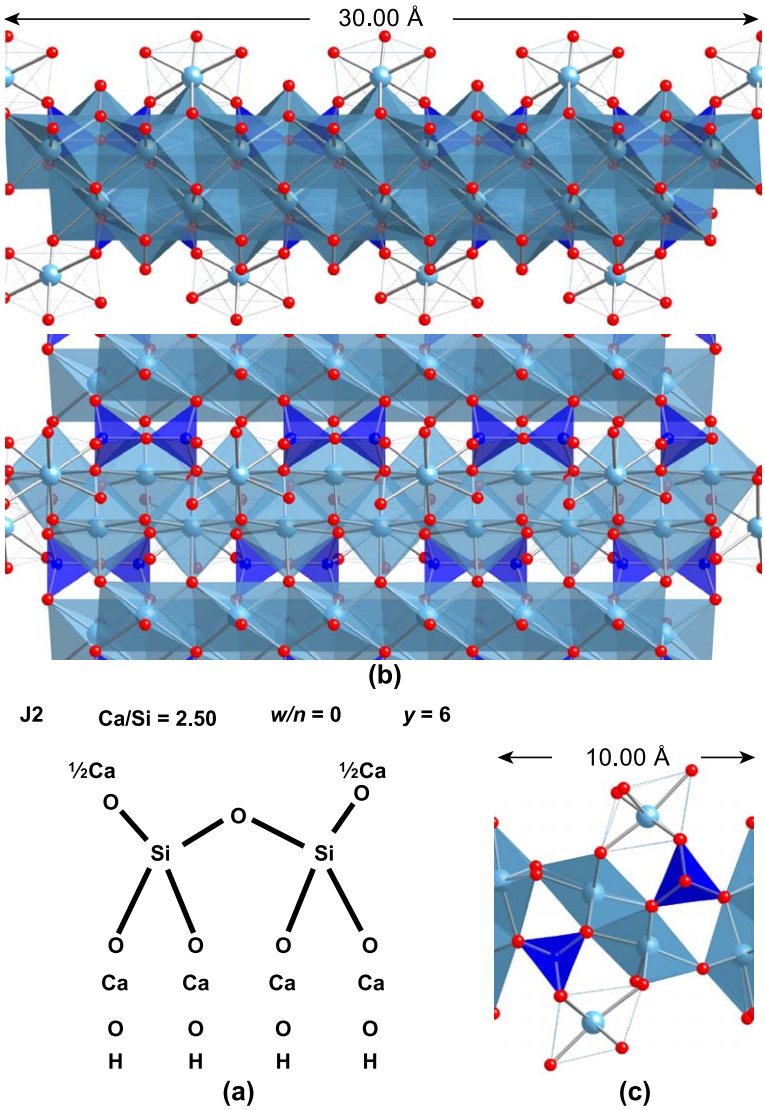


Fig. 31. As Fig. 29 but for the minimum degree of protonation of the silicate chains ($w/n = 0$).

in this equation, $Q^1$ or $Q^2$ correspond to the amount of each species measured by solid-state $^{29}$Si NMR—then,

$$\text{Mean silicate chain length, MCL} = (3n-1) = \frac{2}{q} \tag{6}$$

$$\text{Mean connectivity, } \bar{Q} = 2 - q \tag{7}$$

Fraction of bridging tetrahedra

$$= \frac{n-1}{3n-1} = \frac{Q^2}{3(Q^1+Q^2)} = \frac{1-q}{3} \tag{8}$$

Fraction of paired tetrahedra

$$= \frac{2n}{3n-1} = Q^1 + 2\Big/3Q^2Q^1 + Q^2 = \frac{2+q}{3} \tag{9}$$

Ratio of bridging to paired tetrahedra

$$= \frac{n-1}{2n} = \frac{Q^2}{3Q^1+2Q^2} = \frac{1-q}{2+q} \tag{10}$$

### 4.2. Summary of the structural flexibility of Richardson and Groves' model

The T units in Richardson and Groves' model are derived from the dreierkette structure of 1.4 nm tobermorite, which has the idealized constitutional formula $Ca_5(Si_6O_{18}H_2)\cdot 8H_2O$. Changes in the Ca/Si ratio above or below 0.83, the theoretical value for infinite chains of 1.4 nm tobermorite [40], can result from several types of structural modification. These are outlined in points (i) to (iii) below, with reference to Fig. 40, which is the same as Fig. 25 but with letters added to assist discussion (it is also the same as Fig. 3

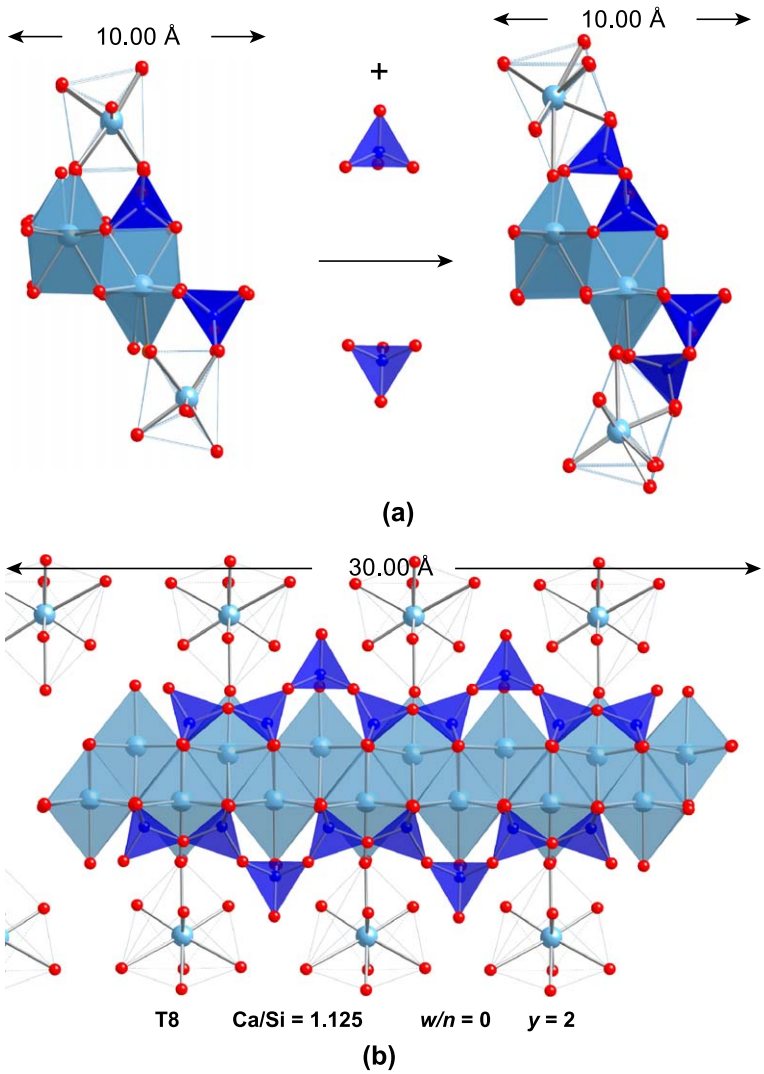


Fig. 32. Diagrams illustrating the polymerization of tobermorite-based dimer ($n=1$) that has the minimum degree of protonation ($w/n=0$). (a) Edge-on views of the silicate chains before and after the insertion of monomers at bridging sites. (b) Tobermorite-based octamer ($n=3$) with the same degree of protonation; this should be compared with Fig. 28 (b), which shows the corresponding view of the dimeric structure (i.e., before polymerization). The values of the variables in Richardson and Groves' model [18] are indicated.

in Ref. [18]). Point Y corresponds to crystalline tobermorite with infinite silicate chains; its degree of protonation corresponds to $w/n=1$ in Richardson and Groves' model. Further increases in Ca/Si ratio are achieved by the incorporation of elements of jennite- and/or CH-based structure, which is outlined in point (iv). Point (i) and the jennite aspect of point (iv) are also implicit in Taylor's earlier model (see Ref. [17] and Section 4.4.1), whilst points (ii) and (iii) were added by Richardson and Groves [18].

(i) *Omission of bridging tetrahedra.* This results in a decrease in the MCL and an increase in the Ca/Si ratio; it corresponds to moving from point Y → G on Fig. 40. Point G corresponds to removal of all the bridging tetrahedra, i.e., dimer with Ca/Si = 1.25; its structure is illustrated in Fig. 27. Line Y–G represents Taylor's tobermorite-based structural units (the lower line of Fig. 2 in Ref. [17]); this composition–chain length relationship was formularized by Richardson and Groves [18] (see Section 4.4.1).

(ii) *Increased content of $Ca^{2+}$ ions balanced by a reduction in Si–OH groups*, i.e., a decrease in the level of protonation, $w/n$, of the silicate chains from 1 to the limit of 0 (in the model, formula (3), there is an associated increase in $y$ from 1 to 2 (see Fig. 24)). This results in an increase in Ca/Si ratio. This is illustrated below for the limiting chain lengths of $\infty$ and 2, but of course applies to structural units of any length within the sequence 2, 5, 8,. . .etc.:

(a) For tobermorite with infinite chains, this corresponds to moving along the line Y → X on Fig. 40 (i.e., reduction in $w/n$ from 1 to 0), the limiting Ca/Si being 1.0. This is the upper limit Ca/Si ratio given by Hamid [71] for tobermorite. The structure

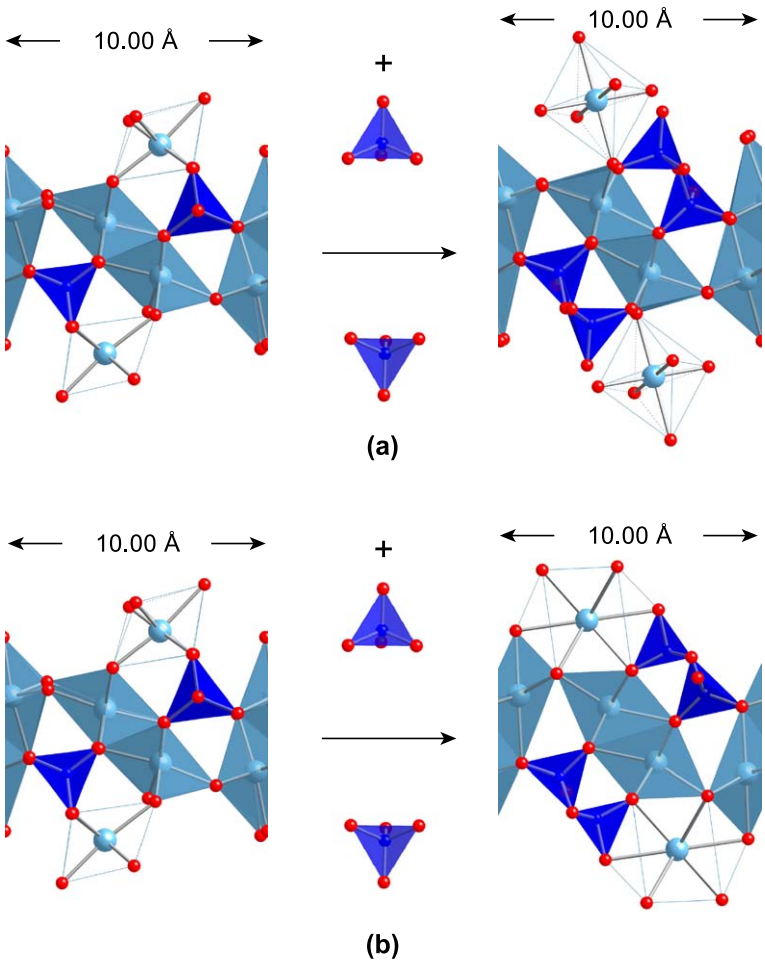


Fig. 33. Diagrams illustrating the polymerization of jennite-based dimer ($n=1$) that has the minimum degree of protonation ($w/n=0$). (a) Edge-on views of the silicate chains before and after the insertion of monomers at bridging sites, derived from crystal structure data for jennite [20]. (b) The same as (a) but derived from data for metajennite [70]. (c) Jennite-based octamer ($n=3$) with the same degree of protonation; this should be compared with Fig. 31 (b), which shows the corresponding view of the dimeric structure (i.e., before polymerization). The values of the variables in Richardson and Groves' model [18] are indicated.

of a longer chain unit (actually octamer) with the same degree of protonation as at point X is illustrated in Fig. 32 (Ca/Si = 1.125, $n=3$, $w/n=0$, $y=2$).

(b) For tobermorite-based dimer (all bridging tetrahedra removed), this corresponds to moving along the line G → F on Fig. 40, the limiting Ca/Si being 1.5, i.e., from the structure illustrated in Fig. 27 (Ca/Si = 1.25, $n=1$, $w/n=1$, $y=1$) to that in Fig. 28 (Ca/Si = 1.50, $n=1$, $w/n=0$, $y=2$).

(iii) *Decreased content of $Ca^{2+}$ ions balanced by an increase in Si–OH groups*, i.e., an increase in the level of protonation, $w/n$, of the silicate chains (the reverse of (ii)) from 1 to the limit of 2 (in the model, formula (3), there is an associated decrease in $y$ from 1 to 0; see Fig. 24). This results in a decrease in Ca/Si ratio.

(a) For tobermorite with infinite chains, this corresponds to moving along the line Y → Z on Fig. 40, the limiting Ca/Si being 0.67. This is the lower limit Ca/Si ratio given by Hamid [71] for tobermorite.

(b) For tobermorite-based dimer (all bridging tetrahedra removed), this corresponds to moving along the line G → H on Fig. 40, the limiting Ca/Si being 1.0; i.e., from the structure illustrated in Fig. 27 (Ca/Si = 1.25, $n=1$, $w/n=1$, $y=1$) to that in Fig. 26 (Ca/Si = 1.00, $n=1$, $w/n=2$, $y=0$).

It clear from points (ii) and (iii) that it is theoretically possible to have C-S-H with a Ca/Si ratio of 1.0 with infinite chains (point X on Fig. 40; structure illustrated in Fig. 32; $w/n=0$, $y=2$) or completely dimeric (point H; structure illustrated in Fig. 26; $w/n=2$, $y=0$).

(iv) *Incorporation of additional $Ca^{2+}$ ions balanced by additional OH ions.* This results in an increase in Ca/Si ratio. On the T/J viewpoint it is the difference between the tobermorite- and jennite-based structural units. The line D–V represents Taylor's jennite-based structural

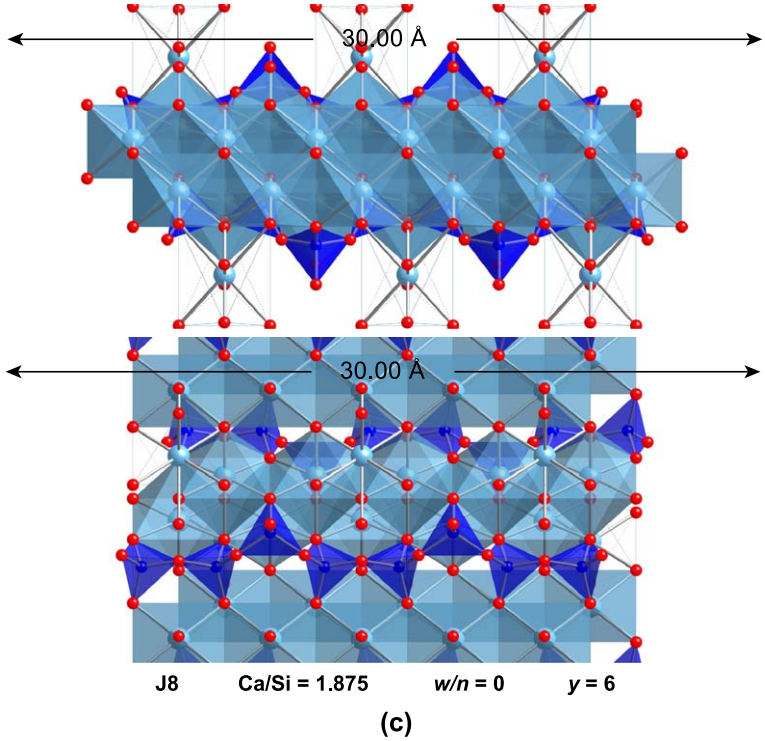


Fig. 33 (*continued*).

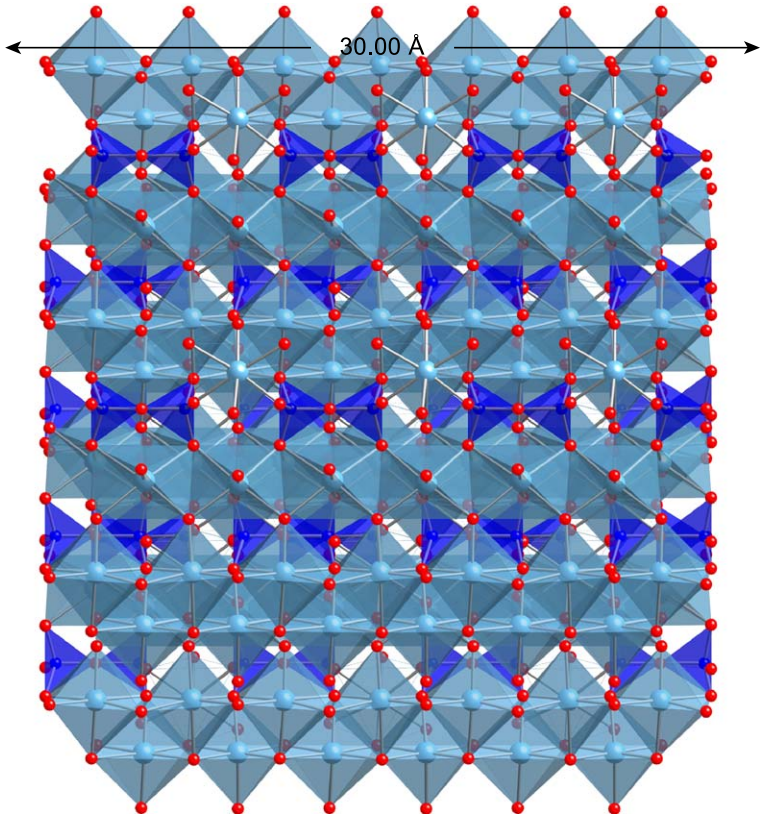


Fig. 34. Schematic diagram showing a view of an approximately 3-nm-sized particle, consisting entirely of J dimer with the minimum degree of protonation ($w/n = 0$). The silicate chains are aligned across the page; a monomer is evident at the extreme right of the top row of silicate tetrahedra.

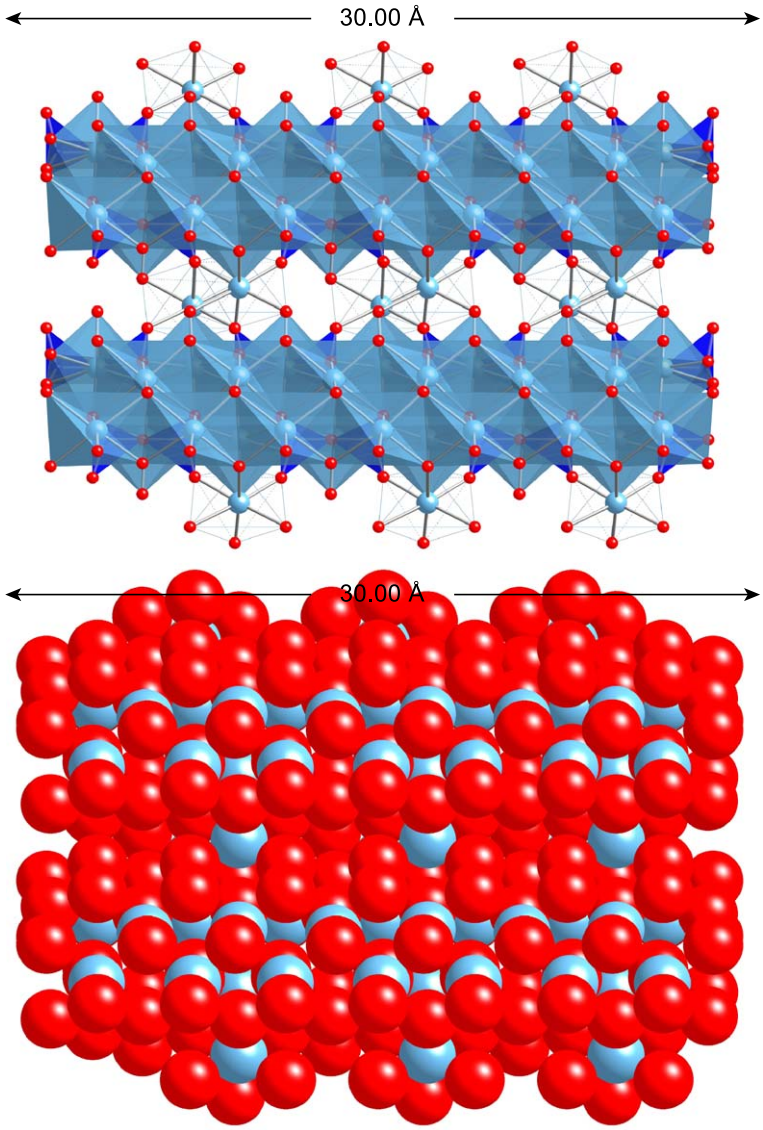


Fig. 35. An alternative view of the particle in Fig. 34 revealing two Ca–O main layers (perpendicular to the plane of the page); the view is shown as both polyhedral and space-filling models.

units (upper line of Fig. 2 in Ref. [17]); the composition–chain length relationship was formularized by Richardson and Groves [18] (see Section 4.4.1) (i.e., $y=5$, and the protonation level $w/n=1$). The structure at point D is illustrated in Fig. 30 (Ca/Si = 2.25, $n=1$, $w/n=1$, $y=5$). The structural modifications outlined in (i), (ii), and (iii) also apply to jennite-based units, the minimum ($w/n=0$) and maximum ($w/n=2$) levels of protonation being represented by lines U–C and W–E, respectively. The structures at points C and E are illustrated in Figs. 31 (Ca/Si = 2.50, $n=1$, $w/n=0$, $y=6$) and 29 (Ca/Si = 2.00, $n=1$, $w/n=2$, $y=4$), respectively, and that of a longer chain unit (actually octamer) with the same degree of protonation as along U–C is illustrated in Fig. 33 (Ca/Si = 1.875, $n=3$, $w/n=0$, $y=6$).

On the alternative to the T/J viewpoint, the T/CH viewpoint, this involves the incorporation of layers of CH [14–16,72–74]. It corresponds to an increase in $y$ in formula (3), or to moving vertically on Fig. 40 towards the region C-E-W-U.

### 4.3. C-S-H incorporating substituents

Richardson and Groves extended their model to allow for the incorporation of substituents into C-S-H [19]. The modified model may be represented as formula (10):

$$\{Ca_{2n}H_w(Si_{1-a}R_a^{[4]})_{(3n-1)}O_{(9n-2)}\}I_{\frac{a}{c}(3n-1)}^{c+} \cdot (OH)_{w+n(y-2)} \cdot Ca_{\frac{n\cdot y}{2}} \cdot Ca_{n\cdot y} \cdot mH_2O \quad (11)$$

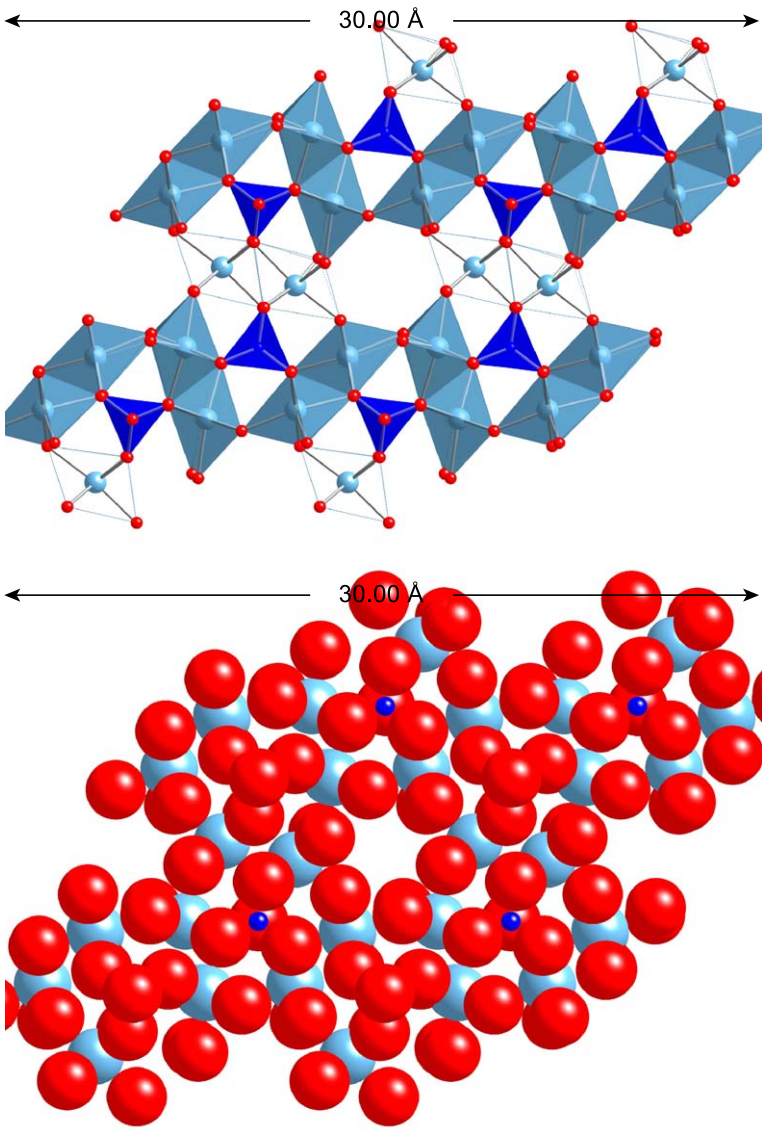


Fig. 36. An alternative view of the particle in Fig. 34 with the silicate chains aligned perpendicular to the plane of the page (i.e., edge on); the view is shown as both polyhedral and space-filling models.

where $R^{[4]}$ is a trivalent cation, mainly $Al^{3+}$, in tetrahedral coordination and $I^{c+}$ is an interlayer ion, either a monovalent alkali cation or $Ca^{2+}$, charge-balancing the $R^{3+}$ substitution for $Si^{4+}$. Al only substitutes for Si in the bridging tetrahedra of the dreierkette structure, consistent with the experimental evidence discussed in Section 3.3. Since there are $n-1$ bridging sites, $0 \le a \le (n-1)/(3n-1)$. The insertion of bridging tetrahedra is shown schematically in Fig. 41.

The Ca/Si ratio and aluminosilicate anion structure are now linked by Eq. (12), on the assumption that charge compensation of the $R^{3+}$ substitution for $Si^{4+}$ is entirely by alkali cations:

$$\mathrm{Ca/Si} = \frac{n(4+y)}{2(1-a)(3n-1)} \tag{12}$$

A slightly smaller value of $y$ is obviously obtained on the assumption that some or all of the charge compensation of the $R^{3+}$ substitution for $Si^{4+}$ is by $Ca^{2+}$ ions; if entirely by $Ca^{2+}$ ions, Eq. (12) is modified to:

$$\mathrm{Ca/Si} = \frac{n(4+y') + a(3n-1)}{2(1-a)(3n-1)} \tag{13}$$

These equations are potentially very useful because most of the parameters are measurable experimentally. The mean Ca/Si and Al/Si (and thus $a$) can be determined by X-ray microanalysis of thinned sections in the TEM (in real cement pastes, this is the only technique capable of giving compositions for C-S-H free of admixture with other phases; see Ref. [22] and references therein). The mean aluminosilicate chain length $(3n-1)$ can be determined using solid-state $^{29}Si$ NMR [33] (NMR also gives a check on the Al/Si

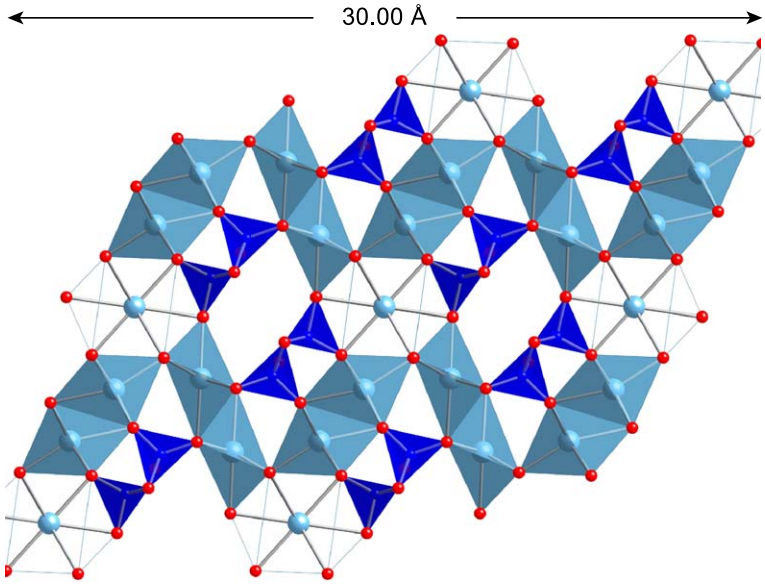


Fig. 37. Schematic diagram showing the same view of the particle in Fig. 36—with the silicate chains aligned perpendicular to the plane of the page (i.e., edge on) and a similar distance between the Ca–O main layers—but in this case, the $Ca^{2+}$ ions present at the bridging sites in Fig. 36 have been displaced by silicate monomers.

ratio). Substitution of these into Eqs. (12) or (13) therefore gives a value for $y$, and thus also for a possible range of values for the degree of protonation of the silicate chains, $w/n$. Additional information on bound water content is then needed to give exact values of $w/n$ and $m$ (water that is bound but not present as hydroxyl groups). Any octahedrally coordinated Al ($Al^{[6]}$) was assumed to be present in layers of AFm or hydrotalcite-like structure interstratified with layers of C-S-H. This assumption is supported by the excellent agreement between Al/Si ratios (>0.1) calculated from NMR and determined directly in the TEM [23] and has been confirmed for C-S-H in alkali-activated slag cements by electron energy loss spectroscopy in the TEM [42]. With $a=0$, Taylor's T-type structural units are derived from formula (11) if $y=1$ and $w/n=1$ and J-type if $y=5$ and $w/n=1$. Richardson and Groves also presented an alternative formulation for the T/CH viewpoint:

$$Ca_X H_{(6n-2X)}(Si_{1-a}R_a^{[4]})_{(3n-1)}O_{(9n-2)}\cdot I_{\frac{a}{c}(3n-1)}^{c+} \cdot zCa(OH)_2\cdot mH_2O \quad (14)$$

The MCL and Al/Si ratio can be calculated from $^{29}Si$ NMR data using the following expressions [33]:

$$\text{Mean alumino silicate chain length, MCL} = \frac{2}{\left(\frac{Q^1}{Q^1+Q^2(0Al)+{}^3/_2\,Q^2(1Al)}\right)} \quad (15)$$

$$\text{Al/Si atom ratio} = \frac{{}^1/_2\,Q^2(1Al)}{Q^1+Q^2(0Al)+Q^2(1Al)} \quad (16)$$

The proportion of bridging tetrahedra that are occupied by Al is

$$\frac{\text{Bridging tetrahedra occupied by Al}}{\text{Bridging tetrahedra occupied by Al and Si}} = \frac{Q^2(1Al)}{{}^2/_3\,Q^2(0Al)+Q^2(1Al)}$$

### *4.4. Relationship of Richardson and Groves' model to other dreierkette-based models for the structure of C-S-H*

#### *4.4.1. Taylor*

Taylor's 1986 model [17] was a development of his earlier discussion, published 30 years earlier with Howison [13] on ways in which C-S-H(I) might attain higher Ca/Si ratios (up to 1.75) than tobermorite (with a Ca/Si of 0.83). The model envisages that C-S-H of high Ca/Si is composed of structural units derived from jennite ($Ca_9Si_6O_{32}H_{22}$) and to a lesser extent 1.4-nm tobermorite ($Ca_5Si_6O_{26}H_{18}$) [17]. Finite silicate chains containing 2, 5, 8,...etc. tetrahedra (i.e., $3n-1$ where $n=1$, 2, 3,...etc.) would result from either structure if bridging tetrahedra (B) were missing. As noted earlier, this chain length sequence is consistent with the silicate anion structure observed in hardened $C_3S$ and OPC pastes (Section 3.3). Taylor assumed that each bridging tetrahedron carries only one H atom and that when one of these tetrahedra is missing only one of the broken ends of the chain is terminated by a H atom. Thus, the net charge remains unchanged and the omission of a tetrahedron requires no change in the amount of interlayer Ca. He stated that, "there is no direct evidence for this assump-

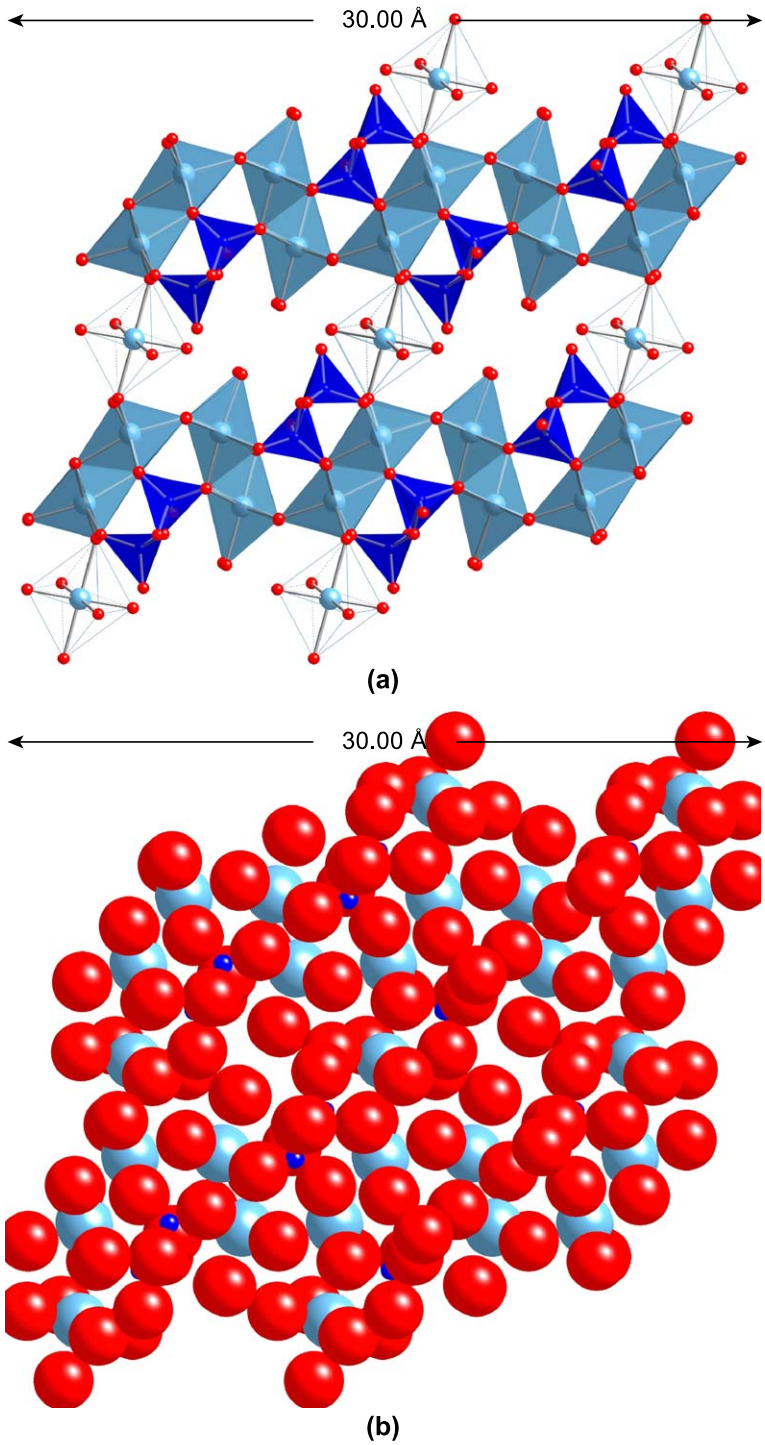


Fig. 38. Schematic diagram showing the same view of the particle in Fig. 37 but in this case the Ca–O main layers are further apart; the view is shown as both polyhedral and space-filling models.

tion, but it is crystal—chemically reasonable and leads to a number of results that agree with experimental data." The Ca/Si ratios of the structural units resulting from the omission of B from the structures of 1.4 nm tobermorite and jennite vary linearly with the reciprocal of the silicate chain length (see Fig. 2 of Ref. [17]). Taylor proposed that the observed composition (Ca/Si = 1.7 → 1.8) and structure of C-S-H gel in hardened $C_3S$ or OPC pastes might be achieved by an intimate mix of these structural units [17]. In young pastes, where only dimer is present, the Ca/Si ratio is achieved by a mixture of J2 and T2. In more mature pastes where pentamer and higher polymeric

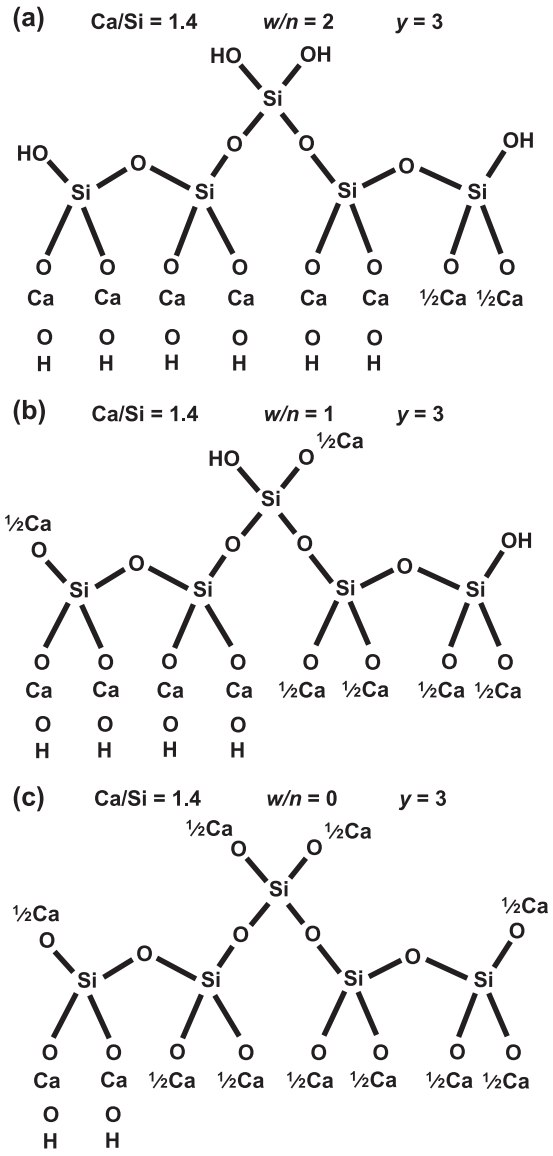


Fig. 39. Schematic diagrams outlining how the distribution between J- and T-based structural units can be altered for a C-S-H of fixed MCL (5) and Ca/Si ratio (1.4) by varying the hydroxyl water content.

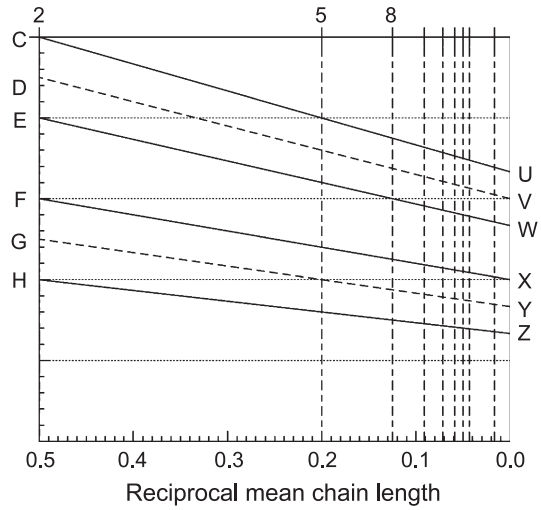


Fig. 40. The same as Fig. 25 but with letters added to assist the discussion in Section 4.2.

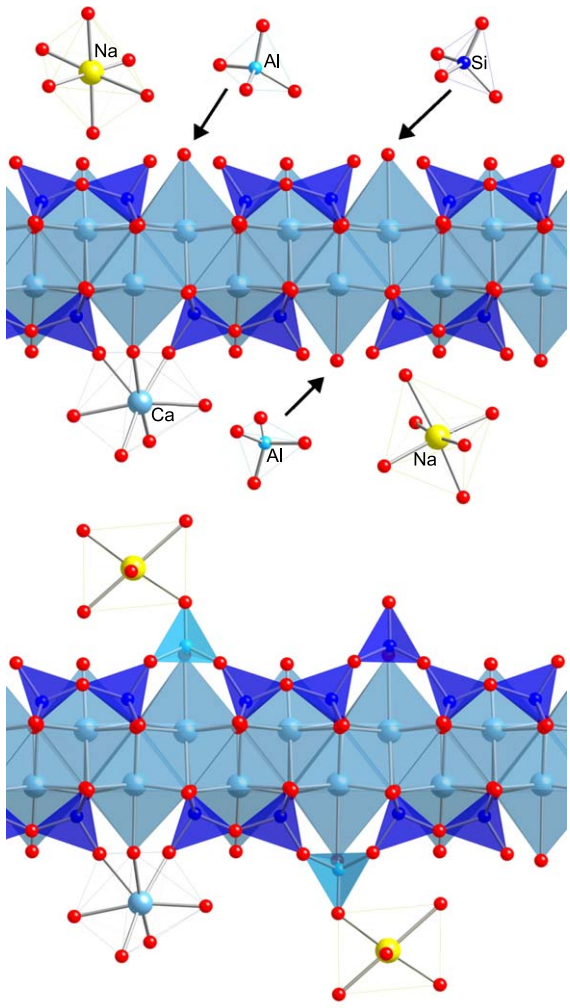


Fig. 41. Schematic diagrams illustrating the polymerization of tobermorite-based dimer by the insertion of both silicate and aluminate monomers at bridging sites. The positions of the ions and water molecules are entirely speculative and purely for the purpose of illustrating the polymerization process.

chains become evident, the composition is achieved by a mix of J5, J8, etc., and lower proportions of J2 and T2. Taylor considered that the fact that the dimeric structural units, whether J2 or T2, are furthest in both structure and composition from the corresponding crystalline hydrates provides a thermodynamic explanation for the condensation process.

Richardson and Groves' [18] noted that Taylor's model can be considered a special case of their formulation based on very specific structural considerations, namely as a mixture of structural units based on jennite and tobermorite where one of the chain-end tetrahedra and each bridging tetrahedron carries a proton. Each structural unit therefore has *n* silanol groups—dimer has one silanol group, pen-

tamer two, octamer three, and so on—and $n/2$ interlayer $Ca^{2+}$ ions; or, in terms of formula (3),

$$(w + n(y-2)) = 2\left(\frac{n \cdot y}{2} - \frac{n}{2}\right)$$

and so, $w = n$.

For tobermorite-based units, $y = 1$, which is the minimum value of $y$ for this level of protonation (represented by point •T on Fig. 24), and for jennite-based units $y = 5$, which is the maximum value of $y$ for this level of protonation (point •J on Fig. 24). Thus, substituting $w = n$ and $y = 1$ or 5 into formula (3) and writing the contents of the main layers of the two structures in square brackets give the formula for Taylor's T($3n-1$) units ($y = 1$) as:

$$[Ca_{2n}H_nSi_{(3n-1)}O_{(9n-2)}] \cdot \frac{1}{2}Ca \cdot mH_2O \quad (18)$$

and for his J($3n-1$) units ($y = 5$) as:

$$[Ca_{4n}H_nSi_{(3n-1)}O_{(9n-2)}(OH)_{4n}] \cdot \frac{1}{2}Ca \cdot mH_2O \quad (19)$$

Substitution of $y = 1$ into Eq. (4) gives the structure–composition relationship for Taylor's T($3n-1$) units [18]:

$$Ca/Si = \frac{5n}{2(3n-1)} \quad (20)$$

and substitution of $y = 5$ gives the structure–composition relationship for his J($3n-1$) units [18]:

$$Ca/Si = \frac{9n}{2(3n-1)} \quad (21)$$

Eqs. (20) and (21) can be rewritten in terms of mean chain length (MCL = $3n-1$; $n$=(MCL + 1)/3) so that for T($3n-1$),

$$Ca/Si = \frac{5}{6}\left(\frac{1}{MCL}\right) + \frac{5}{6} \quad (22)$$

and for J($3n-1$),

$$Ca/Si = \frac{3}{2}\left(\frac{1}{MCL}\right) + \frac{3}{2} \quad (23)$$

which are the equations that are graphically represented in Fig. 2 of Taylor's 1986 article on C-S-H [17], and as lines D–V and G–Y in Fig. 40.

#### 4.4.2. Cong and Kirkpatrick

Cong and Kirkpatrick's [75] 'defect-tobermorite' model was developed during wide-ranging studies of synthetic C-S-H phases [75–78]. Their model is not essentially different from Richardson and Groves' general formulation, formula (3) [18]. Cong and Kirkpatrick used two equations to describe the structure–composition relationship for their model [75], namely,

$$C/S = \frac{r}{\left(1 - \frac{m}{3}\right)} \quad (24)$$

and

$$QRT = \frac{2}{\left(\frac{3}{m} - 1\right)} \quad (25)$$

where $r$ is the composition when the silicate chains are of infinite length, $m$ is the fraction of bridging tetrahedra (B) missing, and $QRT = Q^1/(Q^1 + Q^2)$. In Taylor's and Richardson and Groves' models, the structure of C-S-H of sufficiently low C/S ratio is based on 1.4 nm tobermorite with some or all the B missing. As discussed earlier, with B missing, the chain length sequence is 2, 5, 8…($3n-1$), where $n$ is integer. Thus, if $n = 1$, the structural unit is a dimer; if 2, a pentamer; if 3, an octamer, and so on. With $n = 1$ (dimer), all the B are missing, and so in Cong and Kirkpatrick's model, $m = 1$; for $n = 2$ (pentamer), 50% of B are missing and so $m = 1/2$; for $n = 3$ (octamer), 33.3% of B are missing and $m = 1/3$; and so on. Thus, it is clear that $m = 1/n$. If the constitutional formula for 1.4 nm tobermorite with infinite chains is taken as $Ca_5(Si_6O_{18}H_2)\cdot 8H_2O$, then the C/S ratio and so $r$ in Eq. (24) is 5/6 (Cong and Kirkpatrick used $r = 9/10$, although this corresponds to an mean chain length of about 11).

Substituting $m = 1/n$ and $r = 5/6$ into Eq. (24) gives Eq. (20), i.e., Eq. (11) in Richardson and Groves' earlier article [18]. Substituting $m = 1/n$ into Eq. (25) and rearranging gives

$$(3n-1) = \frac{2}{QRT}$$

which is the same as Eq. (6) above (i.e., Eq. (9) in Richardson and Groves' article [18] (Cong and Kirkpatrick's QRT is the same as Richardson and Groves' $q$).

The limits placed on the variables in Richardson and Groves' general model, formula (3), essentially amount to the 'defects' proposed by Cong and Kirkpatrick. For example, Cong and Kirkpatrick started their charge–balance calculations from the assumption that nonbridging oxygens (NBO) are balanced preferentially by $Ca^{2+}$ ions forming Si–O–Ca– linkages. In the terms that they used in their discussion, this corresponds to 2C/S–NBO = 0, i.e., there are just sufficient $Ca^{2+}$ ions to maintain electrical neutrality (NBO here means NBO per tetrahedron). In terms of Richardson and Groves' model, this corresponds to $y = 2$ and the degree of protonation, $w/n = 0$. If 2C/S–NBO < 0, there are insufficient $Ca^{2+}$ ions and the extra NBOs must be charge-balanced by the formation of Si–OH linkages: in Richardson and Groves' model, this corresponds to $w/n > 0$, and for purely tobermorite-based units, $y$ would decrease. If 2C/S-NBO>0, there are extra $Ca^{2+}$ and these must form –Ca–OH linkages to maintain electrical neutrality, or in Richardson and Groves' formulation $w/n$ and $y$ increase. Cong and Kirkpatrick stated that "This process can be expressed as: $NBO(Si-O-Ca) + H_2O \rightarrow Ca-OH + Si-OH$" (p. 1590 of Ref. [75]), which is the same as Richardson and Groves' "An increase in w above its minimum

value is compositionally equivalent to the addition of elements of $H_2O$, but structurally corresponds to increasing the number of Si–O–Ca–OH and Si–OH bonds at the expense of Si–O–Ca–O–Si" (p. 1009 of Ref. [18]).

#### 4.4.3. Nonat and Lecoq

Nonat and Lecoq [79] proposed another model based on tobermorite [79]. It was presented in terms of two hypotheses, which essentially applied to different compositional ranges. Their first hypothesis (p. 204) simply corresponds to tobermorite-based structural units with no Si–OH groups, or on Richardson and Groves' model, formula (3), to $y=2$, and a degree of protonation of the silicate chains, $w/n=0$ (where Taylor's tobermorite-based units are represented by $y=1$ and $w/n=1$). Their second hypothesis (p. 205) involves the presence of $OH^-$ and $Ca^{2+}$ ions in the interlayer space, in which respect it is similar to an earlier model by Stade [80], Stade and Wieker [81], Stade et al. [82–84], and Stade and Müller [85]. However, it appears to be different from Taylor's, Richardson and Groves', and Cong and Kirkpatrick's models in that any Si–O–Ca–OH linkages involve interlayer rather than main-layer Ca.

#### 4.4.4. Chen et al.

Chen et al. [86] discussed the ways in which the Ca/Si ratio of C-S-H can vary in a dreierkette-based structural model; their arguments are not different from those present in Richardson and Groves' model [18]. For example, their Table 5 presents the results of charge-balance calculations to determine the Ca/Si ratio above which –Ca–OH must be present in C-S-H; their formulae, which they present for MCLs of 2, 3, 4, 5, and $\infty$, all correspond to T units with $w/n=0$ and $y=2$ in formula (3), which is also the same as Nonat and Lecoq's first hypothesis, discussed above.

### 4.5. Examples of the applicability of Richardson and Groves' model

The applicability of Richardson and Groves' model to the experimental data outlined in Section 3 is discussed in the following section, starting with those systems that have the greatest degree of long-range order.

#### 4.5.1. Alkali-activated pastes

The Op C-S-H present in alkali hydroxide-activated systems very often gives SAED patterns that are consistent with C-S-H (I); it can therefore be considered T-type in structure. This is true at both low and high Ca/Si ratio. Since this C-S-H is also always foil-like in morphology, it seems reasonable to associate foil-like morphology with T-type structure. Fig. 5 shows TEM analyses of Op C-S-H in a KOH-activated synthetic slag paste ($\times$); these data are reproduced from Ref. [33]. The compositions of a number of structural units are indicated in the figure. The J2 label corresponds to J dimer with a degree of protonation $w/n=1$ (i.e., Taylor's jennite-based dimer), the structure of which is illustrated in Fig. 30. T2 is the T dimer with the same degree of protonation, which is illustrated in Fig. 27, and $T_p2$ is T dimer that is totally protonated ($w/n=2$), which is illustrated in Fig. 26. The structural units directly above these two T dimers—which have the same degrees of protonation as they do correspond to longer chains that are saturated with respect to Al. There are of course many other possible units that for simplicity are not shown. For example, T5 with $w/n=1$ has the same composition as $T_p2$, and T8 with only one of its two bridging sites occupied by Al has Si/Ca = 1.167 and Al/Ca = 0.167 when $w/n=2$ but it has Si/Ca = 0.933 and Al/Ca = 0.133 when $w/n=1$. The full line on the figure is the regression line derived from the mean compositions of Op C-S-H in a range of water-activated slag-containing cements [31]; the line meets the Si/Ca axis (i.e., zero Al) at the composition for J dimer; J2 cannot of course accommodate Al because it has no bridging tetrahedra. Since it is assumed that Al does not substitute for Si in longer J-type units—which is discussed in Ref. [19]—this compositional trend seems to suggest that in the water-activated blends the C-S-H consists of T units that can contain Al, intermixed with J units that do not (this is discussed further in Section 4.5.2). Whilst the individual analyses for the Op C-S-H in the KOH-activated synthetic slag paste are clustered along the regression line, given that the MCL is nearly 5 and the proportion of bridging tetrahedra that are occupied by Al is 91%, it seems most likely that the trend is due largely to pentameric T-type units with varying degrees of protonation, rather than there being significant involvement of J-type units. This is well illustrated by comparing the chemical/structural formulae of the T units labelled T5 and $T_p5$ on Fig. 5 with that derived for the C-S-H from the data in Ref. [33] (note that the label for $T_p5$ is offset slightly to the right to avoid overlap with the data points). The T5 and $T_p5$ units correspond to T-type pentamers—with 100% bridging tetrahedra occupied by Al—that have degrees of protonation, $w/n$, of 1 and 2, respectively. In terms of formula (11), T5 ($w/n=1$) has the formula:

$$[Ca_4H_2(Si_{0.8}Al_{0.2})_5O_{16}]\cdot K\cdot Ca\cdot mH_2O \quad (26)$$

where the contents of the main (tobermorite-like) layer are contained within the square brackets. $T_p5$ ($w/n=2$) has the formula

$$[Ca_4H_4(Si_{0.8}Al_{0.2})_5O_{\cdot 16}]K\cdot mH_2O \quad (27)$$

The formula for the C-S-H is established using formula (11) and Eq. (12): Assuming values (from Ref. [33]) for mean Ca/Si = 1.09, Al/Si = 0.215, and MCL = 4.83, $a$ is calculated as 0.177 (since $Al/Si=a/(1-a)$) and $n$ as 1.94 (since $(3n-1)=4.83$); substitution into Eq. (12) gives $y=0.46$ on the assumption that the $Al^{3+}$ substitution for $Si^{4+}$ is charge compensated entirely by $K^+$, which is not unreasonable in this KOH-activated low-Ca system. Assuming the minimum degree of protonation ($w/n=2-y=1.54$) to

make the comparison most straightforward, substitution into formula (11) gives the average formula for the C-S-H as

$$[Ca_{3.89}H_{2.99}(Si_{0.82}Al_{0.18})_{4.83}O_{15.48}] \cdot K_{0.85} \cdot Ca_{0.45} \cdot mH_2O \quad (28)$$

The minimum ratio of hydroxyl groups to (Si + Al) is therefore 0.62 (the slight charge imbalance is due to rounding).

Fig. 5 also shows TEM analyses of Op C-S-H in a PC–metakaolin blend with 20% metakaolin and activated with 5 M KOH solution. SAED showed that all analyses were free of admixture with crystalline CH. The MCL for the C-S-H in this paste varied very significantly over a short period [45], with a peak value of about 18. On inspection, it is evident that the distribution of TEM analyses on Fig. 5 are well explained by the T/CH structural viewpoint, formula (14) (shown by the dotted line), but cannot be accounted for on the T/J viewpoint. Some of the data points can be accounted for by variations in the degree of protonation of the silicate chains with no –Ca–OH groups present.

Fig. 4 shows TEM analyses of Op C-S-H for 5-M KOH-activated neat PC (+) and slag–PC blends with 50% (□) and 90% (◇) slag. The MCLs were 2.8, 3.6, and 4.2, respectively; the percentage of bridging sites occupied by Al in the blends was 72% for the 50% (□) blend and 83% for the 90% (◇) blend. The TEM analyses for the 90% blend (◇)—which are more scattered than when activated with water (Fig. 3)—can all be accounted for by short-chain T-type units (mainly dimers and pentamers) with varying degrees of protonation, with no need for extra Ca present in J units or as 'solid-solution' CH. This is a useful example to again illustrate the use of Eq. (12) and formula (3) to establish the formula that represents an average structural unit in the C-S-H. Assuming values (from Ref. [31]) for mean Ca/Si = 1.15, Al/Si = 0.17, and MCL = 4.21, $a$ is calculated as 0.145 (since Al/Si = $a/(1-a)$) and $n$ as 1.74 (since $(3n-1) = 4.21$); substitution into Eq. (12) gives $y = 0.77$ on the assumption that the $Al^{3+}$ substitution for $Si^{4+}$ is charge compensated entirely by $Na^+$ or $K^+$, which is again not unreasonable in this low-Ca system. A value of 0.77 for $y$ means that the degree of protonation ($w/n$) must be between 1.23 and 2. Additional information on bound water content is needed to decide upon an exact value (and also to determine $m$); if the minimum value is chosen, then substitution of these values into formula (11) gives

$$[Ca_{3.47}H_{2.14}(Si_{0.85}Al_{0.15})_{4.21}O_{13.63}] \cdot (Na,K)_{0.61} \cdot Ca_{0.67} \cdot mH_2O \quad (29)$$

This structure is entirely T-type, with no need for J-type units or 'solid-solution' CH. Such units are, however, required if the degree of protonation of the silicate chains is higher than the minimum, which seems likely from the distribution of the points on Fig. 4. Since the microstructural evidence (i.e., the SAED patterns, foil-like morphology, and presence of microcrystalline CH) clearly favours the T/CH model, the formula (from formula (14)) with maximum degree of protonation would be

$$Ca_{3.47}H_{3.47}(Si_{0.85}Al_{0.15})_{4.21}O_{13.63} \cdot (Na,K)_{0.61} \cdot 0.67Ca(OH)_2 \cdot mH_2O \quad (30)$$

Or with the contents of the main (T-type) layer written within square brackets,

$$[Ca_{3.47}H_{3.47}(Si_{0.85}Al_{0.15})_{4.21}O_{13.63}] \cdot (Na,K)_{0.61} \cdot 0.67Ca(OH)_2 \cdot mH_2O \quad (31)$$

Note that the minimum and maximum values of the ratio of hydroxyl groups to (Si + Al) are 0.51 and 0.82, respectively.

All the analyses for the Op C-S-H in the 50% blend and in the neat PC on Fig. 4 can be accounted for on the T/CH model. Whilst most, but not all of them, can also be accounted for by the T/J approach, the microstructural evidence clearly favours the T/CH, in which case, the formula for the C-S-H in the 50% blend with minimum degree of protonation ($w/n = 0$)—and with the substitution of $Si^{4+}$ by $Al^{3+}$ balanced entirely by alkali cations ($y = 2.50$)—would (from formula (14), assuming from Ref. [31] Ca/Si = 1.55, Al/Si = 0.12, and MCL = 3.60) be

$$Ca_{4.60}(Si_{0.89}Al_{0.11})_{3.60}O_{11.80} \cdot (Na,K)_{0.39} \cdot 0.38Ca(OH)_2 \cdot mH_2O \quad (32)$$

This can be written with the contents of the main (T-type) layer within square brackets ($2n$ $Ca^{2+}$ ions are main layer $Ca^{2+}$ ions and $n - (w/2)$ $Ca^{2+}$ ions are interlayer $Ca^{2+}$ ions required for charge-balance), in which case the formula is

$$[Ca_{3.07}(Si_{0.89}Al_{0.11})_{3.60}O_{11.80}] \cdot (Na,K)_{0.39} \cdot Ca_{1.53} \cdot 0.38Ca(OH)_2 \cdot mH_2O \quad (33)$$

With maximum degree of protonation ($w/n = 2$), the formula is

$$Ca_{3.07}H_{3.07}(Si_{0.89}Al_{0.11})_{3.60}O_{11.80} \cdot (Na,K)_{0.39} \cdot 1.92Ca(OH)_2 \cdot mH_2O \quad (34)$$

or

$$[Ca_{3.07}H_{3.07}(Si_{0.89}Al_{0.11})_{3.60}O_{11.80}] \cdot (Na,K)_{0.39} \cdot 1.92Ca(OH)_2 \cdot mH_2O \quad (35)$$

The substitution of $Si^{4+}$ by $Al^{3+}$ is not of course necessarily balanced entirely by alkali cations; on the assumption that—at the other extreme—it is balanced entirely by $Ca^{2+}$ ions ($y' = 2.25$), with minimum degree of protonation ($w/n = 0$), the formula is

$$Ca_{4.79}(Si_{0.89}Al_{0.11})_{3.60}O_{11.80} \cdot 0.19Ca(OH)_2 \cdot mH_2O \quad (36)$$

or

$$[Ca_{3.07}(Si_{0.89}Al_{0.11})_{3.60}O_{11.80}] \cdot Ca_{1.72} \cdot 0.19Ca(OH)_2 \cdot mH_2O \quad (37)$$

With maximum degree of protonation ($w/n = 2$), it is

$$Ca_{3.26}H_{3.07}(Si_{0.89}Al_{0.11})_{3.60}O_{11.80} \cdot 1.72Ca(OH)_2 \cdot mH_2O \quad (38)$$

or

$$[Ca_{3.07}H_{3.07}(Si_{0.89}Al_{0.11})_{3.60}O_{11.80}] \cdot Ca_{0.19} \cdot 1.72Ca(OH)_2 \cdot mH_2O \quad (39)$$

Extra information on the bound water content and the extent of charge compensation by alkali cations is needed to establish a more exact average formula.

#### 4.5.2. Water-activated pastes

The TEM analyses on Fig. 3 for Op C-S-H in water-activated blends are less scattered than those in Fig. 4. The MCLs for the C-S-H were 4.1 and 6.5 for the blends with 50% (○) and 90% (△) slag, respectively; the percentage of bridging sites occupied by Al in the blends was 54% for the 50% (○) blend and 63% for the 90% (△) blend (i.e., three quarters of the values for the corresponding KOH-activated pastes) [31]. Those for the 90% blend fall in an essentially vertical line and can again be accounted for by an entirely T-type structure, in this case involving in particular pentamer and octamer that has both Si and Al in bridging tetrahedra. The degree of protonation of the aluminosilicate chains would be variable.

Repeating the procedure used above gives a value for $y$ of 1.63 (using mean Ca/Si = 1.265, Al/Si = 0.17, MCL = 6.45, $a = 0.145$, $n = 2.48$) assuming that the $Al^{3+}$ substitution for $Si^{4+}$ is charge compensated entirely by $Na^+$ or $K^+$, which means that the degree of protonation $w/n$ of the *average* structural unit must be between 0.37 and 2. Charge compensation entirely by $Ca^{2+}$ would give values of 0.75 and 2. Again, additional information on bound water is needed to establish a more exact value, but consideration of the distribution of the individual analyses on Fig. 3 with the compositions of pentameric and octameric T units indicates strongly that the degree of protonation is close to the minimum; indeed some of the individual analyses would

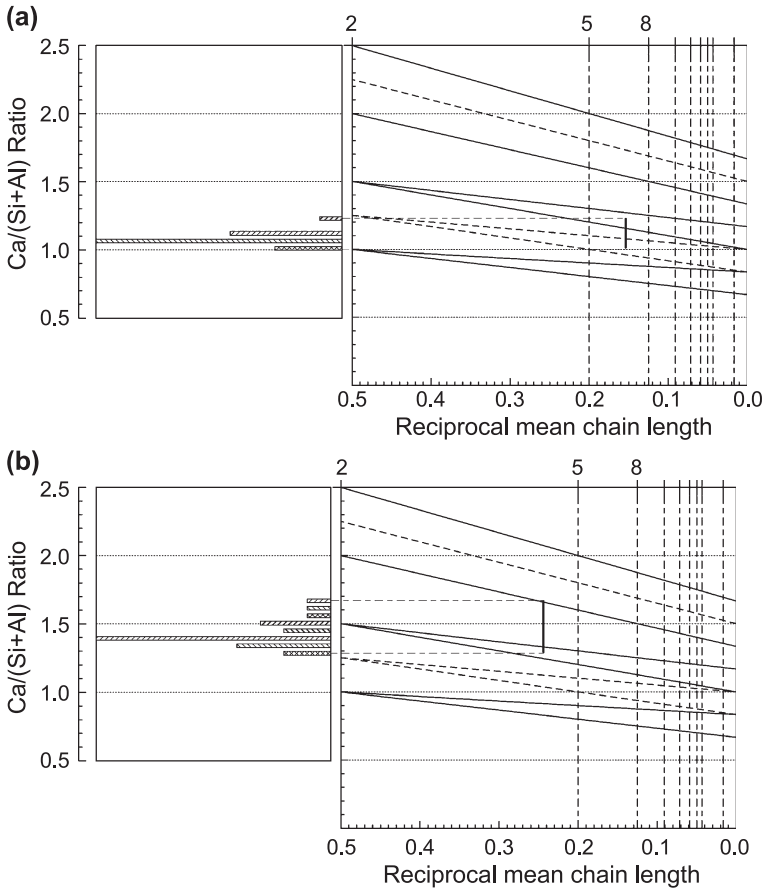


Fig. 42. Ca/(Si + Al) ratio frequency histogram of the TEM analyses of Op C-S-H present in hardened water-activated white PC/GGBS blends with (a) 90% slag and (b) 50% slag (see Fig. 3) placed against the Ca/Si–MCL plot of Fig. 25. The inclusion of $Al^{3+}$ substituted for $Si^{4+}$ does not affect the compositional position of the points for the T units (>5 tetrahedra) unless the charge difference is in part compensated by $Ca^{2+}$ ions; the alternative lines in the T region (i.e., those not present on Fig. 25) represent the greatest possible change in the position of the units (i.e., maximum Al balanced totally by Ca).

correspond to zero degree of protonation if the $Al^{3+}$ substitution for $Si^{4+}$ is charge compensated entirely by $Na^{+}$ or $K^{+}$. This point is perhaps better illustrated on Fig. 42(a), which shows a Ca/(Si + Al) ratio frequency histogram of the TEM analyses placed against the Ca/Si–MCL plot of Fig. 25; the MCL of the C-S-H is indicated by a bold vertical line (which is the height of the histogram). The inclusion of $Al^{3+}$ substituted for $Si^{4+}$ does not affect the compositional position of the points for the T units (>5 tetrahedra) unless the charge difference is in part compensated by $Ca^{2+}$ ions; the alternative lines on the figure represent the greatest possible change in the position of the units (i.e., maximum Al balanced totally by Ca). On inspection, it is clear that the composition and MCL are well explained by T units, and that the aluminosilicate chains must be protonated to only a modest extent since the vertical bar is close to the upper line, which corresponds to zero protonation, $w/n = 0$ (the middle line corresponds to the intermediate level of protonation ($w/n = 1$; i.e., Taylor's assumption) and the lower line to the maximum degree of

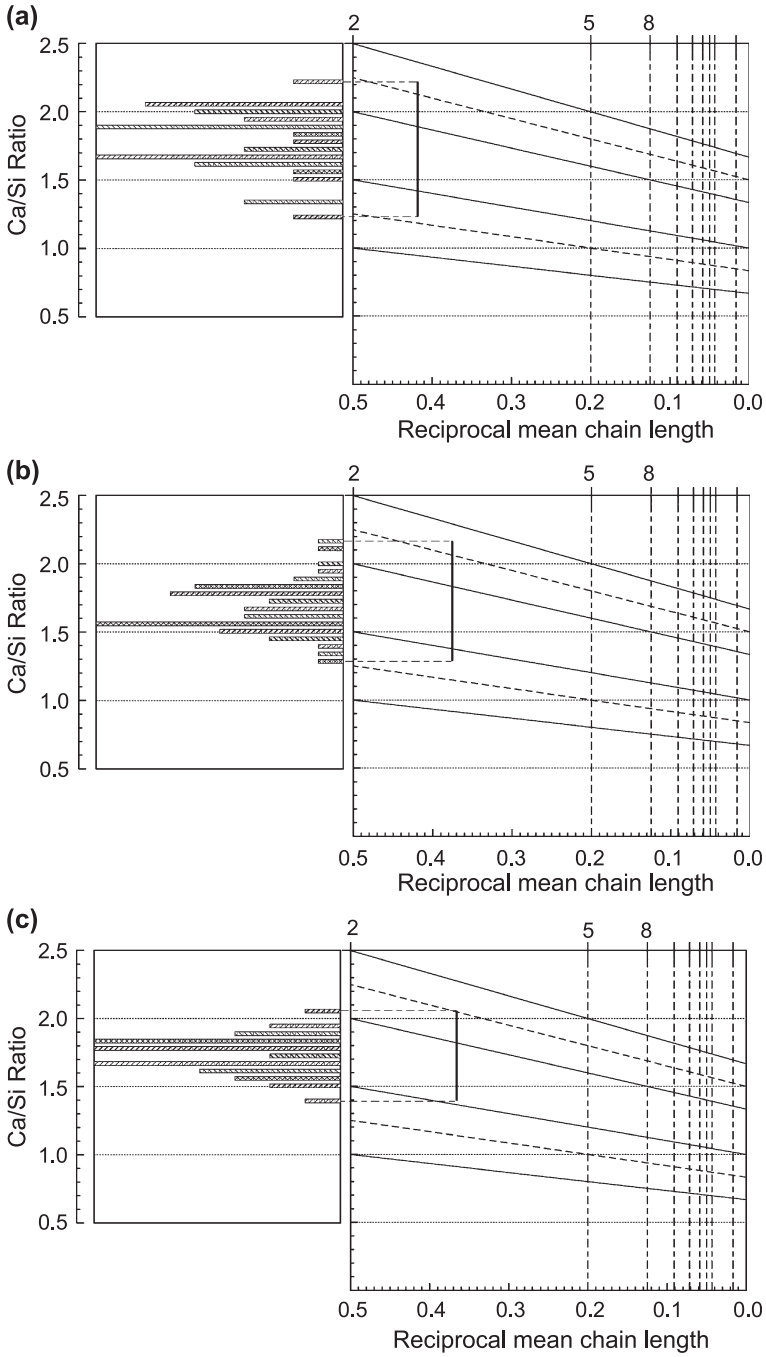


Fig. 43. Ca/Si ratio frequency histograms of the TEM analyses of C-S-H present in hardened water-activated ordinary PC pastes (replotted from Ref. [28]) placed against the Ca/Si–MCL plot of Fig. 25, for ages (a) 1 day, (b) 1 week, (c) 3 months, (d) 1 year, and (e) 2 years, with typical MCL data taken from Ref. [59].

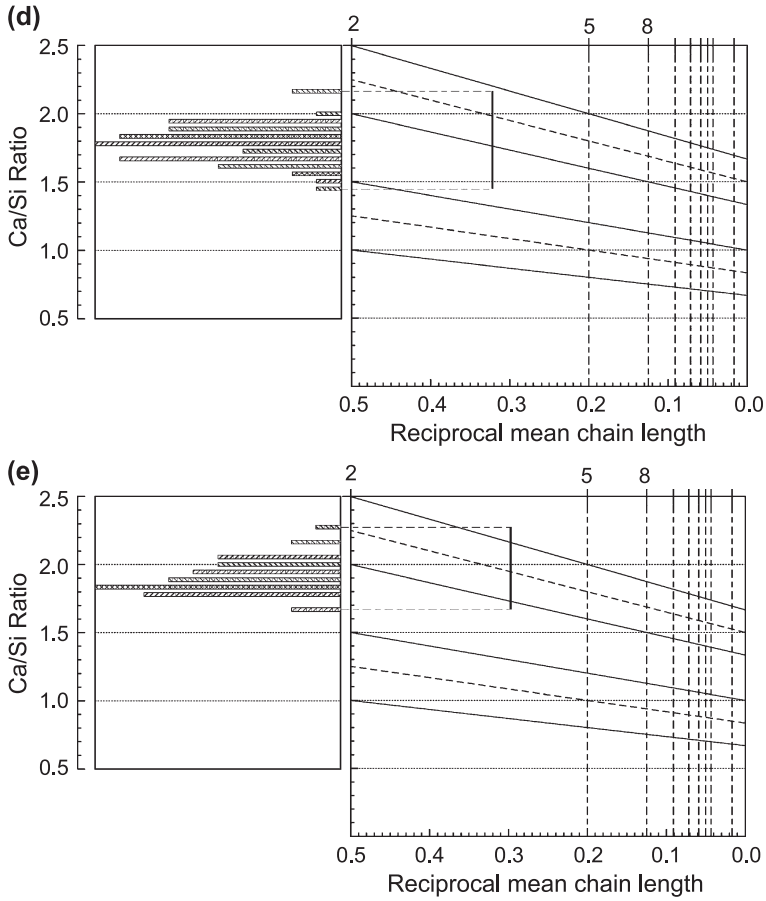


Fig. 43 (*continued*).

protonation, $w/n = 2$). Thus, if the minimum value for the degree of protonation is chosen—together with charge compensation by alkali cations—the formula that represents an average structural unit in this system is

$$[Ca_{4.96}H_{0.92}(Si_{0.85}Al_{0.15})_{6.45}O_{20.32}] \cdot (Na, K)_{0.94} \cdot Ca_{2.02} \cdot mH_2O \quad (40)$$

Interestingly, the ratio of hydroxyl groups to (Si + Al) in this formula is only 0.14, which is much lower than the values established above for KOH activation; it should be possible to test this conclusion using NMR techniques. The Op C-S-H again has foil-like morphology, but the foils are more crumpled than with KOH activation, and it does not give a C-S-H (I) SAED pattern. So, whilst the foils obviously grow mainly in two dimensions (the foils are only a few nanometers thick), there is no long-range structural order.

Fig. 42(b) shows a Ca/(Si + Al) ratio frequency histogram of the TEM analyses for the Op C-S-H present in the water-activated blend with 50% slag placed against the Ca/Si–MCL plot of Fig. 25. Inspection of this figure and Fig. 3 shows that the data—which, like the 90% blend, are less scattered than with KOH activation—can be accounted for on both structural viewpoints. Since the MCL is 4.1 and the proportion of bridging tetrahedra that are occupied by Al is 54%, on the assumptions that the aluminosilicate chains are not highly protonated and that Al only substitutes for Si in T units—both of which seem probable—the best explanation for the data on the T/J viewpoint is that the C-S-H consists of a mixture of J2, T2, T5 (with and without Al), and T8 (1Al). It is perhaps odd that this explanation requires the presence of J2 units (but not longer-chain J units), which are furthest away in composition from the mean value. The T/CH viewpoint would, of course, account for the data by the interstratification of CH layers with those of T-type structure.

The requirement of J units or CH layers in water-activated systems coincides with a change in morphology of Op C-S-H from foil-like to fibrillar, so it is would seem reasonable to associate their presence with fibrillar morphology. The change is not, however, simply a result of their incorporation per se (i.e., of increasing Ca/Si ratio) because foil-like C-S-H with high Ca/Si ratio is formed in some systems, for example, in KOH-activated PC pastes; in that case, the T/CH viewpoint is clearly more appropriate than the T/J because SAED patterns are often typical of C-S-H (I) and microcrystalline CH is present. It might therefore be concluded that the change in morphology is due to the presence of J units rather than ‘solid-solution’ CH. However, it is possible that it is simply due to differences in the

chemistry of the systems that affect the rate at which complexes are transferred from solution to the growing particles of C-S-H, such that T-type layers that form in KOH systems essentially grow in two dimensions, albeit in a very disordered way, which results in the formation of sheets, whilst those in water-activated systems are essentially one dimensional, resulting in rods; the sheets or rods may be interstratified with CH-type structure, ultimately forming crumpled foils or fibrils.

The Op C-S-H present in neat water-activated ordinary PC pastes also has fibrillar morphology, and again, microcrystalline CH is never detected with normal w/c ratios and ambient curing temperatures, so the T/J approach is perhaps appropriate. Fig. 43(a)–(e) shows the Ca/Si ratio frequency histograms from Ref. [28] (TEM data) placed against the Ca/Si–MCL plot of Fig. 25, for ages ranging from 1 day to 2 years, with typical MCL data taken from Ref. [59]; the small amount of Al present in the C-S-H has been neglected but would not affect the discussion unduly. There are many possibilities of mixtures of different units that could account for the data, but these are reduced significantly if it is assumed that the silicate chains are not protonated, as seems quite likely [75,87,88]; i.e., that the J units have compositions along C–U on Fig. 40 and the T units along F–X. Fig. 43(a) certainly demonstrates well how the bimodal distribution at early age is nicely explained by the T/J viewpoint—the higher modal value having more J units than the lower—although the T/CH viewpoint could of course still account for the distribution: some regions would simply have less CH-like structure than others. The mean Ca/Si ratio does not essentially change as the MCL increases, but the bimodularity diminishes (Fig. 43(a)–(e)); there is a tendency towards compositional equilibrium. Since the Ca/Si ratio of J units gets closer to the mean value upon polymerisation, whilst that of T units departs further from it, a plausible explanation for the disappearance of the bimodularity is that polymerization occurs mainly within J-type structural units. This would also provide an explanation for the large amount of dimer that remains even after several decades (see Section 3.3). However, some longer chain T-type structure must be present to accommodate tetrahedral $Al^{3+}$. Polymerization might become increasingly difficult as the MCL approaches 5 because of restricted access to bridging sites in the interior of the particles of C-S-H, as discussed in Section 4.1.

Figs. 44(a) and (b) show the Ca/Si ratio frequency histograms from Ref. [28] (TEM data) for 3.5- and 26-year-old $C_3S$ pastes, respectively, and Fig. 44(c) for a β-$C_2S$ paste, placed against the Ca/Si–MCL plot of Fig. 25, with the MCL of the C-S-H again indicated by a bold vertical bar (as measured by $^{29}Si$ NMR). Since silanol groups probably do not occur to any large extent in C-S-H in hardened $C_3S$ or β-$C_2S$ pastes hydrated at normal temperature and w/c ratios [87], in terms of an entirely jennite-based model, this would mean that the structural units would occur along the line C–U on Fig. 40 (i.e., $w/n = 0$). As discussed in Section 3, TMS studies show that both the $C_3S$ systems would have ≈40% dimer and substantial fractions of pentamer and octamer; the older specimen would also contain larger anions with some tens of tetrahedra [54]. On inspection, it is clear that on the T/J model with no silanol groups ($w/n = 0$), entirely J-type structural units cannot account for the data, since none of the distributions fall on the line C–U of Fig. 40. It is necessary to have elements of T-type structure in all three cases. Although much of the polymer fraction in the older $C_3S$ paste would be J type, it seems likely that the dimer would be T. Entirely J-type structural units would require very significant protonation of the silicate chains. The increase in MCL that occurs between 3.5 and 26 years would mainly be due to the formation of J8 (and longer) units by the insertion of monomers at bridging sites of shorter J chains, which would result in a reduction in the local Ca/Si ratio, and so tend to narrow the Ca/Si ratio distribution. Since the polymerization of T2 units also leads to a reduction in Ca/Si ratio, it would tend to broaden the distribution. Since this is the opposite of what occurs, it seems unlikely that T-type chains would lengthen to any appreciable extent. Instead, extra Ca must be incorporated in those regions, perhaps by the formation of new J2, or on the T/CH approach by additional layers of CH-type structure.

The C-S-H particles in the Ip regions of relatively large grains (i.e., of relatively low surface area and slower reaction) do not grow beyond small globules. However, as discussed in Section 3.2.6, the C-S-H that forms in the Ip region of small, fully reacted grains tends to be foil-like. It is thus plausible that the C-S-H in these regions is essentially T-based. In neat PC pastes, it would be largely dimeric (because dimer has the highest Ca/Si ratio of T-type units; Ca/Si = 1.5 when $w/n = 0$), with small amounts of 'solid-solution' CH; the possibility that the C-S-H in these Ip regions has a very different nanostructure—and so different properties—to that elsewhere in a paste could have important implications.

#### 4.5.3. Carbonation of water-activated $C_3S$ pastes

A useful illustrative example of the use of the generalized formula is set out next for a hypothetical C-S-H formed from the hydration of $C_3S$ at around 20 °C for about 9 months. It uses guide data from the literature for values of Ca/Si ratio (1.75 [28]), the MCL of the C-S-H (2.9 [50]), and of bound $H_2O$/Ca ratio (1.4 [89]); this exercise would, of course, be more meaningful if these data were all available for the same sample. If it is assumed that this hypothetical C-S-H contains no silanol groups, as indicated by $^1H$ NMR investigations of high Ca/Si systems [87] (i.e., $w/n = 0$), it follows that in terms of the general 'solid-solution' formulation (formula (2))—the T/CH viewpoint—the C-S-H would be represented by

$$Ca_{3.9}Si_{2.9}O_{9.7} \cdot 1.17Ca(OH)_2 \cdot 5.9H_2O \quad (41)$$

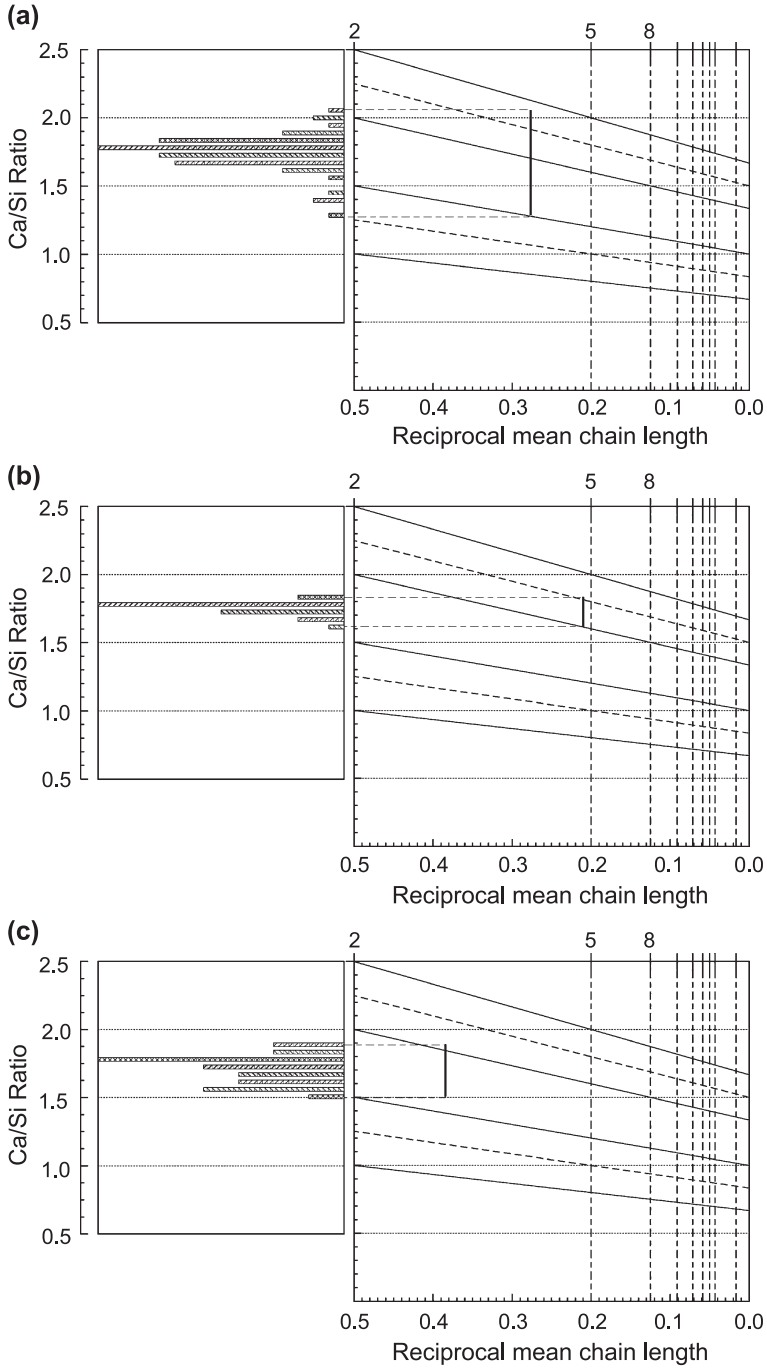


Fig. 44. Ca/Si ratio frequency histograms of the TEM analyses of C-S-H present in hardened water-activated $C_3S$ pastes (replotted from Ref. [28]) placed against the Ca/Si–MCL plot of Fig. 25, for ages (a) 3.5 and (b) 26 years; (c) is the same for a β-$C_2S$ paste hydrated for 3 months.

Or in terms of formula (3), by

$$[Ca_{2.6}Si_{2.9}O_{9.7}](OH)_{2.34} \cdot Ca_{2.47} \cdot 5.9H_2O \quad (42)$$

In terms of the T/J viewpoint, this must be rearranged to place the $(OH)^-$ ions and all but $n-(w/2)$ (= 1.3) $Ca^{2+}$ ions within the square brackets, i.e., in the main layer of the structure. Thus, the formula becomes

$$[Ca_{3.77}Si_{2.9}O_{9.7}(OH)_{2.34}]Ca_{1.3} \cdot 5.9H_2O \quad (43)$$

The C-S-H represented by formulae (41) and (42) (i.e., the T/CH viewpoint) and formula (43) (i.e., the T/J viewpoint) might be expected to have very different degradation characteristics: On the T/CH viewpoint, nearly twice as many Ca ions are not in the main layer (outside the square brackets) than on the T/J viewpoint, and so the former might be expected to degrade (leach, carbonate, etc.) more readily. For example, Groves et al. [64] reported that a 9-month-old $C_3S$ paste carbonated for 2 months in air at a relative

humidity of 72.6% contained a relatively homogeneous C-S-H of mean Ca/Si = 1.02 and MCL = 4.5 (silica gel had not yet formed); the data are illustrated on Fig. 45. Substituting these into Eq. (4) gives $y = 1$, and so assuming the minimum number of silanol groups (which corresponds in this case to Taylor's assumption), the C-S-H may be represented by

$$[Ca_{3.67}H_{1.83}Si_{4.5}O_{14.5}]Ca_{0.92} \cdot mH_2O \quad (44)$$

Formula (44) has no $Ca(OH)_2$ or jennite-like elements. It is plausible that the Ca in excess of that required for charge-balancing the silicate chains with $Ca^{2+}$ ions (i.e., the $zCa(OH)_2$ in formula (2)) should be the first Ca to be withdrawn from the C-S-H on reaction with carbon dioxide. It is not obvious why $Ca(OH)_2$ in the T/J viewpoint should be as reactive because in that case it forms an integral part of the main layer in a jennite-like (although disordered) layer structure.

#### 4.5.4. $C_3S$/PC–silica pastes

Brough et al. reported that the C-S-H formed in a $C_3S$–silica system that had an overall Ca/Si of 1.0 and that had been hydrated for 3 months at 40 °C (w/s = 0.7), had an MCL of 8 [62]; since the silica had reacted completely, the C-S-H was assumed to have a Ca/Si ratio of 1. Substitution of these values into Eq. (4) gives $y = 1.33$, which means that the degree of protonation of the silicate chains, $w/n$, must be between 0.67 and 2. So, assuming the minimum degree of protonation, which avoids the co-existence of Si–OH and –Ca–OH groups, the formula for an average structural unit is

$$[Ca_6H_2Si_8O_{25}]Ca_2 \cdot mH_2O \quad (45)$$

Data in the same article for pastes hydrated at 20 °C, which had either the silica or $C_3S$ selectively enriched in $^{29}Si$, showed that the C-S-H was not homogeneous, but that a region of hydrate existed that contained Si mainly originating from the silica, and that it was of substantially greater chain length than the rest. Since there is no reason to suppose that the situation would be different in the system hydrated at 40 °C, it seems likely that much of the dimer would be in separate regions to the long-chain units, which are presumably largely in the neighbourhood of reacting silica rather than $C_3S$ particles. Nevertheless, it is probable that they would all have T-type structure, with a degree of protonation greater than zero. The data do not exclude the possibility of J-type dimer, but their presence would necessitate an even greater degree of protonation of the silicate chains, as is clear on inspection of Fig. 45, which includes this system (♦) as well as the data for the carbonated paste.

Groves and Rodger [63] reported results for a PC–silica fume paste, which had >50% silica and was hydrated for 3 months at 40 °C (w/s = 0.7). The C-S-H had a mean Ca/Si ≈ 0.7 → 0.8 and an MCL of 8.5, which make it a particularly noteworthy example because the silicate chains have to be totally protonated ($w/n = 2$), placing it is at the very limit of the model. This is illustrated on Fig. 45 (◇). Substitution into formula (3) gives the formula for the average structural unit as

$$[Ca_{6.33}H_{6.33}Si_{8.5}O_{26.5}] \cdot mH_2O \quad (46)$$

## 5. Summary and conclusions

Ip C-S-H in relatively large grains of $C_3S$ or alite appears to consist of small globular particles, which are ≈ 4–8 nm in size in pastes hydrated at 20 °C but smaller at elevated temperatures, ≈ 3–4 nm. Fibrils of Op C-S-H in $C_3S$ or β-$C_2S$ pastes appear to consist of aggregations of long thin particles that are about 3 nm in their smallest dimension and of variable length, ranging from a few nanometers to many tens of nanometers. Op C-S-H in PC pastes is typically of finer morphology, with fewer coarse fibrils. The decalcification of C-S-H during carbonation leads first to a lengthening of the particles in the fibrils, followed by fragmentation, and ultimately in the formation of microporous silica.

In water-activated slag–PC pastes, the mean Ca/Si ratio of Op C-S-H decreases as the slag loading is increased. The C-S-H retains a linear directional morphology until the mean Ca/Si ratio drops below about 1.5. A further reduction

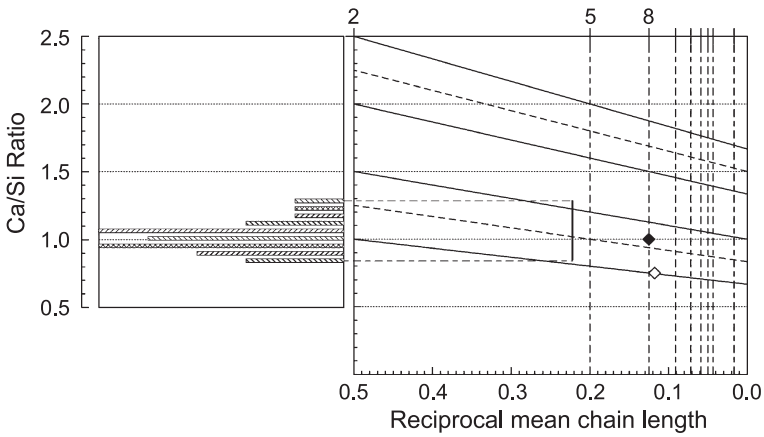


Fig. 45. Ca/Si ratio frequency histogram of the TEM analyses of C-S-H present in a partially carbonated $C_3S$ paste (replotted from Ref. [64]) placed against the Ca/Si–MCL plot of Fig. 25. Mean data are also included for C-S-H present in $C_3S$/PC–silica pastes from Ref. [62] (♦) and Ref. [63](◇).

results in a change to a crumpled-foil morphology, which suggests strongly that as the Ca/Si ratio is reduced, a transition occurs from essentially one-dimensional growth of the C-S-H particles to two-dimensional; i.e., long thin particles (aggregations of which form fibrils) to foils.

The morphology of Op C-S-H present in KOH-activated slag–PC pastes is generally foil-like at both low and high Ca/Si ratio. This C-S-H is also better ordered than in water-activated pastes, giving SAED patterns consistent with C-S-H (I), which is related to 1.4 nm tobermorite. CH is largely microcrystalline with KOH activation but forms as mostly large crystals with water activation unless cured at elevated temperature. The Op C-S-H is again foil-like in KOH-activated metakaolin–PC pastes.

Richardson and Groves' 1992 model for the structure of C-S-H, which includes formulations for both T/J and T/CH structural viewpoints, is explained more clearly than previously with the use of schematic diagrams. The close similarity with other recent dreierkette-based models is demonstrated.

A number of conclusions have been drawn regarding the applicability of the alternative structural viewpoints in Richardson and Groves' model to experimental data for C-S-H present in a range of cementitious systems, including

(i) The C-S-H present in a hydrated KOH-activated synthetic slag glass is entirely T-type in structure, with varying degrees of protonation of the silicate chains.
(ii) Data for the C-S-H present in a hydrated KOH-activated metakaolin–PC paste is well explained by the T/CH structural viewpoint and cannot be accounted for on the T/J.
(iii) Data for the C-S-H present in hydrated KOH-activated slag–PC pastes favour the T/CH viewpoint.
(iv) The C-S-H present in a hydrated water-activated slag–PC paste containing 90% slag is entirely T-type in structure, with only a modest level of protonation of the silicate chains.
(v) Both structural viewpoints can account for compositional and structural data for the C-S-H in water-activated neat PC pastes. The T/J approach nicely explains the bimodal distribution in Ca/Si ratio that is observed at early ages. The tendency to a unimodal distribution on aging could be explained by polymerization occurring largely in J-based units and not in T-based. This would also provide an explanation for the large amount of dimer that remains even after several decades of reaction. However, some longer chain T-type structure must be present to accommodate tetrahedral $Al^{3+}$. Polymerization might also become increasingly difficult because of restricted access to the bridging sites in the interior of particles of C-S-H.
(vi) The compositional and structural data for C-S-H in old $C_3S$ pastes cannot be accounted for on an entirely J-type structure unless there is very significant protonation of the silicate chains, which seems unlikely.
(vii) The C-S-H present in hydrated blends of PC or $C_3S$ with reactive silica is entirely T-based; in one particular example, the silicate chains must be totally protonated.

Sheet or foil-like morphology can be associated with T-type structure. The requirement of J units or CH layers in water-activated systems coincides with a change in morphology of Op C-S-H from foil-like to fibrillar, so it would seem reasonable to associate their presence with fibrillar morphology. The change is not, however, simply a result of their incorporation per se (i.e., of increasing Ca/Si ratio) because foil-like C-S-H with high Ca/Si ratio is formed in some systems, for example, in KOH-activated PC pastes, where the T/CH viewpoint is clearly more appropriate than the T/J. It might therefore be concluded that the change in morphology is due to the presence of J units rather than 'solid-solution' CH. However, it is possible that it is simply due to differences in the chemistry of the systems that affect the rate at which complexes are transferred from solution to the growing particles of C-S-H, such that T-type layers that form in KOH systems essentially grow in two dimensions, albeit in a very disordered way, which results in the formation of sheets, whilst those in water-activated systems are essentially one dimensional, resulting in rods; the sheets or rods may be interstratified with CH-type structure, ultimately forming crumpled foils or fibrils.

The C-S-H present in small fully hydrated alite grains, which has high Ca/Si ratio, contains a less dense product with substantial porosity; its morphology is quite similar to the fine foil-like Op C-S-H that forms in water-activated neat slag pastes, which has a low Ca/Si ratio. It is thus plausible that the C-S-H in small grains is essentially T-based (and largely dimeric). Since entirely T-based C-S-H is likely to have different properties to C-S-H consisting largely of J-based structure, it is possible that the C-S-H in small fully reacted grains will have different properties to the C-S-H formed elsewhere in a paste; this could have important implications.

The small size of the particles of C-S-H in water-activated $C_3S$, $\beta$-$C_2S$, and PC pastes is likely to result in significant edge effects, which would seem to offer a reasonable explanation for the persistence of $Q^0$(H) species. This would also explain why there is more $Q^0$(H) at elevated temperatures, where the particles seem to be smaller, and apparently less in KOH-activated pastes where the Op C-S-H has a foil-like morphology, which presumably has fewer chain-end edges than the particles in the fibrils present in water-activated pastes.

## Acknowledgements

Thanks are due to the Engineering and Physical Sciences Research Council for funding under Grant No. GR/S45874/01 and to Drs. Adrian R. Brough and Rik M.D. Brydson for valuable discussions.

## References


[1] L. Erdmenger, Fortschritte in der Cement-Industrie, Chemiker-Zeitung 17 (1893) 982–986.
[2] W.S. Michaëlis, The setting of calcareous hydraulic cements, Z. Chem. Ind. Kolloide 5 (1909) 9–22.
[3] H. Kühl, The "swelling theory" of Portland cement, Tonind.-Ztg. 33 (1909) 556–557.
[4] H. Le Chatelier, Recherches expérimentales sur la constitution des ciments et la théorie de leur prise (Experimental researches on the constitution of cements and the theory of their setting), C. R. Acad. Sci., Paris 94 (1882) 867–869.
[5] H. Le Chatelier, Crystalloids against colloids in the theory of cements, Trans. Faraday Soc. 14 (1–2) (1919) 8–11.
[6] S.B. Newberry, M.M. Smith, Constitution of hydraulic cements. J. Soc. Chem. Ind. 22 (1903) 94–95.
[7] G.A. Rankin, The setting and hardening of Portland cement, Trans. Faraday Soc. 14 (1–2) (1919) 23–28.
[8] R.H. Bogue, The Chemistry of Portland Cement, 2nd ed., Reinhold, New York, 1955.
[9] J.D. Bernal, J.W. Jeffery, H.F.W. Taylor, Crystallographic research on the hydration of Portland cement. A first report on investigations in progress, Mag. Concr. Res. 4 (11) (1952) 49–54.
[10] H.F.W. Taylor, Hydrated calcium silicates. Part 1. Compound formation at ordinary temperatures. J. Chem. Soc., (1950) 3682–3690.
[11] H.D. Megaw, C.H. Kelsey, Crystal structure of tobermorite, Nature 177 (1956) 390–391.
[12] E. Bonaccorsi, S. Merlino, H.F.W. Taylor. Crystal structures of jennite and tobermorites: New data for understanding the nanostructure of Portland cement. Paper presented at *Congress of the Italian Association of Crystallography*, 2002.
[13] H.F.W. Taylor, J.W. Howison, Relationships between calcium silicates and clay minerals, Clay Miner. Bull. 3 (1956) 98–111.
[14] D.L. Kantro, S. Brunauer, C.H. Weise, Development of surface in the hydration of calcium silicates. II. Extension of investigations to earlier and later stages of hydration, J. Phys. Chem. 66 (1962) 1804–1809.
[15] H.G. Kurczyk, H.E. Schwiete, Concerning the hydration products of $C_3S$ and $\beta$-$C_2S$, Proc 4th Int. Symp. Chem. Cem. 1.
[16] J.D. Birchall, N.L. Thomas, The mechanism of retardation of setting of OPC by sugars. Proc. Br. Ceram. Soc. 35 (1984) 305–315.
[17] H.F.W. Taylor, Proposed structure for calcium silicate hydrate gel, J. Am. Ceram. Soc. 69 (6) (1986) 464–467.
[18] I.G. Richardson, G.W. Groves, Models for the composition and structure of calcium silicate hydrate (C-S-H) gel in hardened tricalcium silicate pastes, Cem. Concr. Res. 22 (1992) 1001–1010.
[19] I.G. Richardson, G.W. Groves, The incorporation of minor and trace elements into calcium silicate hydrate (C-S-H) gel in hardened cement pastes, Cem. Concr. Res. 23 (1993) 131–138.
[20] E. Bonaccorsi, S. Merlino, H.F.W. Taylor, The crystal structure of jennite, $Ca_9Si_6O_{18}(OH)_6{\cdot}8H_2O$, Cem. Concr. Res., 34 (2004) 1481–1488.
[21] Report from RILEM TC 170-CSH, The structure of C-S-H (2004).
[22] I.G. Richardson, Electron microscopy of cements, in: P. Barnes, J. Bensted (Eds.), Chapter 22 in Structure and Performance of Cements, 2nd ed., Spon Press, London, 2002, pp. 500–556.
[23] I.G. Richardson, The nature of C-S-H in hardened cements, Cem. Concr. Res. 29 (1999) 1131–1147.
[24] L.S. Dent Glasser, E.E. Lachowski, K. Mohan, H.F.W. Taylor, A multi-method study of $C_3S$ hydration, Cem. Concr. Res. 8 (1978) 733–740.
[25] N.J. Clayden, C.M. Dobson, C.J. Hayes, S.A. Rodger, Hydration of tricalcium silicate followed by solid-state $^{29}$Si N.M.R. spectroscopy, J. Chem. Soc., Chem. Commun., (1984) 1396–1397.
[26] P.J. Le Sueur, D.D. Double, G.W. Groves, Chemical and morphological studies of the hydration of tricalcium silicate, Trans. Br. Ceram. Soc. 35 (1984) 177–191.
[27] H.F.W. Taylor, D.E. Newbury, Calcium hydroxide distribution and calcium silicate hydrate composition in tricalcium silicate and $\beta$-dicalcium silicate pastes, Cem. Concr. Res. 14 (1984) 93–98.
[28] I.G. Richardson, G.W. Groves, Microstructure and microanalysis of hardened ordinary Portland cement pastes, J. Mater. Sci. 28 (1993) 265–277.
[29] I.G. Richardson, The nature of the hydration products in hardened cement pastes, Cem. Concr. Compos. 22 (2000) 97–113.
[30] I.G. Richardson, G.W. Groves, Microstructure and microanalysis of hardened cement pastes involving ground granulated blast-furnace slag, J. Mater. Sci. 27 (1992) 6204–6212.
[31] I.G. Richardson, G.W. Groves, The structure of the calcium silicate hydrate phases present in hardened pastes of white Portland cement/blast-furnace slag blends, J. Mater. Sci. 32 (1997) 4793–4802.
[32] C.A. Love, PhD thesis, University of Leeds (2002).
[33] I.G. Richardson, A.R. Brough, G.W. Groves, C.M. Dobson, The characterization of hardened alkali-activated blast-furnace slag pastes and the nature of the calcium silicate hydrate (C-S-H) phase, Cem. Concr. Res. 24 (1994) 813–829.
[34] R.B. Williamson, Solidification of Portland cement, Prog. Mater. Sci. 15 (1972) 189–286.
[35] G.W. Groves, TEM studies of cement hydration, Mater. Res. Soc. Symp. Proc. 85 (1987) 3–12.
[36] A.J. Allen, C.G. Windsor, V. Rainey, D. Pearson, D.D. Double, N. McN Alford, A small-angle neutron-scattering study of cement porosities, J. Phys., D. Appl. Phys. 15 (1982) 1817–1833.
[37] D. Pearson, A.J. Allen, A study of ultrafine porosity in hydrated cements using small angle neutron scattering, J. Mater. Sci. 20 (1985) 303–315.
[38] H.M. Jennings, B.J. Dalgleish, P.L. Pratt, Morphological development of hydrating tricalcium silicate as examined by electron microscopy techniques, J. Am. Ceram. Soc. 64 (1981) 567–572.
[39] Å. Grudemo, The crystal structures of cement hydration—A review and a new gel structure model, CBI (Cement och Betong Institutet [Swedish Cement and Concrete Research Institute]) Report ra 1·86 (1986) 3–16. (Reprinted from Nordic Concrete Research, 1984).
[40] H.F.W. Taylor, Cement Chemistry, 2nd ed., Thomas Telford, London, 1997.
[41] L.E. Copeland, E.G. Schulz, Electron optical investigation of the hydration products of calcium silicates and Portland cement, J. PCA Res. Dev. Lab. 4 (1962) 2–12.
[42] R. Brydson, I.G. Richardson, D.W. McComb, G.W. Groves, Parallel electron energy loss spectroscopy study of Al-substituted calcium silicate hydrate (C-S-H) phases present in hardened cement pastes, Solid State Commun. 88 (1993) 183–187.
[43] H.F.W. Taylor, Nanostructure of C-S-H: Current status, Adv. Cem. Based. Mater. 1 (1993) 38–46.
[44] Å. Grudemo, Discussion following the paper by J.D. Bernal on "The structure of cement hydration compounds", 3rd Int. Symp. Cem. Chem, London, Cement and Concrete Association, London, 1954, pp 247–253.
[45] C.A. Love, I.G. Richardson, A.R. Brough (in preparation).
[46] I.G. Richardson, S.A. Rodger, G.W. Groves, The porosity and pore structure of hydrated cement pastes as revealed by electron microscopy techniques, Mater. Res. Soc. Symp. Proc. 137.
[47] G.W. Groves, D.I. Rodway, I.G. Richardson, The carbonation of hardened cement pastes, Adv. Cem. Res. 3 (1990) 117–125.
[48] I.G. Richardson, G.W. Groves, A.R. Brough, C.M. Dobson, The carbonation of OPC and OPC/silica fume hardened cement pastes in air under conditions of fixed humidity, Adv. Cem. Res. 5 (1993) 81–86.
[49] G.W. Groves, D.I. Rodway, I.G. Richardson, The carbonation of hardened cement pastes, Adv. Cem. Res. 3 (1990) 117–125.
[50] S.A. Rodger, G.W. Groves, N.J. Clayden, C.M. Dobson, A study of tricalcium silicate hydration from very early to very late stages, Mater. Res. Soc. Symp. Proc. 85 (1987) 13–20.
[51] J.F. Young, Investigations of calcium silicate hydrate structure using

silicon-29 nuclear magnetic resonance spectroscopy, J. Am. Ceram. Soc. 71 (1988) C-118–C-120.
[52] A.R. Brough, C.M. Dobson, I.G. Richardson, G.W. Groves, In situ solid-state NMR studies of $Ca_3SiO_5$: Hydration at room temperature using $^{29}Si$ enrichment, J. Mater. Sci. 29 (1994) 3926.
[53] L.S. Dent-Glasser, E.E. Lachowski, M.Y. Qureshi, H.P. Calhoun, D.J. Embree, W.D. Jamieson, C.R. Masson, Identification of some of the polysilicate components of trimethylsilylated cement. Cem. Concr. Res. 11 (1981) 775–780.
[54] K. Mohan, H.F.W. Taylor, A trimethylsilylation study of tricalcium silicate pastes, Cem. Concr. Res. 12 (1982) 25–31.
[55] J. Hirljac, Z.-Q. Wu, J.F. Young, Silicate polymerization during the hydration of alite, Cem. Concr. Res. 13 (1983) 877–886.
[56] F. Massazza, M. Testolin, Trimethylsilylation in the study of pozzolana-containing pastes, Il cemento 80 (1) (1983) 49–62.
[57] I.G. Richardson, A.R. Brough, R. Brydson, G.W. Groves, C.M. Dobson, The location of aluminum in substituted calcium silicate hydrate (C-S-H) gels as determined by $^{29}Si$ and $^{27}Al$ NMR and EELS, J. Am. Ceram. Soc. 76 (1993) 2285–2288.
[58] M.D. Anderson, H.J. Jakobsen, J. Skibsted, Incorporation of aluminium in the calcium silicate hydrate (C-S-H) of hydrated Portland cements: A high-field $^{27}Al$ and $^{29}Si$ MAS NMR investigation, Inorg. Chem. 42 (2003) 2280–2287.
[59] S.A. Rodger, The chemistry of admixture interaction during cement hydration, D.Phil. thesis, University of Oxford (1984).
[60] S.A. Rodger, G.W. Groves, N.J. Clayden, C.M. Dobson, Hydration of tricalcium silicate followed by $^{29}Si$ NMR with cross-polarization, J. Am. Ceram. Soc. 71 (2) (1988) 91–96.
[61] A.R. Brough, C.M. Dobson, I.G. Richardson, G.W. Groves, Alkali activation of reactive silicas in cements: in situ $^{29}Si$ MAS NMR studies of the kinetics of silicate polymerization, J. Mater. Sci. 31 (1996) 3365–3373.
[62] A.R. Brough, C.M. Dobson, I.G. Richardson, G.W. Groves, A study of the pozzolanic reaction by solid-state $^{29}Si$ nuclear magnetic resonance using selective isotopic enrichment, J. Mater. Sci. 30 (1995) 1671–1678.
[63] G.W. Groves, S.A. Rodger, The hydration of C3S and ordinary Portland cement with relatively large additions of microsilica, Adv. Cem. Res. 2 (1989) 135–140.
[64] G.W. Groves, A. Brough, I.G. Richardson, C.M. Dobson, Progressive changes in the structure of hardened $C_3S$ cement pastes due to carbonation, J. Am. Ceram. Soc. 74 (1991) 2891–2896.
[65] F.P. Glasser, E.E. Lachowski, D.E. Macphee, Compositional model for calcium silicate hydrate (C-S-H) gels, their solubilities and free energies of formation, J. Am. Ceram. Soc. 70 (7) (1987) 481–485.
[66] S. Merlino, E. Bonaccorsi, T. Armbruster, Tobermorites: Their real structure and order–disorder (OD) character, Am. Mineral. 84 (1999) 1613–1621.
[67] S. Merlino, E. Bonaccorsi, T. Armbruster, The real structure of clinotobermorite and tobermorite 9 Å: OD character, polytypes, and structural relationships, Eur. J. Mineral. 12 (2000) 411–429.
[68] S. Merlino, E. Bonaccorsi, T. Armbruster, The real structure of tobermorite 11 Å: normal and anomalous forms, OD character and polytypic modifications, Eur. J. Mineral. 13 (2001) 577–590.
[69] N.A. Yamnova, Kh. Sarp, Yu.K. Egorov-Tismenko, D.Yu. Pushcharovskii, Crystal structure of jaffeite, Crystallogr. Rep. 38 (4) (1993) 464–466 (c/c of Kristallografiia).
[70] H.F.W. Taylor, personal communication 2000.
[71] S.A. Hamid, The crystal structure of the 11 Å natural tobermorite $Ca_{2.25}[Si_3O_{7.5}(OH)_{1.5}]\cdot 1H_2O$, Zeit. Krist. 154 (1981) 189–198.
[72] S.A. Greenberg, T.N. Chang, E. Anderson, Investigation of colloidal hydrated calcium silicates. I. Solubility products, J. Phys. Chem. 64 (1960) 1151–1157.
[73] S.A. Greenberg, T.N. Chang, Investigation of the colloidal hydrated calcium silicates. II. Solubility relationships in the calcium oxide–silica–water system at 25 °C, J. Phys. Chem. 69 (1965) 182–188.
[74] K. Fujii, W. Kondo, Heterogeneous equilibrium of calcium silicate hydrate in water at 30 °C, J. Chem. Soc., Dalton Trans. 2 (1981) 645–651.
[75] X. Cong, R.J. Kirkpatrick, $^{29}Si$ MAS NMR study of the structure of calcium silicate hydrate, Adv. Cem. Based Mater. 3 (1996) 144–156.
[76] X. Cong, R.J. Kirkpatrick, $^{1}H$-$^{29}Si$ CPMAS NMR study of the structure of calcium silicate hydrate, Adv. Cem. Res. 7 (1995) 103–111.
[77] R.J. Kirkpatrick, J.L. Yarger, P.F. McMillan, P. Yu, X. Cong, Raman spectroscopy of C-S-H, tobermorite, and jennite, Adv. Cem. Based. Mater. 5 (1997) 93–99.
[78] R.J. Kirkpatrick, G.E. Brown, N. Xu, X. Cong, Ca X-ray absorption spectroscopy of C-S-H and some model compounds, Adv. Cem. Res. 9 (1997) 31–36.
[79] A. Nonat, X. Lecoq, The structure, stoichiometry and properties of C-S-H prepared by $C_3S$ hydration under controlled conditions, in: P. Grimmer, A.-R. Grimmer, H. Zanni, P. Sozzani (Eds.), Nuclear Magnetic Resonance Spectroscopy of Cement-Based Materials, Springer, Berlin, 1998, pp. 197–207.
[80] H. Stade, On the structure of ill-crystallized calcium hydrogen silicates. II. A phase consisting of poly- and disilicate, Z. Anorg. Allg. Chem. 470 (1980) 69–83 (in German).
[81] H. Stade, W. Wieker, On the structure of ill-crystallized calcium hydrogen silicates. I. Formation and properties of an ill-crystallized calcium hydrogen disilicate phase, Z. Anorg. Allg. Chem. 466 (1980) 55–70 (in German).
[82] H. Stade, W. Wieker, G. Garzo, On the structure of ill-crystallized calcium hydrogen silicates. IV. Anion composition of the hydration products of tricalcium silicate, Z. Anorg. Allg. Chem. 500 (1983) 123–131.
[83] H. Stade, D. Müller, G. Scheler, On the structure of ill-crystallized calcium hydrogen silicates. V. Studies on the coordination of Al in C-S-H(di,poly) by $^{27}Al$ NMR spectroscopy, Z. Anorg. Allg. Chem. 510 (1984) 16–24.
[84] H. Stade, A.-R. Grimmer, G. Engelhardt, M. Magi, E. Lipmaa, On the structure of ill-crystallized calcium hydrogen silicates. VII. Solid state silicon-29 NMR studies on C-S-H (Di,Poly), Z. Anorg. Allg. Chem. 528 (1985) 147–151 (in German).
[85] H. Stade, D. Müller, On the coordination of Al in ill-crystallized C-S-H phases formed by hydration of tricalcium silicate and by precipitation reactions at ambient temperature, Cem. Concr. Res. 17 (1987) 553–561.
[86] J.J. Chen, J.J. Thomas, H.F.W. Taylor, H.M. Jennings, Solubility and structure of calcium silicate hydrate, Cem. Concr. Res. 2950 (this issue).
[87] D. Heidemann, W. Wieker, Characterization of protons in C-S-H phases by means of high-speed $^{1}H$ MAS NMR investigations, in: P. Grimmer, A.-R. Grimmer, H. Zanni, P. Sozzani (Eds.), Nuclear Magnetic Resonance Spectroscopy of Cement-Based Materials, Springer, Berlin, 1998, pp. 169–179.
[88] P. Yu, R.J. Kirkpatrick, B. Poe, P.F. McMillan, X. Cong, Structure of calcium silicate hydrate (C-S-H): near-, mid-, and far- infrared spectroscopy. J. Am. Ceram. Soc. 82 (1999) 742–748.
[89] H.F.W. Taylor, Bound water in cement pastes and its significance for pore solution compositions, Mater. Res. Soc. Symp. Proc. 85 (1987) 47–54.